UNIVERSITY OF SOUTHAMPTON

FACULTY OF NATURAL AND ENVIRONMENTAL SCIENCES

Ocean and Earth Science

Astronomical climate forcing during the Oligo-Miocene

by

Diederik Liebrand

A thesis submitted in partial fulfillment for the degree of Doctor of Philosophy

October 2014

UNIVERSITY OF SOUTHAMPTON

ABSTRACT

FACULTY OF NATURAL AND ENVIRONMENTAL SCIENCES
OCEAN AND EARTH SCIENCE

Doctor of Philosophy

ASTRONOMICAL CLIMATE FORCING DURING THE OLIGO-MIOCENE

by Diederik Liebrand

In this thesis newly generated high-resolution Oligo-Miocene climate proxy records from Walvis Ridge ODP Site 1264 (south-eastern Atlantic Ocean) are presented (Chapters 2 and 3). The records are tuned to an eccentricity solution (Chapter 3) and they are compared to published Atlantic and Pacific palaeoclimate chronologies (Chapters 2 and 4). The main research objectives are 1) to identify astronomical pacemakers of global significance and test earlier pacing theories, 2) to describe global climate and oceanographic change on astronomical and tectonic time scales and 3) to test the strong hysteresis in ice sheet models that suggest a very stable Antarctic ice sheet once formed.

Chapter 1 gives a general introduction on the "mid"-to-late Oligocene climatic, oceanographic, geographic and cryospheric settings. Climate evolution and dynamics, together with the major underlying processes are introduced.

In Chapter 2, high-resolution early Miocene stable oxygen and carbon isotope chronologies from Walvis Ridge Site 1264 are presented. The data are analysed on an untuned age model to identify the principal astronomical pacemakers, without introducing power on orbital frequencies. A dominance of variance in all datasets on 100-kyr timescales is found. The $\delta^{18}O$ data are used to parameterize a suite of 1D ice sheet models and show that between 20 – 80% (avg. ~50%) of the $\delta^{18}O$ signal can be explained by changes in Antarctic ice volume. (This chapter has been published as: *D. Liebrand, L. J. Lourens, D. A. Hodell, B. de Boer, R. S. W. van de Wal and H. Pälike*. Antarctic ice sheet and oceanographic response to eccentricity forcing during the early Miocene. *Climate of the Past*, 7, 869–880, 2011)

In Chapter 3, extended stable-isotope records together with X-ray fluorescence core scanning data from Walvis Ridge Site 1264 are presented. The records span an 11-Myr mid Oligocene through early Miocene time interval. Ages are calibrated to eccentricity, are in good agreement with the GTS2012 and independently confirm the Oligo-Miocene time scale to the ~100-kyr level. The ~2.4-Myr long-period eccentricity cycle is identified as the main pacemaker of Oligo-Miocene climate events, as identified in the benthic isotope records, at shorter astronomical (eccentricity) periodicities.

In Chapter 4, the high-resolution Oligo-Miocene benthic stable-isotope chronology from Site 1264 is compared to published records from the Atlantic and Pacific to further identify and explore possible global climate pacemakers. In addition, an investigation of long-term trends and inter-/intra-basin isotopic gradients and their implications for ice volume reconstruction and palaeoceanographic studies are discussed. Methods are explored to quantify the apparent change in geometry of ~100-kyr cycles in our benthic $\delta^{18}O$ data and the analyses indicate an increased cycle asymmetry (i.e. sawtooth patterns) throughout the Oligo-Miocene. This change in cycle geometry is interpreted as a measure of changing boundary conditions and used to track the evolution of a threshold response mechanism in Earth's climate system.

In Chapter 5 the main results of this thesis are summarised, the implications for our understanding of the Oligo-Miocene are discussed and perspectives are given on future work.

List of Contents (1 of 3) **Page**

List of Contents (2 of 3) **Page**

List of Contents (3 of 3) **Page**

List of Tables **Page**

List of Figures (1 of 2) **Page**

List of Figures (2 of 2) **Page**

List of Appendices

This thesis is accompanied by only one appendix (Appendix A), which is too large to print.

Appendix A: An Excel file titled "Appendix_To_Thesis_Liebrand.xlsx" containing

Table 1: 1264 Affine
Table 2: 1264 Splice
Table 3: 1265 Affine
Table 4: 1265 Splice
Table 5: 1265 PMAG
Table 6: 1266 Affine
Table 7: 1266 Splice
Table 8: 1266 PMAG
Table 9: 1265 – 1264 tie-points
Table 10: 1266 – 1264 tie-points
Table 11: 1264 PMAG age-model
Table 12: 1264 405-kyr tuning
Table 13: 1264 100-kyr tuning
Table 14: 1264 Mag. Sus.
Table 15: 1264 Col. Refl.
Table 16: 1264 XRF
Table 17: 1264 Isotopes
Table 18: 1264 Match test ages

has been made digitally available to H. Pälike and L. J. Lourens. After publication the data presented in this thesis will be available on request and/or will be stored in a public database.

Declaration of Authorship

I, *Diederik Liebrand*, declare that the thesis entitled "Astronomical climate forcing during the Oligo-Miocene" and the work presented in the thesis are both my own, and have been generated by me as the result of my own original research. I confirm that:

- this work was done wholly or mainly while in candidature for a research degree at this University;
- where any part of this thesis has previously been submitted for a degree or any other qualification at this University or any other institution, this has been clearly stated;
- where I have consulted the published work of others, this is always clearly attributed;
- where I have quoted from the work of others, the source is always given. With the exception of such quotations, this thesis is entirely my own work;
- I have acknowledged all main sources of help;
- where the thesis is based on work done by myself jointly with others, I have made clear exactly what was done by others and what I have contributed myself;
- Chapter 2 of this thesis has been published as: *D. Liebrand, L. J. Lourens, D. A. Hodell, B. de Boer, R. S. W. van de Wal and H. Pälike*. Antarctic ice sheet and oceanographic response to eccentricity forcing during the early Miocene. *Climate of the Past*, 7, 869–880, 2011.

Signed:

Date:

Acknowledgements

I would like to thank Heiko Pälike for supervising this PhD-research. During the project you encouraged my curiosity and supported me all along, for which I am very grateful. Your earlier Oligo-Miocene studies have inspired me greatly. I would like to thank Paul Wilson for his help and advise. We discussed many ideas and I look forward to do so over the coming years during a postdoc under your supervision. Sailing on IODP Expedition 342 was an opportunity I couldn't decline and it was a fantastic experience. Lucas Lourens, you have taught me the principles of cyclostratigraphy, skills I will not forget. Thank you for offering technical support when the lab in Southampton was down. I appreciate that you are always keen to discuss ideas. Steven Bohaty, I would like to thank you for many scientific discussions and for the help you gave to Paul and me during the proposal writing. Eelco Rohling, thank you for being an excellent panel chair. I enjoyed that many panel meetings (strictly only about progress) ended in scientific discussions. Frits Hilgen, thank you for being such an inspiring stratigrapher, palaeoclimatologist, teacher and science enthusiast during my time in Utrecht and during the ColdiGioco summer school.

The results presented in this thesis could never have been generated without the help and/or technical support of many people. I am especally indebted to Geert Ittman, Arnold van Dijk, Jan Drenth, Jason Curtis, Giana Brown, Walter Hale, Alex Wülbers, Dominika Kasjaniuk, Thomas Westerhold, Ursula Röhl and Anastasia Tsiola.

This thesis benefited greatly from discussions with (amongst others): Helen Beddow, Dave Hodell, Rosanna Greenop, David Naafs, Martin Ziegler, Clara Bolton, Lucy Stap, Tanja Kouwenhoven, Sietske Batenburg, Christian Zeeden, Cristina Sghibartz, Sarah O'Dea, Ellen Thomas, Dick Kroon, Franck Bassinot, Luc Beaufort, Daniel Clay Kelly, Alice Lefebvre, Ian Croudace, Mischa Saes, Cindy Schrader, Isabella Raffi, Samantha Gibbs and Doug Wilson.

The members of the GTS-next network are thanked for many pleasant (field) trips, workshops and summer schools all over Europe. Especially Klaudia Kuiper is thanked for making the project run as smoothly as it did.

Thanks to all (former) office mates for creating such a nice work environment. In Southampton: Clara, Debbie, Alice, Maike, Cristina, Sarah, Ben, Dave L., Dave A.-M., and Pin-Ru; in Utrecht: Christian, Hemmo, Joyce, Helen, Vitoria and Tiuri; and in Frankfurt: Oliver.

All (former) colleagues of the palaeoclimatology/palaeoceanography and geochemisty-groups at NOCS are thanked for scientific discussions and collaborations.

Many housemates made me feel welcome in Southampton. I would especially like to thank my former housemates Nadia, Ida, Patrick, James, Alex, Juan, Mark, Ewa, Dat, Soraya and Matt, and my present housemates Anya and Megan.

I would like to thank Hans and Ineke, Janwillem, Riti and Katalin, Andrea and Marte, extended family members and Sietske and family for being there for me and supporting me. I could not have written this thesis without you!

Thomas, Gijske, Martijn, Ramon, Stijn, Robbert, Roderic, Thomas, Jochem, Tim, Ronald, Doeke and other friends in Utrecht/the Netherlands are thanked for support, discussions and many good memories of the past years.

Frits Hilgen (Utrecht University) and Steven Bohaty (University of Southampton), the examiners during my viva, took time to read this thesis and give feedback on the ideas presented in it. For doing so, I am very grateful.

I would like to acknowledge the help of the Graduate School (GS-NOCS) during my PhD.

This research used samples provided by the Ocean Drilling Program, sponsored by the US National Science Foundation and participating countries under the management of Joint Oceanographic Institutions (JOI), Inc.

This research has been made possible by a European Community's Seventh Framework Programme (FP7/2007-2013) Marie Curie grant (215458) to the "GTS-next" initial training network (Southampton participants: Heiko Pälike and Diederik Liebrand) and by a VIDI-grant (864.02.007) and VICI-grant (865.10.001) of the Dutch Science Foundation (NWO) to Lucas Lourens.

List of Definitions and Abbreviations

ATNTS = Astronomically Tuned Neogene Time Scale

benthic = benthonic = organisms that live on the bottom of the ocean (or lake)

$CaCO_3$ est. = calcium carbonate estimates

CAR = Carbonate Accumulation Rate

CO_2 = carbon dioxide

DSDP = Deep Sea Drilling Project

EAIS = East Antarctic Ice Sheet

EOT = Eocene Oligocene (Climatic) Transition

ETP = artificial mix of Eccentricity, Tilt (obliquity) and Precession

E2011 = Laskar 2011 eccentricity solution

ET2004 = artificial mix of Laskar 2004 Eccentricity and Tilt

ETP2004 = artificial mix of Laskar 2004 Eccentricity, Tilt (obliquity) and Precession

insolation = incoming solar radiation

kyr = thousand years

Ma = Mega annum = (proverbially) million years ago

MAR = Mass Accumulation Rate

mcd = meters composite depth

MMCO = Mid Miocene Climatic Optimum

Myr = million years

NH = Northern Hemisphere

ODP = Ocean Drilling Program

OMT = Oligocene – Miocene (Climatic) Transition

pCO_2 = partial pressure of atmospheric carbon dioxide

planktic = planktonic = organisms that live in the water column and cannot swim

rmcd = revised meter composite depth

SH = Southern Hemisphere

SST = Sea Surface Temperature

WAIS = West Antarctic Ice Sheet

XRF = X-ray fluorescence

$\delta^{13}C$ (‰) = $(({}^{13}C/{}^{12}C)_{sample} / ({}^{13}C/{}^{12}C)_{standard} -1) \times 1000$ = stable carbon isotopic composition

$\delta^{18}O$ (‰) = $(({}^{18}O/{}^{16}O)_{sample} / ({}^{18}O/{}^{16}O)_{standard} -1) \times 1000$ = stable oxygen isotopic composition

CHAPTER 1

INTRODUCTION

1.1 Overview of Oligocene and Early Miocene Climate

The Oligocene through early Miocene time interval (34 Ma – 17 Ma) comprises the late Palaeogene through early Neogene period. Directly following the Doubthouse – Icehouse transition broadly contemporaneous with the Eocene – Oligocene boundary and bracketed, at the younger end, by the onset of the Early/Mid Miocene Climatic Optimum, the Oligo-Miocene constitutes the earliest phase of Earth's Cenozoic glaciated history with continental size ice sheet on Antarctica (Fig. 1.01). Superimposed on a long-term Cenozoic cooling trend, the Oligo-Miocene forms ~17 Myr interval of relative stability that was interrupted by the late Oligocene warm interval, the transient glaciations associated with the "mid"-Oligocene cold phase, the OMT and other high-frequency climate variability on astronomical time scales. Earth is thought to have resided in a unipolar Icehouse state during (almost) the entire Oligo-Miocene, with no significant land ice on the Northern Hemisphere, probably resulting in more moderate pole to equator temperature gradients than today.

The exact loci and size of the major ice sheets during the Oligo-Miocene is matter of debate and the presence or absence of land ice on West Antarctica [*Wilson and Luyendyk*, 2009] and in the Northern Hemisphere [*Moran et al.*, 2006] are still poorly understood. Ice-rafted debris off coast Greenland has been recorded from as early as the middle Eocene [*Eldrett et al.*, 2007; *Moran et al.*, 2006; *Tripati et al.*, 2005] suggesting that at least some land-ice or coastal glaciers must have been present at high Northern latitudes. Deep-water formation (predominantly) took place in the Southern Ocean, filling all major ocean basins with Antarctic-sourced bottom waters [*Billups et al.*, 2002]. This view is however debated for the Atlantic Ocean, where perhaps as early as the EOT [*Katz et al.*, 2011], or even the early-to-mid Eocene [*Hohbein et al.*, 2012], the formation of North Atlantic deep water and the modern stratification of water masses had already manifested itself. Deep-water temperatures in the Atlantic and Pacific probably averaged around 4°C [*Lear et al.*, 2000; *Lear et al.*, 2004], not much warmer than today. Only very sparse SST estimates are currently available (see review [*Norris et al.*, 2013]), but planktic foraminifer $\delta^{18}O$ data suggest that SSTs may have been highly variable on astronomical timescales across the OMT

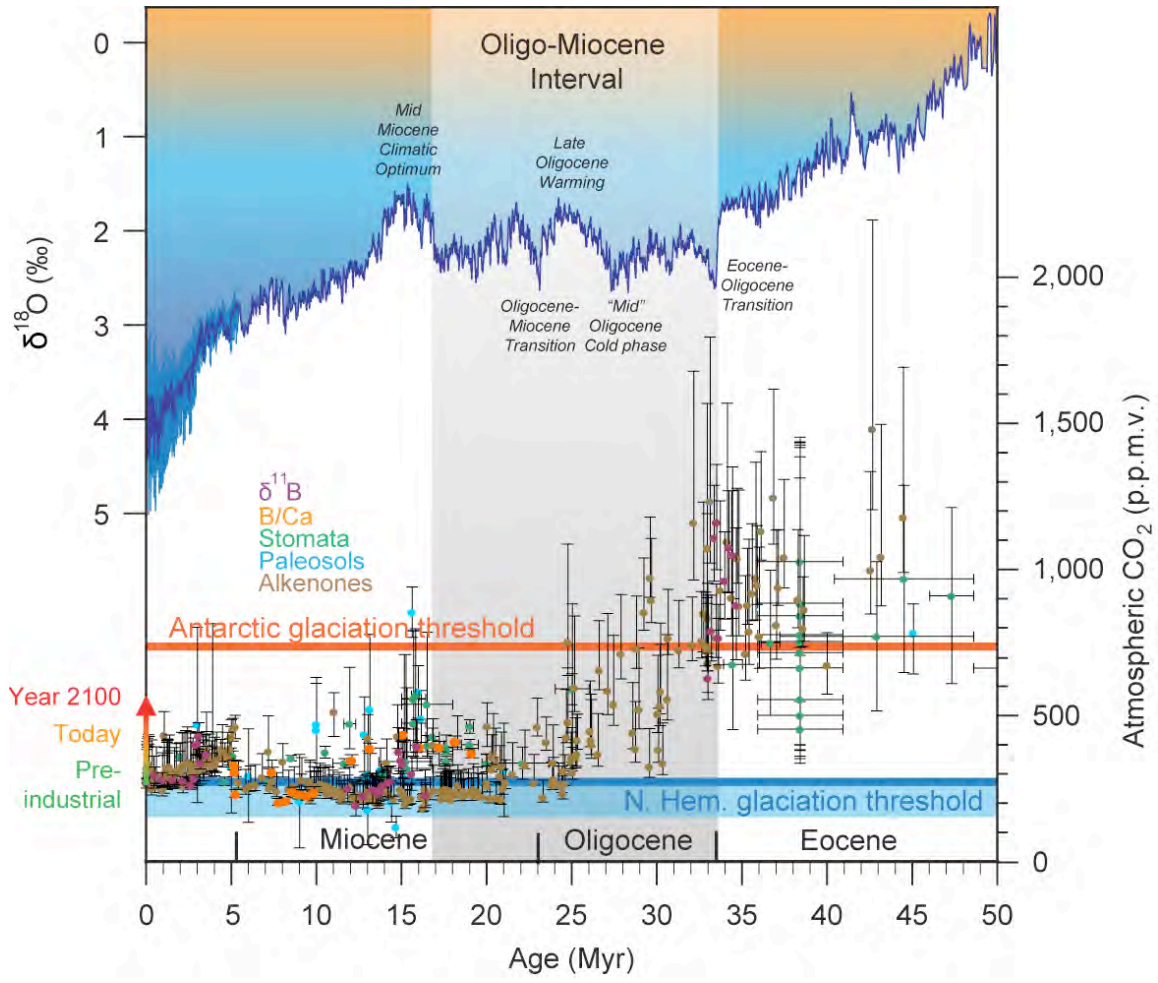

Figure 1.01: *Global compilation of benthic $\delta^{18}O$ [Lisiecki and Raymo, 2005; Zachos et al., 2008] (resampled) showing the largest inferred glaciations of the early (unipolar) Icehouse and a global compilation of atmospheric CO_2 proxy records [Beerling and Royer, 2011; Zhang et al., 2013]. Orange and blue horizontal lines represent CO_2 thresholds for major Antarctic & NH glaciation as defined in a coupled climate-ice sheet model [DeConto et al., 2008].*

[*Pearson et al.*, 1997]. Reconstructions of atmospheric CO_2 concentrations are limited, however, those available indicate a persistent lowering of values from around ~650 ± 350 ppmv prior to ~27 Ma to ~400 ± 100 ppmv post ~24Ma [*Pagani et al.*, 2005; *Zhang et al.*, 2013]. Surprisingly, this drop in pCO_2 is broadly contemporaneous with relatively light benthic $\delta^{18}O$ values of the late Oligocene warm phase. Further evidence for decoupling between pCO_2 and global climate comes

from the major glaciations across OMT that apparently are not accompanied by lowering of pCO_2, as far as the currently available records can resolve (Fig. 1.01).

The best resolved chronologies of (global) Oligo-Miocene climate dynamics on astronomical timescales come from (land-based) marine archives [*Abels et al.*, 2007; *Hüsing et al.*, 2007; *Hüsing et al.*, 2009; *Zeeden et al.*, 2014]. Benthic $\delta^{18}O$ records show variability on precession, obliquity and short and long eccentricity time-scales indicating that several linear and non-linear response mechanisms influenced deep sea temperatures and ice volume [*Pälike et al.*, 2006a; *Pälike et al.*, 2006b], reminiscent of late Pleistocene climate dynamics [*Hays et al.*, 1976]. Benthic oxygen isotope records are generally interpreted in terms of the combined contributions of calcification temperature (i.e. bottom water temperature) and the isotopic composition of the water (i.e. a measure of global ice volume), thereby recording predominantly high latitude climate variability where deep-water formation takes place. Despite the presence of all astronomical periodicities in globally integrated proxy data, episodes with enhanced sensitivity to ~100-kyr eccentricity periodicity have been identified [*Liebrand et al.*, 2011, Chapter 2; *Pälike et al.*, 2006b; *Zachos et al.*, 1997] suggesting that during brief periods global climate responded to eccentricity-modulated precession.

1.2 Global Change During the Oligocene and Miocene

1.2.1 Long-Term Trends

Strontium isotope records across the Oligocene and early Miocene indicate a persistent increase in seawater $^{87}Sr/^{86}Sr$ ratios since ~40 Ma [*Hodell and Woodruff*, 1994; *Zachos et al.*, 1999]. Both the exposure of rock lithologies resulting from tectonic events (physical weathering) and global climate (through the rate of chemical weathering and solute transport) control the Sr ratio of seawater. It is generally thought that the long term Cenozoic increase in $^{87}Sr/^{86}Sr$ of seawater is the direct result of increased global topography, primarily related to the uplift of the Tibetan plateau [*Raymo et al.*, 1988]. However the exact dates of significant uplift are debated and the effect of global climate on weathering rates and Sr ratios should not be underestimated [*Zachos et al.*, 1999]. Silicate weathering causes carbonic acid (i.e. dissolved CO_2, in seawater for example) to be consumed and bicarbonate to form. The global increase in the weathering rates of silicate

rocks is therefore also reflected in Cenozoic compilations of pCO_2 that show a progressive decrease (Fig. 1.01).

No clear constraints exist on the opening and/or closure of major ocean gateways during the Oligocene. However, it is thought that perhaps the Panamanian (i.e. Central American) seaway, and hence the deep-water connection between the Pacific and Atlantic Oceans started to shoal during the early to mid Miocene [*Newkirk and Martin*, 2009]. Final closure did not occur until the late Miocene [*Campbell Jr et al.*, 2010], as recorded by the Great American (Faunal) Interchange, but a deep-water closure could affect ocean circulation patterns in both the Pacific and Atlantic [*Newkirk and Martin*, 2009; *Omta and Dijkstra*, 2003], pole-to-equator heat transport, the hydrological cycle and North Atlantic deep water formation due to salinisation of the Atlantic ocean [*Broecker*, 2002]. It is likely that the on-going closure of the Tethys and Panamanian seaways, the widening of the Atlantic ocean and the amplification of the Atlantic overturning circulation, the gulf stream etc. affected regional and global climate during the Oligocene and Miocene and perhaps even contributed to the global change associated with the OMT [*Edinger and Risk*, 1994; *Von der Heydt and Dijkstra*, 2005; *Von der Heydt and Dijkstra*, 2006]. The Drake Passage and Tasmanian Gateway were already open to such an extent during the late Eocene, that a circum-Antarctic current had been established [*Bijl et al.*, 2013; *Scher and Martin*, 2006].

1.2.2 Astronomical Climate Forcing

Milankovitch [1941], building on work of (amongst others) Adhémar and Croll, proposed that the recurrent Pleistocene 'ice-ages' on the Northern Hemisphere were related to cyclic changes in the distribution of insolation across the Earth over 10^4 – 10^5 years. The first 'tuning' to Milankovitch's 65°N insolation 'target-curve' was by *Köppen and Wegener* [1924], who aligned maximum extent of glaciers in the Swiss Alps to calculated NH summer insolation minima. Conclusive proof for an astronomical 'pacemaker of the ice-ages' had to wait until deep-sea drilling techniques (such as piston coring) had improved and Pleistocene high-resolution benthic stable oxygen isotope records were generated [*Hays et al.*, 1976]. The precession and obliquity cycles (approx. 20-kyr and 40-kyr respectively) determine the distribution of insolation throughout the year and across the globe. The eccentricity cycle modulates the amplitude of the precession cycle and thereby it constitutes the third astronomical variable to which system Earth

can synchronise, however only through (quadratic) nonlinear response mechanisms to precession [*King*, 1996]. Strictly speaking the Milankovitch Theory only applies to the (NH) ice age cycles of the late Pleistocene. A generalised theory of 'astronomical climate forcing' is now widely accepted in the field of palaeoclimatology and applied in studies of Icehouse (e.g. [*Hays et al.*, 1976; *Holbourn et al.*, 2007; *Pälike et al.*, 2006b]), Greenhouse (e.g. [*Lourens et al.*, 2005]) and Greenhouse-Icehouse transitional (e.g. [*Coxall et al.*, 2005]) intervals of Earth history. The latest astronomical (eccentricity) solutions La2010 [*Laskar et al.*, 2011a] and La2011 are stable back to 50 – 55 Ma [*Westerhold et al.*, 2012], but will most likely not be constrained much further (back into the Palaeocene and Cretaceous) in the foreseeable future because of the chaotic behaviour introduced in the numeral solutions related to the uncertainty in the initial conditions of the proto-planet Ceres, asteroid Vesta and other asteroids [*Laskar et al.*, 2011b].

1.2.3 Stable vs Dynamic Antarctic Ice Sheet

An outstanding problem in the palaeoclimate community is how to reconcile output from coupled climate-ice sheet models, which predict a very stable EAIS once formed [*DeConto and Pollard*, 2003a; b; *Pollard and DeConto*, 2005], with proximal and distal proxy data that indicate considerable variability of the WAIS and EAIS over the past 34 Ma [*Bohaty et al.*, 2012; *Lear et al.*, 2000; *Lisiecki and Lisiecki*, 2002; *Mawbey and Lear*, 2013]. The question is to what extent were the EAIS and WAIS dynamic since the EOT? Most proxy data provide indirect evidence of glacial activity, for example large amplitude variability in benthic $\delta^{18}O$ records suggestive of an (SH) ice sheet contribution to the signal [*Zachos et al.*, 1997]. However, recently compelling evidence has been published showing that at least during the Pliocene the EAIS significantly retreated inland during interglacials [*Cook et al.*, 2013; *Patterson et al.*, 2014]. The extent of ice sheet variability during the Oligocene and Miocene is still a matter of debate.

The first relatively low-resolution (~100 – ~200 kyr) Oligocene and Miocene benthic $\delta^{18}O$ records showed variability of ~1‰ [*Miller et al.*, 1989; *Miller et al.*, 1991; *Woodruff and Savin*, 1989; *Wright and Miller*, 1992]. The largest 'glaciations' were linked to obliquity nodes that resulted in reduced seasonal extremes, with near-average values for obliquity. These nodes are spaced ~1.2-Myr apart and the associated glaciations have been given a Mi (for Miocene glaciations) or Oi (for Oligocene glaciations) preposition. More recent high-resolution benthic chronologies indicate that indeed a multi-Myr spacing between episodes of glaciations is present,

however the largest variability now appears to be associated with astronomical cycles on 40 - ~100-kyr timescales [*Pälike et al.*, 2006b; *Zachos et al.*, 1997; *Zachos et al.*, 2001a], making the traditional Mi and Oi zonations obsolete, apart from perhaps the largest events (Mi-1 and Oi-1).

The true nature of glacial dynamics during the Oligo-Miocene is difficult to test using benthic $\delta^{18}O$ because of the combined influence of temperature and ice volume on this globally integrated proxy. However when benthic $\delta^{18}O$ records are considered together with other, independent deep-water temperature and/or ice volume proxy data, or in combination with (inverse) modelling output, a better understanding of both temperature and ice sheet variability (on astronomical time scales) can be obtained. At present few high-resolution Oligo-Miocene records are available and those available show dominant variability on either 40 or ~100-kyr periods. Outstanding questions therefore remain: If the (Antarctic) ice sheets were dynamic, then on what (astronomical) periodicities? The need for more, and higher resolution records is therefore still current, despite the limitations of deep-sea geologic archives.

1.3 Thesis Outline

In this thesis newly generated high-resolution Oligo-Miocene climate proxy records from Walvis Ridge ODP Site 1264 (south-eastern Atlantic Ocean) are presented (Chapters 2 and 3). The records are tuned to an eccentricity solution (Chapter 3) and they are compared to published Atlantic and Pacific palaeoclimate chronologies (Chapters 2 and 4). The main research objectives are 1) to identify astronomical pacemakers of global significance and test earlier pacing theories, 2) to describe global climate and oceanographic change on astronomical and tectonic time scales and 3) to test the strong hysteresis in ice sheet models that suggest a very stable Antarctic ice sheet once formed.

Chapter 1 gives a general introduction on the "mid"-to-late Oligocene climatic, oceanographic, geographic and cryospheric settings. Climate evolution and dynamics, together with the major underlying processes are introduced.

In Chapter 2, high-resolution early Miocene stable oxygen and carbon isotope chronologies from Walvis Ridge Site 1264 are presented. The data are analysed on an untuned age model to identify the principal astronomical pacemakers, without introducing power on orbital frequencies. A

dominance of variance in all datasets on 100-kyr timescales is found. The δ18O data are used to parameterize a suite of 1D ice sheet models and show that between 20 – 80% (avg. ~50%) of the $\delta^{18}O$ signal can be explained by changes in Antarctic ice volume. (This chapter has been published as: *D. Liebrand, L. J. Lourens, D. A. Hodell, B. de Boer, R. S. W. van de Wal and H. Pälike*. Antarctic ice sheet and oceanographic response to eccentricity forcing during the early Miocene. *Climate of the Past*, 7, 869–880, 2011)

In Chapter 3, extended stable-isotope records together with X-ray fluorescence core scanning data from Walvis Ridge Site 1264 are presented. The records span an 11-Myr mid Oligocene through early Miocene time interval. Ages are calibrated to eccentricity, are in good agreement with the GTS2012 and independently confirm the Oligo-Miocene time scale to the ~100-kyr level. The ~2.4-Myr long-period eccentricity cycle is identified as the main pacemaker of Oligo-Miocene climate events, as identified in the benthic isotope records, at shorter astronomical (eccentricity) periodicities.

In Chapter 4, the high-resolution Oligo-Miocene benthic stable-isotope chronology from Site 1264 is compared to published records from the Atlantic and Pacific to further identify and explore possible global climate pacemakers. In addition, an investigation of long-term trends and inter-/intra-basin isotopic gradients and their implications for ice volume reconstruction and palaeoceanographic studies are discussed. Methods are explored to quantify the apparent change in geometry of ~100-kyr cycles in our benthic $\delta^{18}O$ data and the analyses indicate an increased cycle asymmetry (i.e. sawtooth patterns) throughout the Oligo-Miocene. This change in cycle geometry is interpreted as a measure of changing boundary conditions and used to track the evolution of a threshold response mechanism in Earth's climate system.

In Chapter 5 the main results of this thesis are summarised, the implications for our understanding of the Oligo-Miocene are discussed and perspectives are given on future work.

CHAPTER 2:

ANTARCTIC ICE SHEET AND OCEANOGRAPHIC RESPONSE TO ECCENTRICITY FORCING DURING THE EARLY MIOCENE

This chapter has been published as: *D. Liebrand, L. J. Lourens, D. A. Hodell, B. de Boer, R. S. W. van de Wal and H. Pälike*, under the same title, in *Climate of the Past*, 7, 869–880, 2011.

2.1 Abstract

Here we present stable-isotope records of benthic foraminifera from ODP Site 1264 in the south-eastern Atlantic Ocean, which resolve the latest Oligocene to early Miocene (~24–19 Ma) climate changes at high temporal resolution (<3 kyr). Using an inverse modelling technique, we decompose the oxygen isotope record into temperature and ice volume and find that the Antarctic ice sheet recurrently expanded during the declining phase of the long-term (~405-kyr) eccentricity cycle and subsequent low short-term (~100-kyr) eccentricity cycle. The largest glaciations are separated by multiple long-term eccentricity cycles, indicating the involvement of a non-linear response mechanism that probably resulted from 'initial' athmospheric CO_2 levels, or Antarctic ice sheet configuration, prior to the glacial expansions. Our 1D-modelling results suggest that during the largest (Mi-1) event, the combined East and West Antarctic ice sheets reached up to its present-day volume. In addition, we find that distinct ~100-kyr variability occurs during the termination phases of the major Antarctic glaciations, suggesting that climate and ice-sheet response was more susceptible to short-term eccentricity forcing at these times. During two of these termination-phases, $\delta^{18}O$ bottom water gradients in the Atlantic decreased, indicating a direct link between global climate, enhanced ice-sheet instability and major oceanographic reorganisations.

2.2 Introduction

Earth's climate has gradually cooled during the past 50 million years in conjunction with declining atmospheric pCO_2 conditions [*Pagani et al.*, 2005; *Zachos et al.*, 2008]. Following the cooling and rapid expansion of Antarctic continental ice-sheets in the earliest Oligocene, deep-sea oxygen isotope ($\delta^{18}O$) values remained relatively heavy (2.5 ‰), indicating permanent ice cover

with a mass as large as 50% of that of the present-day and bottom-water temperatures of ~4 °C [*Lear et al.*, 2004]. The Antarctic ice sheets reduced in size during the course of the Oligocene and early Miocene except during several brief periods of glaciation. One such glaciation is the Mi-1 episode/zone [*Miller et al.*, 1991], which encompasses the Oligocene-Miocene transition. Initially, only two Oligocene and six Miocene oxygen isotope zones (Oi-1, Oi-2, Mi-1 – Mi-6) were described [*Miller et al.*, 1991]. Several smaller glaciations were later identified in isotope records spanning the latest Oligocene and early Miocene and were labelled Mi-1a, Mi-1b, Mi-7, Mi-1aa [*Wright and Miller*, 1992], Oi-2b.1, Mi-1.1 [*Billups et al.*, 2002] and one still unnamed zone [*Paul et al.*, 2000]. It has long been suspected that the large-scale changes in Antarctic ice volume are coupled to long-term eccentricity (2.0–2.6 Myr) and obliquity (~1.2 Myr) modulations of the Earth's orbit and axial tilt [*Beaufort*, 1994; *Lourens and Hilgen*, 1997; *Miller et al.*, 1991; *Wright and Miller*, 1992]. But, this theory could only recently be tested through the generation of high-resolution (≤10 kyr) oxygen isotope records [*Billups et al.*, 2002; *Pälike et al.*, 2006a; *Pälike et al.*, 2006b; *Wade and Pälike*, 2004; *Zachos et al.*, 2001a].

In 2003, the Ocean Drilling Program (ODP) revisited Walvis Ridge (29° S) in the south-eastern Atlantic Ocean during Leg 208 [*Zachos et al.*, 2004]. Six sites were drilled along a depth-transect of which two sites, Site 1264 (2505 m) and Site 1265 (3083 m), are used in this study to assess the long-term orbital pacing theory of the early Miocene time interval. Both sites are situated above the level of the present day lysocline and CCD (4.0 and 4.5 km respectively, Fig. 2.01). This offers the unique opportunity to record major changes in regional and/or global ocean carbon chemistry, ocean circulation and intermediate bottom water chemistry and circulation during key palaeoceanographic events [*Zachos et al.*, 2004]. Site 1264 was drilled as the shallow water depth end-member of the Walvis Ridge transect and is characterized by an expanded Oligocene and Neogene sediment sequence [*Zachos et al.*, 2004]. From this site, we have generated a high-resolution (<3 kyr) and continuous stable-isotope record of the benthic foraminiferal species *Cibicidoides mundulus* between ~24–19 Ma. In this paper, we will compare our new isotope results with those of ODP Site 926 Hole B (3° N) at 3598m water depth and ODP Site 929 Hole A (6° N) at 4358m water depth, both from Ceara Rise in the Equatorial Western Atlantic [*Flower et al.*, 1997b; *Pälike et al.*, 2006a; *Paul et al.*, 2000; *Shackleton et al.*, 2000; *Zachos et al.*, 1997; *Zachos et al.*, 2001a], and the composite record of ODP Site 1090, based on Holes D and E, at 3699m water depth from the Agulhas Ridge (43° S) in the Atlantic sector of the Southern Ocean [*Billups et al.*, 2002; *Billups et al.*, 2004]. In addition, we decompose the marine benthic $\delta^{18}O$ record into temperature and ice volume contributions through an inverse modelling technique

[*Bintanja and Van de Wal*, 2008; *De Boer et al.*, 2010], to shed new light upon the orbital pacing theory of the Antarctic ice sheets during the Oligocene/Miocene transition.

2.3 Analytical Methods

Samples of approximately 10 g of sediment were taken every 2–2.5 cm from the uppermost Oligocene and lower Miocene section of the Site 1264. The samples were freeze dried, washed (in tap water), sieved to obtain the larger than 37, 65 and 150 μm fractions for foraminiferal accumulation rates (not presented in this study) and foraminiferal analysis, and dried in evaporation basins. Primarily single specimen samples of the benthic foraminifer species *Cibicidoides mundulus* were picked from the >150 μm fraction and subsequently analysed. For every sample, stable oxygen and carbon isotope ratios ($\delta^{18}O$ and $\delta^{13}C$, respectively) were measured and the $\delta^{18}O$ values were corrected for disequilibrium fractionation with seawater by adding 0.64‰ [*Shackleton*, 1974; *Zachos et al.*, 2001b].

Approximately 80% of the samples were measured at the Faculty of Geosciences of Utrecht University (UU) where (uncleaned) foraminiferal tests were dissolved in a Finnigan MAT Kiel III automated preparation system. Isotopic ratios of purified CO_2 gas were then measured on-line with a Finnigan MAT 253 mass spectrometer and compared to an internal gas standard. The remaining set of samples was measured at the Department of Geological Sciences of the University of Florida (UF) on two inter-calibrated devices. Of the samples with sufficient specimens, subsamples of crushed, washed (in hydrogen peroxide) and ultra-sonically cleaned (in methanol) foraminiferal calcite from several tests (3–6 on average) was reacted using a common acid bath of orthophosphoric acid at 90 °C using a Micromass Isocarb preparation system. Isotope ratios of purified CO_2 gas were measured online using a Micromass Prism mass spectrometer. Of the samples with few *Cibicidoides mundulus* specimens, whole, washed (in hydrogen peroxide) and ultra-sonically cleaned (in methanol) foraminiferal test(s) (1–2 specimen) were dissolved using a Finnigan MAT Kiel III automated preparation system coupled to a Finnigan MAT 252 mass spectrometer to measure the isotopic ratios of purified CO_2 gas. The standard NBS-19 and the in-house (at UU) standard "Naxos" were used to calibrate to Vienna Pee Dee Belemnite (VPDB). Reproducibility (same sample on the same device) is 0.19‰ for $\delta^{18}O$ and 0.13‰ for $\delta^{13}C$ (Supplement Fig. 2.01).

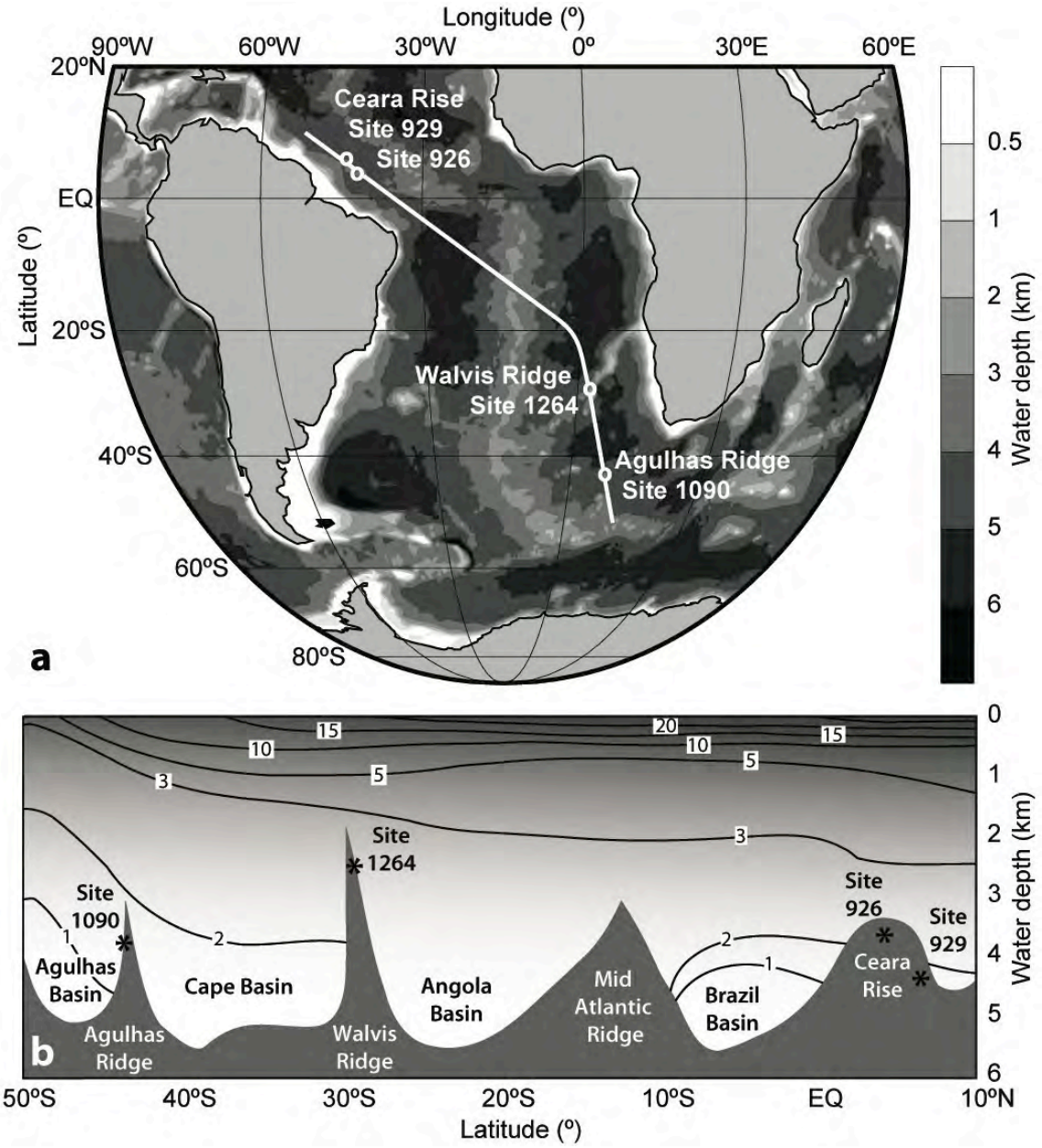

Figure 2.01: *Site locations and Atlantic Ocean transect. (a) Present day map of the drill locations of ODP Sites 929, 926, 1264 and 1090. The white line through the drill locations represents the approximate transect shown in panel (b). (b) Transect through the current Equatorial and Southern Atlantic Ocean. Black stars represent drill locations. Black lines represent present-day water temperatures. Both graphs were constructed using Ocean Data View [Schlitzer, 2010] and were then graphically edited.*

An average offset of ~0.30‰ in $\delta^{18}O$ is found between the analyses of foraminifera from the same samples by the two labs (Supplement Fig. 2.01). No correction has been applied for this offset because a lower resolution record (step size ~100-kyr), spanning the interval of this study and measured entirely at UF, shows no offset with the UU measurements [*Naafs*, 2011]. Furthermore, the relatively small set of samples used to compare the isotope signatures between laboratories might not be representative. Twenty outliers were defined by an upper and lower boundary of 2 standard deviations (of the entire time series) added or subtracted from a 13-point moving average. Because the stable-isotope analysis is paired, outliers defined in $\delta^{13}C$ or in $\delta^{18}O$ were removed from both records (Supplement Fig. 2.02). Where possible, outliers were re-measured. After outlier-removal, the $\delta^{18}O$ and $\delta^{13}O$ records of Site 1264 each contain 1754 data points.

2.4 Age Model

Because Site 1264 lacks a good magnetostratigraphy, we transposed the magnetostratigraphic data [*Bowles*, 2006] from the nearby ODP Site 1265 by correlating the magnetic susceptibility (MS) and colour reflectance (CR, 600/450 nm) records (Fig. 2.02, Table 2.01). Subsequently, we assigned the Astronomically Tuned Neogene Time Scale 2004 (ATNTS2004) ages of *Lourens et al*., [2004] to the magnetic reversals and applied a third order polynomial to inter- and extrapolate the age model. This provided an orbital-based age model without tuning individual peaks to the astronomical solution. We chose to present our data on this un-tuned, but loosely astronomy-based, timescale to re-examine previous interpretations about the Oligocene and Miocene climate dynamics. Finally, the "Match" algorithm [*Lisiecki and Lisiecki*, 2002] was applied to correlate the stable-isotope records of Ceara Rise and the Agulhas Ridge to Site 1264.

2.5 Stable-isotope Results

The $\delta^{18}O$ record of Site 1264 closely matches that of the Agulhas Ridge Site 1090 (Figs. 2.03 and 2.4). However, both records, from Site 1264 and Site 1090, are ~0.5‰ heavier than the $\delta^{18}O$ records of Sites 926 and 929. These distinct $\delta^{18}O$ (and $\delta^{13}C$) gradients between sites decreased, however, during two "events" at ~22.9 Ma and ~21.2 Ma, which are marked by low $\Delta\delta^{18}O$ values

(see arrows in Fig. 2.04). The $\delta^{18}O$ values at Site 929 increased significantly during these events [*Flower et al.*, 1997b; *Zachos et al.*, 1997; *Zachos et al.*, 2001a]. Changes in wind-driven [*Cramer et al.*, 2009], thermal and/or haline ocean circulation and in ocean gateway configurations [*Von der Heydt and Dijkstra*, 2006] have been proposed to explain changing inter- and intra-basinal isotope gradients. We interpret these events with low $\Delta\delta^{18}O$ values as periods where at the Ceara Rise abyss, an Antarctic sourced bottom-water mass was present [*Billups et al.*, 2002; *Woodruff and Savin*, 1989] and hence as periods in which the oceanographic mechanism that kept the prevailing gradients in place, was briefly (<405 kyr) disrupted. The ~0.4‰ difference in the average $\delta^{18}O$ values before and after the O/M transition at Ceara Rise [*Zachos et al.*, 2001a] is not recorded at Site 1264, suggesting that a possible flow reversal through the Panamanian Seaway [*Von der Heydt and Dijkstra*, 2005] or changes in abyssal circulation patterns in the Atlantic [*Miller and Fairbanks*, 1983] did not significantly alter the $\delta^{18}O$ composition of the water mass at Site 1264.

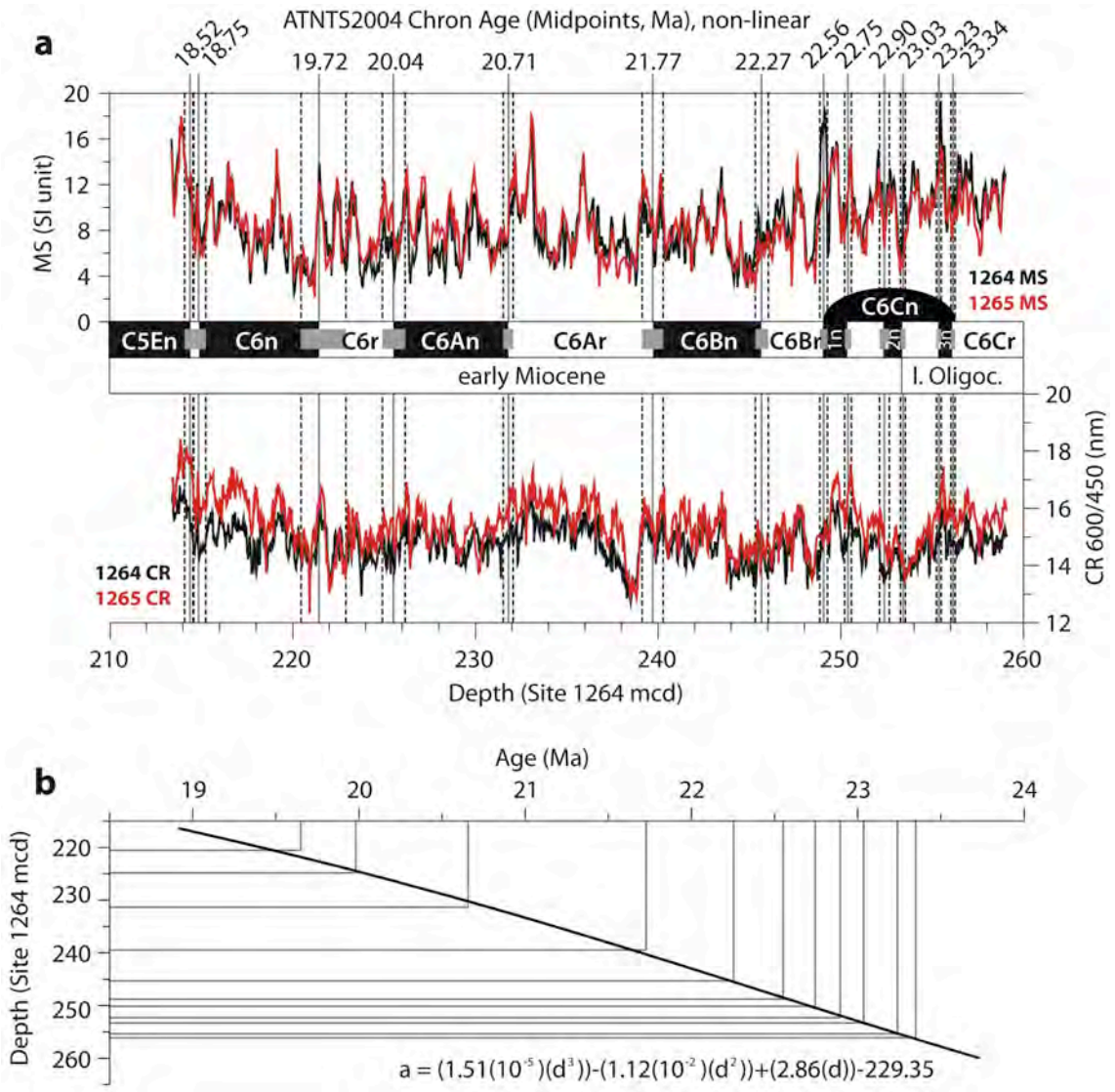

Figure 2.02: *Near-linear depth-age relation Site 1264.* ***(a)*** *Transfer of the magnetostratigraphy [Bowles, 2006] from Site 1265 to Site 1264 by means of magnetic susceptibility (MS) and 600/450 nm colour reflectance (CR) pattern matching. Depth scale is in meters composite depth (mcd). Please note: by transferring the magnetostratigraphic mid-points from Site 1265 mcd to Site 1264 mcd, they may not look like "mid-points" on Site 1264 mcd. Grey bars indicate uncertainties in the chron boundary positions.* ***(b)*** *3rd order polynomial fit of depth "d" through ATNTS2004 [Lourens et al., 2004] chron ages "a".*

Chron	Site 1265 Mid-point depth (mcd)[a]	Site 1264 Mid-point depth (mcd)[b]	ATNTS-2004 age (Ma)[c]	3rd order polynomial age (Ma)[d]
C5En (*o*)	89.745	214.408	18.524	18.564
C6n (*y*)	90.395	214.878	18.748	18.644
C6n (*o*)	97.095	221.450	19.722	19.592
C6An (*y*)	100.420	225.520	20.040	20.102
C6An (*o*)	105.595	231.792	20.709	20.826
C6Bn (*y*)	112.720	239.685	21.767	21.662
C6Bn (*o*)	118.595	245.615	22.268	22.261
C6Cn.1n (*y*)	121.500	248.937	22.564	22.593
C6Cn.1n (*o*)	122.390	250.333	22.754	22.733
C6Cn.2n (*y*)	124.110	252.323	22.902	22.934
C6Cn.2n (*o*)	124.815	253.342	23.030	23.037
C6Cn.3n (*y*)	126.145	255.298	23.230	23.237
C6Cn.3n (*o*)	126.740	256.070	23.340	23.317

Table 2.01: *Chron ages.*

a Midpoints between the top and bottom uncertainties in magnetic reversals (Bowles, 2006). Depth scale is in meters composite depth (mcd).

b Based on calibration shown in Fig. 2.02.

c Astronomically Tuned Neogene Time Scale [Lourens et al., 2004].

d 3rd order polynomial based on the ATNTS2004 [Lourens et al., 2004] graphed in Fig. 2.02.

The benthic $\delta^{13}C$ record of Site 1264 is on average 0.1 to 0.4‰ heavier than those of Sites 1090, 926 and 929, indicating that Site 1264 was bathed in relatively nutrient-depleted intermediate water masses due to its shallower position (Figs. 2.01, 2.03, 2.04). The highest $\delta^{13}C$ value of almost 2.0‰ coincides with the onset of the Oligocene-Miocene Carbon Maximum, CM-OM at ~23.2 Ma [*Hodell and Woodruff*, 1994], and corresponds [*Zachos et al.*, 1997] with the maximum $\delta^{18}O$ values during the O/M climate transition. The sudden decline in $\delta^{13}C$ values of ~0.4 ‰, marking the end of the CM-OM around ~21.8 Ma, coincides with a significant change in the deep-sea carbon reservoir within the entire Atlantic Ocean (Figs. 2.03, 2.04) [*Compton et al.*, 1990; *Compton et al.*, 1993; *Hodell and Woodruff*, 1994].

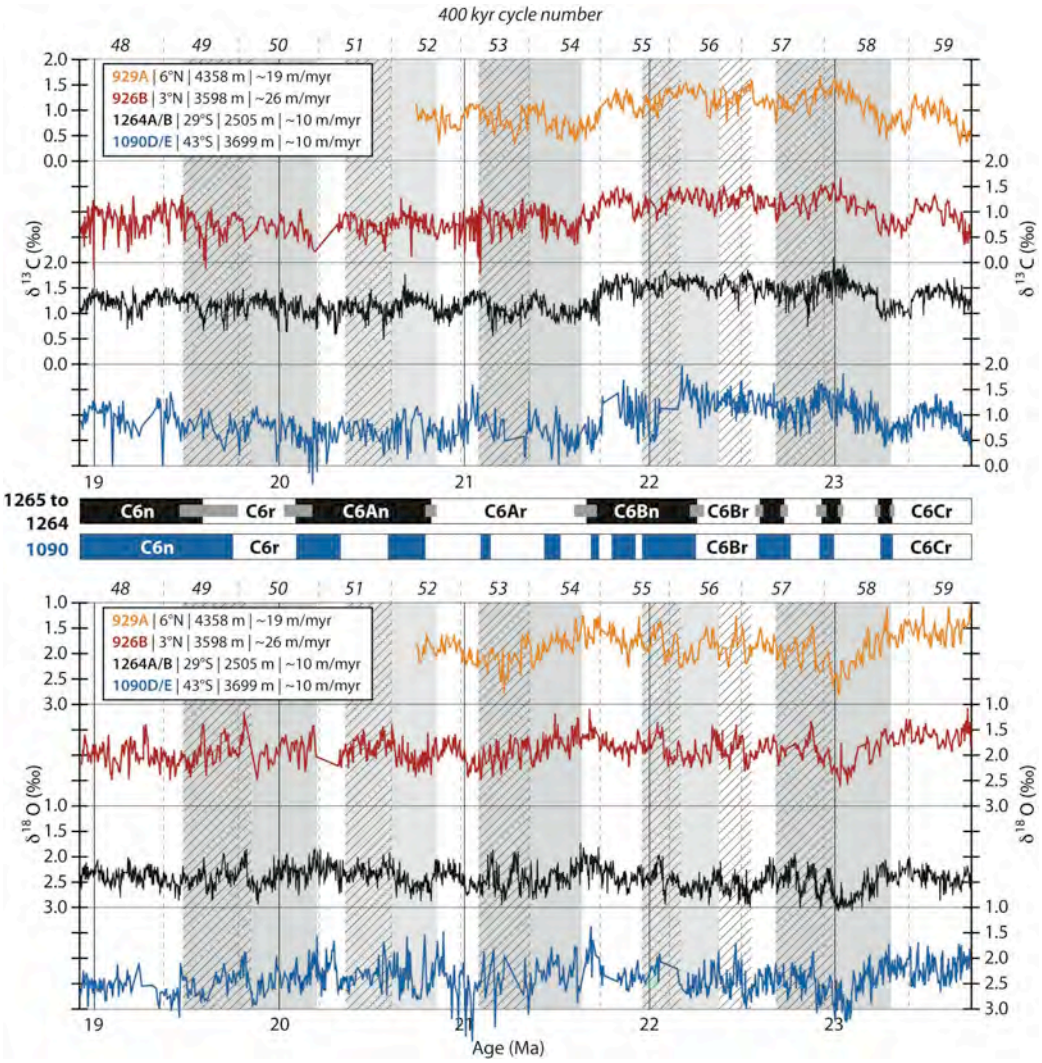

Figure 2.03: *Comparison of early Miocene stable-isotope records. High-resolution Atlantic $\delta^{13}C$ and $\delta^{18}O$ (+0.64‰) records of ODP Sites 929 (C. mundulus), 926 (C. mundulus and C. cresbi, uncorrected) [Flower et al., 1997b; Pälike et al., 2006a; Paul et al., 2000; Shackleton et al., 2000; Zachos et al., 1997; Zachos et al., 2001a], Site 1264 (this study) (C. mundulus) and Site 1090 (C. praemundulus, C. dickersoni, C. eocaenus, C. havanensis, C. mundulus, O. umbonatus, Ordisalis values corrected to combined Cibicidoides values) [Billups et al., 2002; Billups et al., 2004]. Records were matched to Site 1264 in the depth domain using the "Match" algorithm [Lisiecki and Lisiecki, 2002] and then plotted on the ATNTS-based age model of Site 1264. The Walvis Ridge magnetostratigraphy [Bowles, 2006] has been transposed from Site 1265 to Site 1264 (see Fig. 2.02). The vertical dashed lines mark the boundaries of the 405-kyr cycles [Wade and Pälike, 2004]. Latitude, present water depth and average sedimentation rates are given for each site.*

Power spectral analyses indicate the dominance of the long-term (405-kyr) eccentricity cycle in both the $\delta^{13}C$ and $\delta^{18}O$ records (Fig. 2.05). Additional smaller peaks are found at the short (95 and 125 kyr) eccentricity periods and to a lesser degree at the obliquity (41 kyr) period. No clear precession-related peaks are detected in the power spectra even though the resolution of the record (<3 kyr) is well above the Nyquist limit (~10 kyr) for this cycle. The weak imprint of obliquity at Site 1264 is remarkable, since Sites 926 and 929 revealed a dominant obliquity signal throughout this time interval [*Flower et al.*, 1997a; *Paul et al.*, 2000]. The stronger obliquity signal at the tropical deep-water Sites 929 and 926, and the weaker imprint recorded at the high(er) latitude intermediate to deep-water Sites 1264 and 1090 is still open for speculation about possible deep-water sources and teleconnections between the poles and the equator. The weak expression of precession and obliquity is a likely consequence of the relatively low sedimentation rates (~1 cm/kyr) at Site 1264.

Wavelet analysis confirms the dominance of the 405-kyr eccentricity-related variability in the $\delta^{13}C$ and $\delta^{18}O$ records throughout the time interval studied (Fig. 2.05, Supplement Fig. 2.03). The ~100-kyr eccentricity-related variations in $\delta^{18}O$ occur during four distinct and two less distinct periods. These periods are also reflected in the wavelet spectrum of $\delta^{13}C$, although the relative amplitude of the ~100-kyr dominated intervals differs slightly from that of the $\delta^{18}O$ record (Fig. 2.05). Sites 1090, 929 and 926 do not show these prominent ~100-kyr dominated intervals. Since these sites are situated approximately 1–1.5 km deeper than Site 1264, we consider that they were more vulnerable to carbonate dissolution through changes in the position of the CCD and lysocline. Carbonate dissolution and subsequent recrystallization could have preferentially distorted (i.e. amplified in this case) the imprint of the higher astronomical frequencies on the records of Sites 926, 929 and 1090. The higher sedimentation rates at Sites 926 and 929 could also have resulted in more variance being preserved at higher astronomical frequencies, compared to Site 1264, thereby attenuating the relative strength of the ~100-kyr periodicity.

*>> **Figure 2.04**: Comparison of early Miocene stable-isotope records. For more information see figure caption of Fig. 2.03. **(a)** The $\delta^{13}C$ records. **(b)** The $\delta^{18}O$ (+0.64 ‰) records. **(c)* As in panel (b). but without Site 1090. Grey areas in between the isotope records indicate the changes in Atlantic (intermediate) deep-water $\delta^{18}O$ gradients. **(d)** $\Delta\delta^{18}O$ of Sites 1264−929, 1264−926, and 1264−1090, to indicate the changes in Atlantic (intermediate) deep-water $\delta^{18}O$ gradients. Shaded*

lines represent the $\Delta\delta^{18}O$ of the 2 kyr resampled data sets. Resampling was done using a Gaussian-weighted moving average (15 kyr). Thick lines are the corresponding 100-kyr Gaussian-weighted moving averages. Arrows indicate the occurrences of reduced gradients between equatorial and southern Atlantic. These two events occur 4 × 405-kyr apart. ***(e)*** *As in panel (d) but now for 1090−929, 1090−926 and 926−929.*

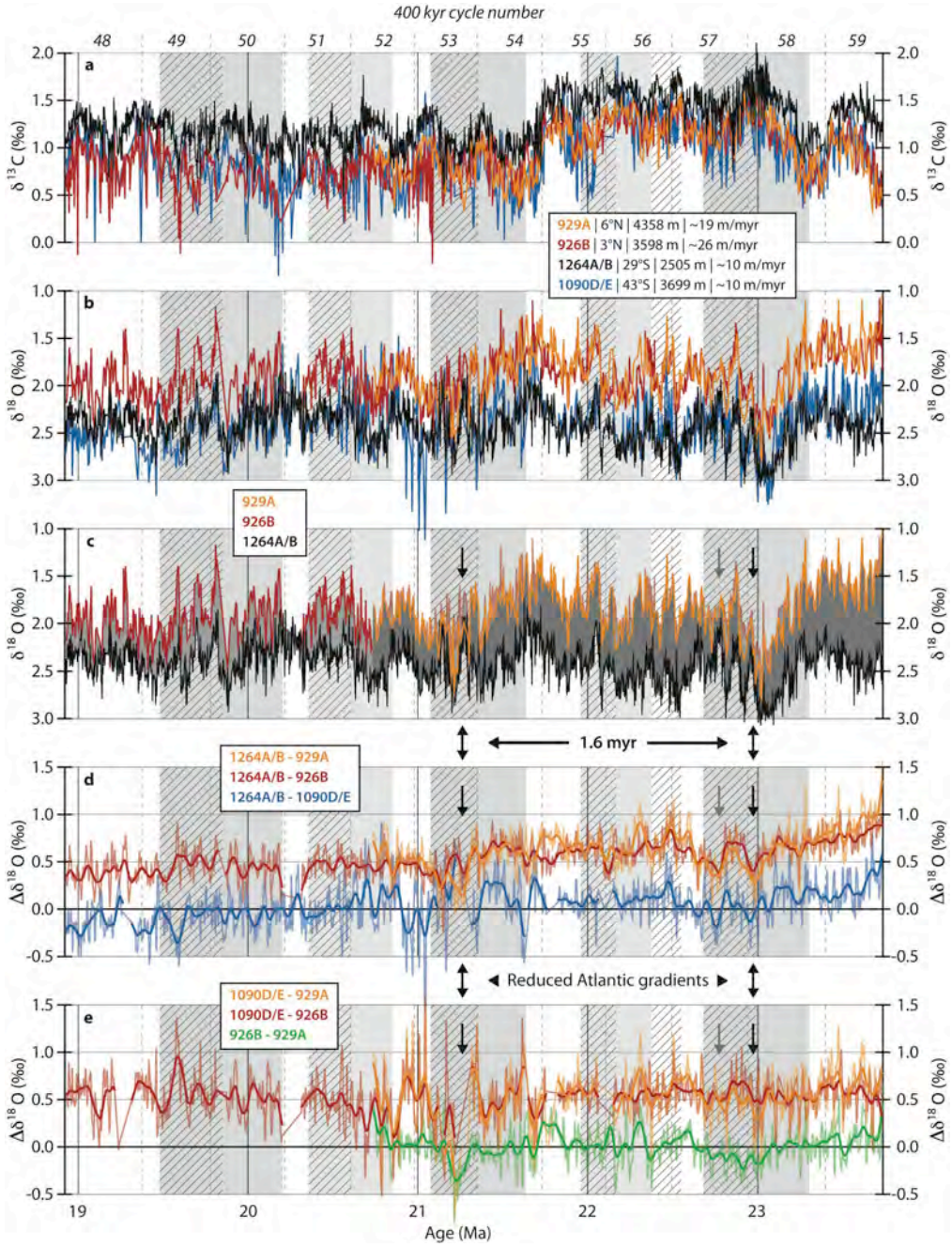

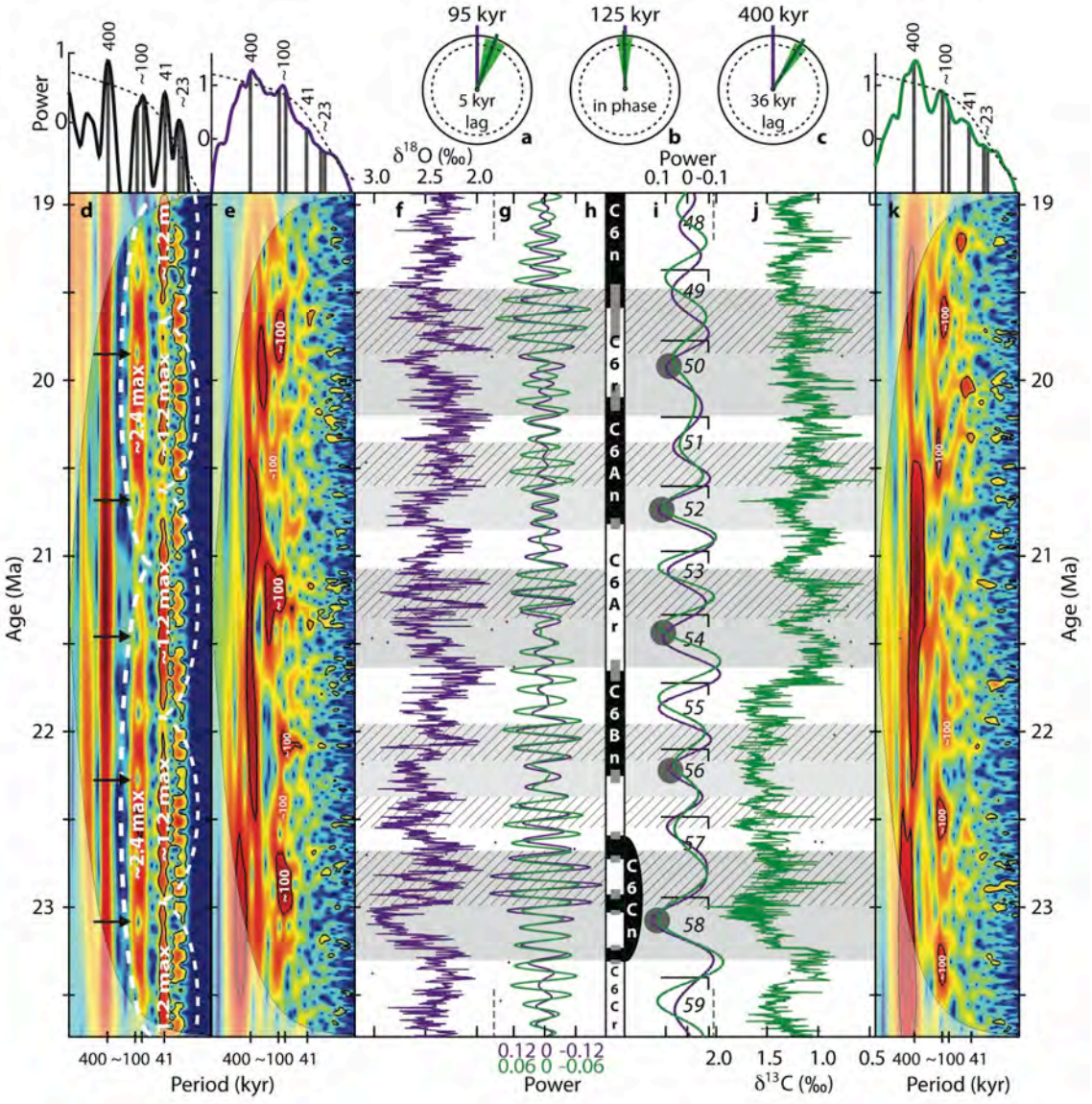
95 kyr
125 kyr
400 kyr
5 kyr lag
in phase
36 kyr lag
a
b
c
Power
400
~100
41
~23
δ18O (‰)
3.0 2.5 2.0
0.1 0 -0.1
d
e
f
g
h
i
j
k
C6n
C6r
C6An
C6Ar
C6Bn
C6Cn
C6Cr
48
49
50
51
52
53
54
55
56
57
58
59
~2.4 max
~1.2 max
Age (Ma)
19
20
21
22
23
Period (kyr)
0.12 0 -0.12
0.06 0 -0.06
Power
2.0 1.5 1.0 0.5
δ13C (‰)

*<< **Figure 2.05**: Walvis Ridge (Site 1264) stable-isotope records. Phase wheels represent the phase relation of $\delta^{13}C$ (green) relative to $\delta^{18}O$ at the **(a)** 95, **(b)** 125 and **(c)** 405-kyr eccentricity periods, where 360° represents one full cycle. Phase lags increase clockwise and the green areas represent the 95% confidence level. Vector length shows coherency (dashed circle 95 %). **(d)** Wavelet analysis [Grinsted et al., 2004] with >95% confidence levels (black lines) of an eccentricity/obliquity/precession mix calculated after the Laskar et al., [2004] astronomical solution. Time step size after re-sampling is 2.75 kyr. White dashed lines indicate the (on average) ~1.2 and ~2.4-Myr amplitude modulation of obliquity and eccentricity. Arrows indicate minima in 405-kyr eccentricity (characterized by a smaller amplitude 100-kyr cycle) that coincide with maximum ice-sheet expansion. These minima are timed 1 ×, 2 × or 4 × 405-kyr apart. The global spectrum with >95% confidence level [Torrence and Compo, 1998] is plotted at the top of each column. **(e)** Wavelet analysis and global spectrum – processed as in panel (d) – of $\delta^{18}O$ record after removal of >0.5 Myr periodicities using a notch filter [Paillard et al., 1996] (f : 0.0, bw: 2.0) and normalisation. **(f)** Benthic oxygen isotope ($\delta^{18}O$ + 0.64 ‰) record from Site 1264. Loose dots represent outliers. **(g)** Gaussian filters [Paillard et al., 1996] (~100-kyr, f : 10.0, bw: 2.0) of the $\delta^{18}O$ (purple) and $\delta^{13}C$ (green) records. **(h)** Transferred magnetostratigraphy [Bowles, 2006] from Site 1265 to Site 1264. Black is normal, white is reversed, gray is uncertain. **(i)** Gaussian filters [Paillard et al., 1996] (405-kyr, f : 2.5, bw: 1.0) of the $\delta^{18}O$ (purple) and $\delta^{13}C$ (green) records, with corresponding 405-kyr cycle numbers [Wade and Pälike, 2004]. Gray circles mark maxima of the ice-sheet expansion phases. **(j)** Benthic carbon isotope ($\delta^{13}C$) record from Site 1264. Loose dots represent outliers. **(k)** Wavelet analysis and global spectrum of $\delta^{13}C$ processed as in panel (d).*

2.6 Inverse Modelling

A set of 1-D ice sheet models for West and East Antarctica, Greenland, North America and Eurasia in combination with an inverse routine was applied to separate the $\delta^{18}O$ signal into a temperature (δ_T) and an ice volume (δ_w) component [*De Boer et al.*, 2012; *De Boer et al.*, 2010]. The model was initially designed to unravel ice-volume and temperature components from a global benthic $\delta^{18}O$ stack [*Bintanja et al.*, 2005; *De Boer et al.*, 2010], which is anchored in the present day (PD). Since we have applied this method to Site 1264 only, we assumed that the average $\delta^{18}O$ value approximates that of the global mean bottom-water for the early Miocene, notwithstanding a mean offset of 0.53‰ to heavier values (for which the $\delta^{18}O$ record of Site 1264 is corrected prior to the model calculations) with respect to the global stack of *Zachos et al*. [2008; 2001b]. All calculations are relative to a PD *Cibicidoides mundulus* $\delta^{18}O$ value of 3.23‰ in the global stack [*Zachos et al.*, 2008]. Previously performed sensitivity tests revealed that the error margin around absolute modelled values is of the order of 10%. For a thorough evaluation of the set of 1-D models utilized in this study we refer to *De Boer et al*. [2010].

The modelled δ_T record is assumed to represent a global value for deep-water temperature (ΔT_{dw}) relative to the present day, and was rescaled into continental mean annual Northern Hemisphere (40 – 80° N) air temperature (ΔT_{NH}) using a simple linear equation [*Bintanja et al.*, 2005]. The ice-volume component (δ_w) can be expressed in the amount of sea level change, which is equivalent to the amount of land-ice storage on Antarctica and the Northern Hemisphere (mainly Greenland). For the 405 and ~100-kyr oscillations we find within the uncertainty band of the cross spectral analyses, an in-phase relation between δ_T and δ_w, which implies that polar cooling and ice-sheet growth occurred (almost) simultaneously (Fig. 2.06). This phase relation is broadly in agreement with those calculated between Plio-Pleistocene deep-sea Mg/Ca temperature reconstructions and $\delta^{18}O_{benthic}$ ice volume estimates that show a small lead (~11 kyr) of temperature relative to ice volume [*Sosdian and Rosenthal*, 2009]. It is also in agreement with model reconstructions of the late Pleistocene ~100-kyr glacial-interglacial rhythm that showed similar in-phase behaviour for the terminations and a small lag of global ice volume to air temperature of ~6 kyr for the glacial inceptions [*Bintanja and Van de Wal*, 2008].

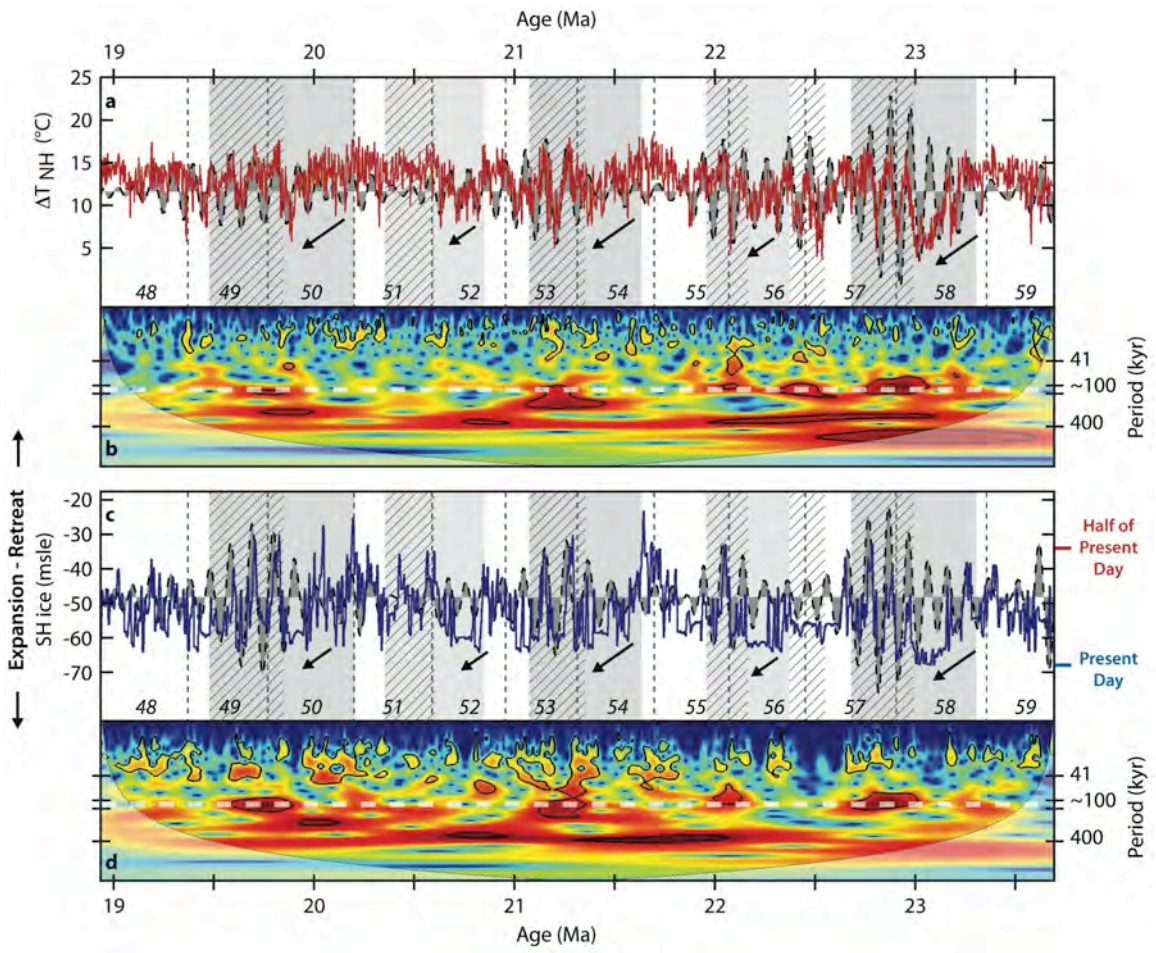

Figure 2.06: *1-D inverse modelling [De Boer et al., 2010] output.* ***(a)*** *Northern Hemisphere (40–80° latitude) annual average air temperature, with ~100-kyr filtered component (f : 10.0, bw: 2.0) [Paillard et al., 1996] depicted in the background.* ***(b)*** *Wavelet analysis [Grinsted et al., 2004] of NH temperature variability. Data processed as in Fig. 2.05.* ***(c)*** *Antarctic ice, with ~100-kyr filtered component (f : 10.0, bw: 2.0) [Paillard et al., 1996] depicted in the background.* ***(d)*** *Wavelet analysis [Grinsted et al., 2004] of Southern Hemisphere (Antarctic) ice variability (in meter sea level equivalent). Data processed as in Fig. 2.05. White dashed lines indicate the ~100-kyr period. Vertical dashed lines and numbers in italic represent the 405-kyr cycle numbers [Wade and Pälike, 2004].*

The outcome of our ice-sheet model simulations show that changes in $\delta^{18}O$ are accompanied by large shifts in ΔT_{NH} of up to 10 – 15 °C (Fig. 2.06, Supplement Fig. 2.04). The main sea level changes are linked to ice-sheet fluctuations on Antarctica. A change from half to full present-day Antarctic ice-sheet configuration is estimated for Mi-1 at 23 million years ago. At this time, the combined West and East Antarctic ice sheets had reached their maximum size of the time interval studied, resulting in a global sea level of ~2.5m above present-day, indicating that the Antarctic ice sheet had reached (almost) its present-day size. These findings are in agreement with estimated apparent sea level variations related to the East Antarctic ice sheet [*Pekar and DeConto*, 2006], which indicate changes of similar amplitude. However, they contrast with sea level estimates from Cape Roberts (Victoria Land basin, Antarctica), which show a relative sea-level lowstand across the OMT [*Naish et al.*, 2001], where (due to the gravitational pull of the large ice sheet) a highstand is expected for such a proximal site. Although there is a very small amount of Greenland ice volume modelled, this is probably not significant considering the uncertainty of the global mean $\delta^{18}O$ value during this interval [*De Boer et al.*, 2012].

Wavelet analyses of the sea level and temperature components of $\delta^{18}O$ revealed an almost similar pattern as the $\delta^{18}O$ record (Fig. 2.06). The episodes of ~100-kyr dominated $\delta^{18}O$ variability, and resultant ~100-kyr dominated ice volume and ΔT_{NH}, are preceded by an interval of gradual cooling and glacial build-up. In fact, the ~100-kyr dominated episodes coincide with the termination phase of periods of large Antarctic ice sheet expansion (Fig. 2.06). Following the astronomical naming scheme based on the 405-kyr cycle of Earth's eccentricity [*Wade and Pälike*, 2004], the oldest recorded Antarctic ice sheet expansion (Mi-1) starts within cycle 58 at ~23.4 Ma and ends within cycle 57 at ~22.6 Ma (Figs. 2.06, 2.07). Similar patterns are reflected by the ice-sheet expansion phases at 22.3 – 21.9 Ma (cycles 56 – 55), 21.6 – 21.1 Ma (cycles 54 – 53), and 20.2 – 19.4 Ma (cycles 50 – 49) of which the latter two periods are close within the age estimates of the Mi-1a and Mi-1aa episodes [*Wright and Miller*, 1992], respectively (Fig. 2.08).

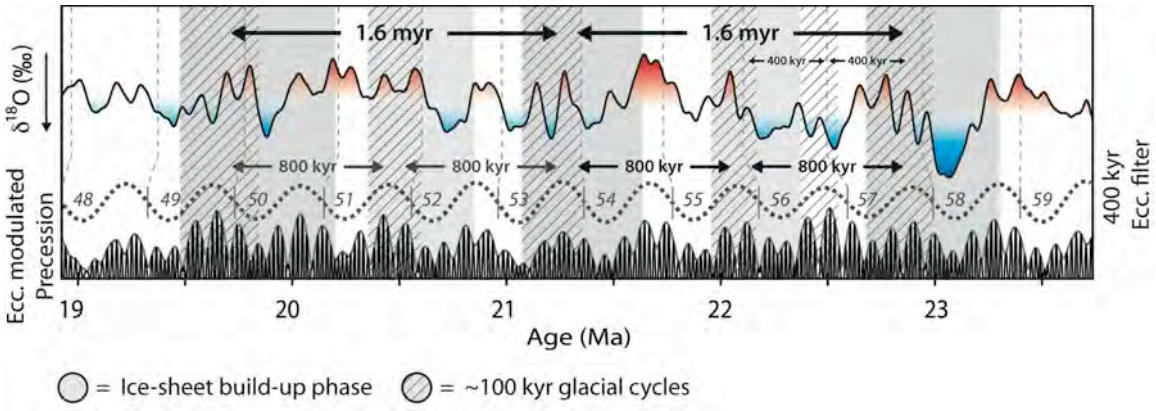

Figure 2.07: *Pacing of ~100-kyr dominated glacial cycles. At the top a Gaussian-weighted moving average (100-kyr) of Site 1264 $\delta^{18}O$ record is depicted. The bottom graphs represent eccentricity modulation precession, eccentricity [Laskar et al., 2004] and a 405-kyr filter (f : 2.5, bw: 1.0) of eccentricity. The 405-kyr numbers of Wade and Pälike, [2004] are shown on top of the 405-kyr eccentricity filter. Because the $\delta^{18}O$ record of Site 1264 is presented on an un-tuned age model, our 405-kyr cycle marking is tentative and no conclusions should be drawn based on the phase relation with eccentricity as depicted. For Figs. 2.03–2.08: grey areas indicate cooling periods with reduced ~100-kyr power, grey and striped areas indicate ~100-kyr "worlds", white areas are intermediate phases characterized by a greater non-linear response to eccentricity modulated precession. These ~100-kyr dominated episodes occur 1 ×, 2 × and 4 × 405-kyr apart from each other. The Oligocene – Miocene transition is one of four/five "similar" early Miocene episodes. It stands apart mainly by the duration of the glaciation phase. Almost comparable absolute high $\delta^{18}O$ values are reached during the other glacial episodes as well, but they are too short to be picked up by the moving average.*

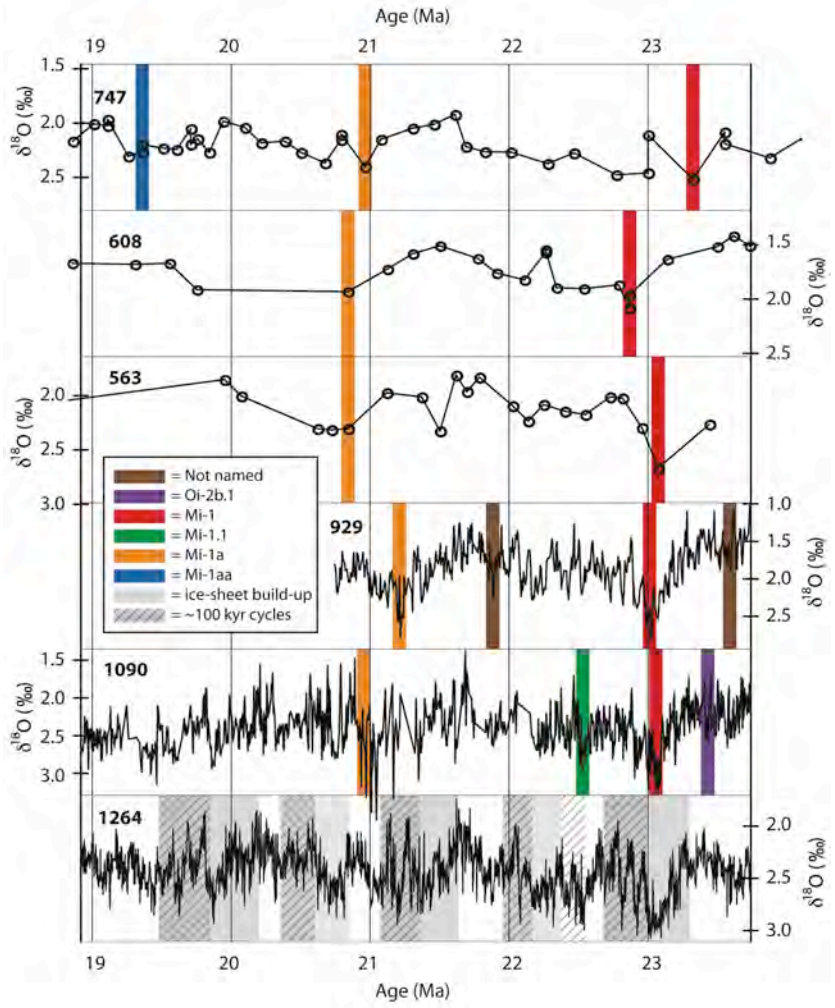

Figure 2.08: *Redevelopment of latest Oligocene and early Miocene Oi- and Mi-naming scheme across consecutive studies. Comparison between isotope records from the Kerguelen Plateau Site 747 and the North Atlantic Sites 563 and 608 [Wright and Miller, 1992; Wright et al., 1992] with Site 1264 (this study). Ages of Sites 563, 608 [Berggren et al., 1995] and magnetostratigraphy of Site 747 [Oslick et al., 1994] have been recalculated to the ATNTS2004 [Lourens et al., 2004]. Site 929 [Paul et al., 2000; Zachos et al., 1997; Zachos et al., 2001a] and Site 1090 [Billups et al., 2002; Billups et al., 2004] are plotted on the Walvis Ridge Site 1264 age model. The Oi- and Mi-zones or episodes were first described at Sites 563, 608 and 747. These names were then (sometimes erroneously) transposed to Sites 929 and 1090. The ~100-kyr dominated intervals described in this study shed new light on the major zones/episodes in the early Miocene and are close within the age estimates of the previously described Mi-1, Mi-1a and Mi-1aa zones or episodes. Nevertheless we support a 405-kyr number-based naming scheme [Wade and Pälike, 2004].*

2.7 Discussion

Cross-spectral analysis between the $\delta^{18}O$ and $\delta^{13}C$ records reveals that both records are highly coherent at the eccentricity periodicities with the $\delta^{13}C$ record slightly lagging $\delta^{18}O$ by 36 ± 8, 0 ± 3 and 5 ± 3 kyr for the 405, 125 and 95 kyr periods, respectively (Fig. 2.05). Similar results were found for the $\delta^{13}C$ and $\delta^{18}O$ records of Ceara Rise and the Pacific Site 1218 for the Oligocene time interval, indicating a strong coupling between climate states and changes in the oceanic carbon reservoir [*Holbourn et al.*, 2005; *Pälike et al.*, 2006b; *Paul et al.*, 2000; *Zachos et al.*, 1997; *Zachos et al.*, 2001a]. Since insolation changes operate predominantly on precession and obliquity time scales, a non-linear mechanism must be involved to transfer power from these high-frequency astronomical periods to the eccentricity band. Using simple box model experiments, *Pälike et al.*, [2006b] showed that the seasonal insolation cycle could drive changes in biosphere productivity and carbon burial on eccentricity time scales due to the long residence time of carbon in the ocean. During periods of increased carbon burial (e.g. high $\delta^{13}C$ values), atmospheric pCO_2 concentrations will drawdown, thereby setting the stage for global cooling and ice-sheet expansion. In turn, during glacial phases the meridional temperature gradient should be stronger, which may have led to enhanced upwelling intensities and carbon burial [*Zachos et al.*, 1997]. A lowering of the sea level may also have enhanced productivity conditions due to erosion of the continental shelves. Evidence for an increase in productivity during the Oligocene/Miocene transition was inferred from benthic foraminifer accumulation rates [*Diester-Haass et al.*, 2011]. These changes in marine primary productivity (as reflected by benthic $\delta^{13}C$) are found to be slightly lagging long- and short-term eccentricity and global climate (as reflected by benthic $\delta^{18}O$). Thus, insolation-forced changes in the carbon cycle may act as an important modulator for global climate change on eccentricity time scales during the early Miocene as was found for the Oligocene [*Pälike et al.*, 2006b].

The major large-scale Antarctic ice-sheet expansions coincide with 405-kyr eccentricity minima when the power of the ~100-kyr eccentricity cycle is significantly suppressed (e.g. at ~23.1, ~22.3, ~21.4, and ~19.8 Ma, black arrows in Fig. 2.05). Since these major ice-sheet expansions do not occur at every 405-kyr eccentricity minimum, one might expect that they are modulated by the long-term eccentricity and obliquity components [*Billups et al.*, 2002; *Lourens and Hilgen*, 1997; *Pälike et al.*, 2006a; *Pälike et al.*, 2006b; *Zachos et al.*, 2001a]. In particular, reduced amplitude of the tilt cycle over hundred thousands of years in combination with low eccentricity values may have favoured Antarctic ice sheet build-up due to on average low summer insolation

values [*Zachos et al.*, 2001a]. Except for Mi-1, the link between the long-term (~1.2-Myr) obliquity and the (~2.4-Myr) eccentricity modulation and the ice-sheet expansion phases are as yet too inconsistent to suggest a strong causal relationship between them (Fig. 2.05). This suggests that another non-linear mechanism is involved. An example of a non-linear mechanism could be that a threshold size for a stable Antarctic ice sheet had been passed, which triggered an episode with large-scale deglaciations every ~100-kyr. During these periods, the ice sheets were probably not adequately shaped [*DeConto and Pollard*, 2003a] to enter a new major growth episode at the next minimum of the 405-kyr cycle.

In summary, long-term tectonic or oceanographic processes may have preconditioned atmospheric pCO_2 levels through changes in the carbon cycle to set the stage for dominantly eccentricity-paced episodes of large Antarctic ice-sheet expansions during the late Oligocene and early Miocene. Such a hypothesis would be in line with modelling studies [*DeConto et al.*, 2008] and reconstructed atmospheric pCO_2 levels for this time interval [*Kürschner et al.*, 2008; *Pagani et al.*, 1999]. The termination phases of these episodes are characterized by enhanced climate variability on ~100-kyr (short eccentricity) time scales. During at least two of these termination-phases, bottom-to-intermediate water $\delta^{18}O$ gradients in the Atlantic were reduced, indicating a direct link between global climate, enhanced ice sheet instability and major oceanographic reorganisations. This succession of global changes could have triggered the major species turnover events as found on the continents during the early Miocene [*Van Dam et al.*, 2006].

2.8 Acknowledgements

We are indebted to Geert Ittman, Arnold van Dijk, Jan Drenth, Jason Curtis, Giana Brown, Walter Hale, Gert-Jan Reichart, and Klaudia Kuiper for their (technical) assistance. David Naafs, Martin Ziegler, Steven Bohaty, Clara Bolton, Lucy Stap, Tanja Kouwenhoven, Sietske Batenburg, Christian Zeeden, Helen Beddow-Twigg, Cristina Sghibartz, Sarah O'Dea, Rosanna Greenop, Frits Hilgen, Ellen Thomas, Dick Kroon, Paul Wilson, Gavin Foster and Eelco Rohling are thanked for discussing the science and/or commenting on an earlier version of this manuscript. We would like to thank the anonymous referee and Franck Bassinot for their insightful comments. Luc Beaufort is thanked for editing the published version of this manuscript. This research used samples provided by the Ocean Drilling Program, sponsored by the US National Science Foundation and participating countries under the management of Joint

Oceanographic Institutions (JOI), Inc. This study has been made possible by NWO VIDI-grant no. (864.02.007) and VICI-grant no. (865.10.001) assigned to L. J. L. and the European Community's Seventh Framework Programme (FP7/2007-2013) under grant agreement no. (215458) to the GTS-next project (D. L. and H. P.).

2.9 Supplementary Figures to Chapter 2

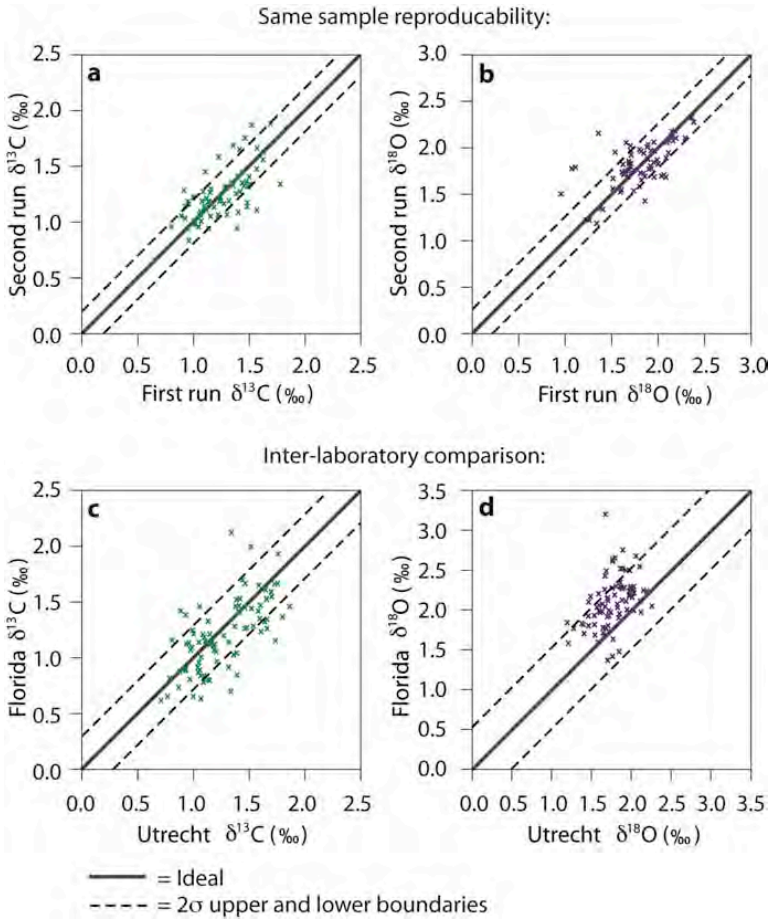

Supplementary Figure 2.09: *Data reproducibility of interlaboratory comparison. (a) Reproducibility between the first and second run $\delta^{13}C$ of the same samples (not necessarily the same foraminifer) on the three intercalibrated mass spectrometers. (b) As in panel (a), but then for $\delta^{18}O$. (c) Reproducibility of $\delta^{13}C$ between measurements done at the University of Florida (UF) and Utrecht University (UU), on specimens from the same sample. (d) As in panel (c), but then for $\delta^{18}O$.*

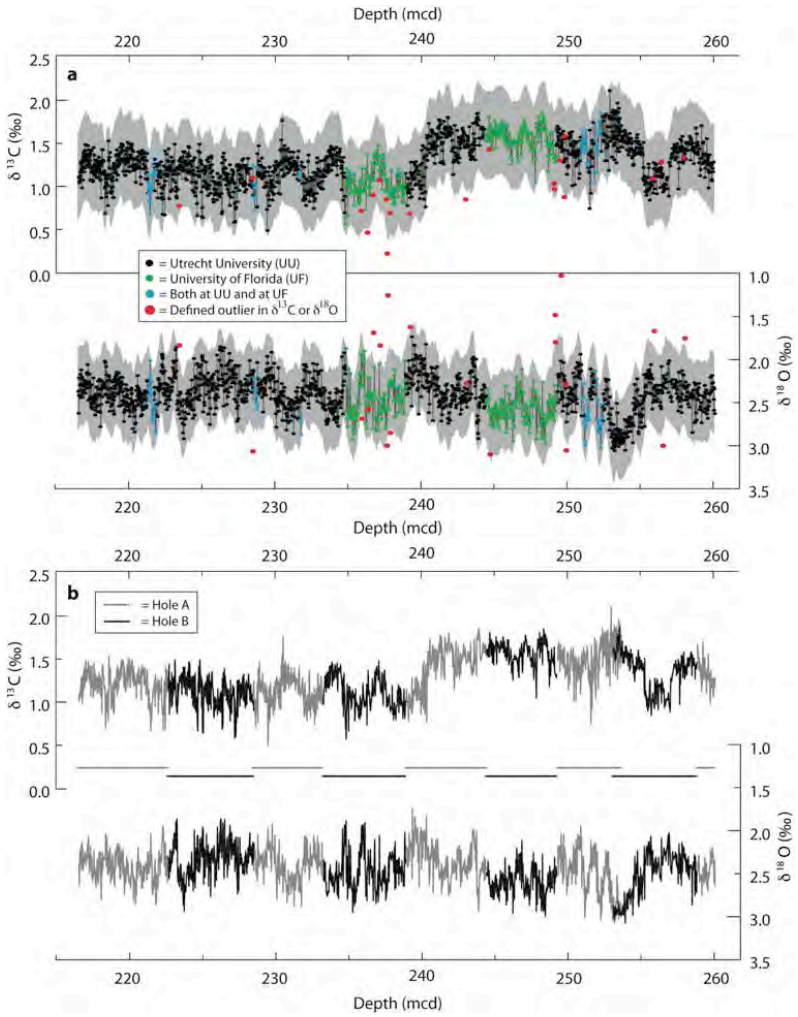

Supplementary Figure 2.10: *Outlier removal and the splice. (a) Specification in which lab each stable-isotope measurement has been done. Outliers were defined by an upper and lower boundary of 2 standard deviations (of the entire series) added or subtracted from a 13-point moving average (gray areas). Outliers defined in* $\delta^{13}C$ *or in* $\delta^{18}O$ *were removed from both records because of the paired analysis. Depth scale is in meters composite depth (mcd). (b) Splice of Site 1264, showing from which hole the samples were taken.*

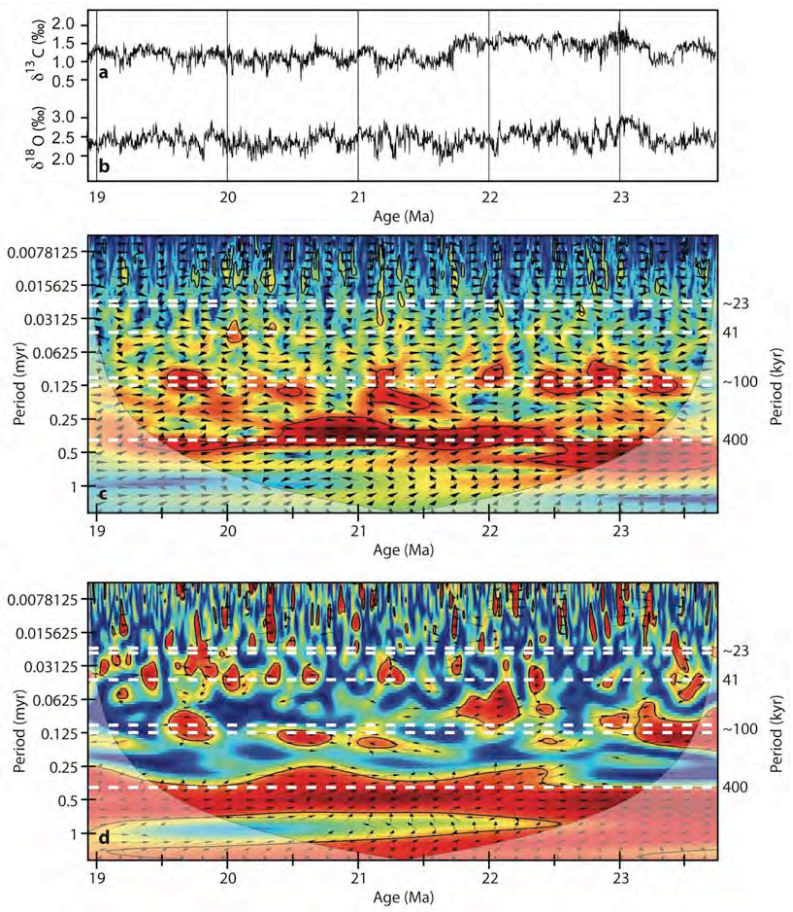

Supplementary Figure. 2.11*: Cross-wavelet transform and wavelet coherence. (a) $\delta^{13}C$ record from Site 1264 of the Walvis Ridge. (b) $\delta^{18}O$ record from Site 1264 of the Walvis Ridge. (c) Cross wavelet transform analysis between the $\delta^{18}O$ and $\delta^{13}C$ records indicating regions in time frequency space where the time series show high common power [Grinsted et al., 2004]. Phase arrows pointing right indicates that $\delta^{18}O$ and $\delta^{13}C$ are in-phase. Phase arrows pointing left indicates that $\delta^{18}O$ and $\delta^{13}C$ are in anti-phase. Phase arrows pointing up means that $\delta^{18}O$ is leading $\delta^{13}C$ by 90°. Phase arrows pointing down means that $\delta^{13}C$ is leading $\delta^{18}O$ by 90°. Black lines represent >95% significance levels. (d) Wavelet coherence analysis [Grinsted et al., 2004] between the $\delta^{18}O$ and $\delta^{13}C$ records indicating regions in time frequency space where the two time series co-vary. However, they do not necessarily have high power on these frequencies [Grinsted et al., 2004]. Phase arrows representation as in panel (a). Black lines represent > 95% Monte Carlo significance levels. Regions in the time frequency space where both records show much power (panel (c)) and where both records are coherent (panel (d)) represent the coupling between climate states and the changes in the oceanic carbon reservoir which has also been described at other Sites [Paul et al., 2000; Zachos et al., 1997; Zachos et al., 2001a].*

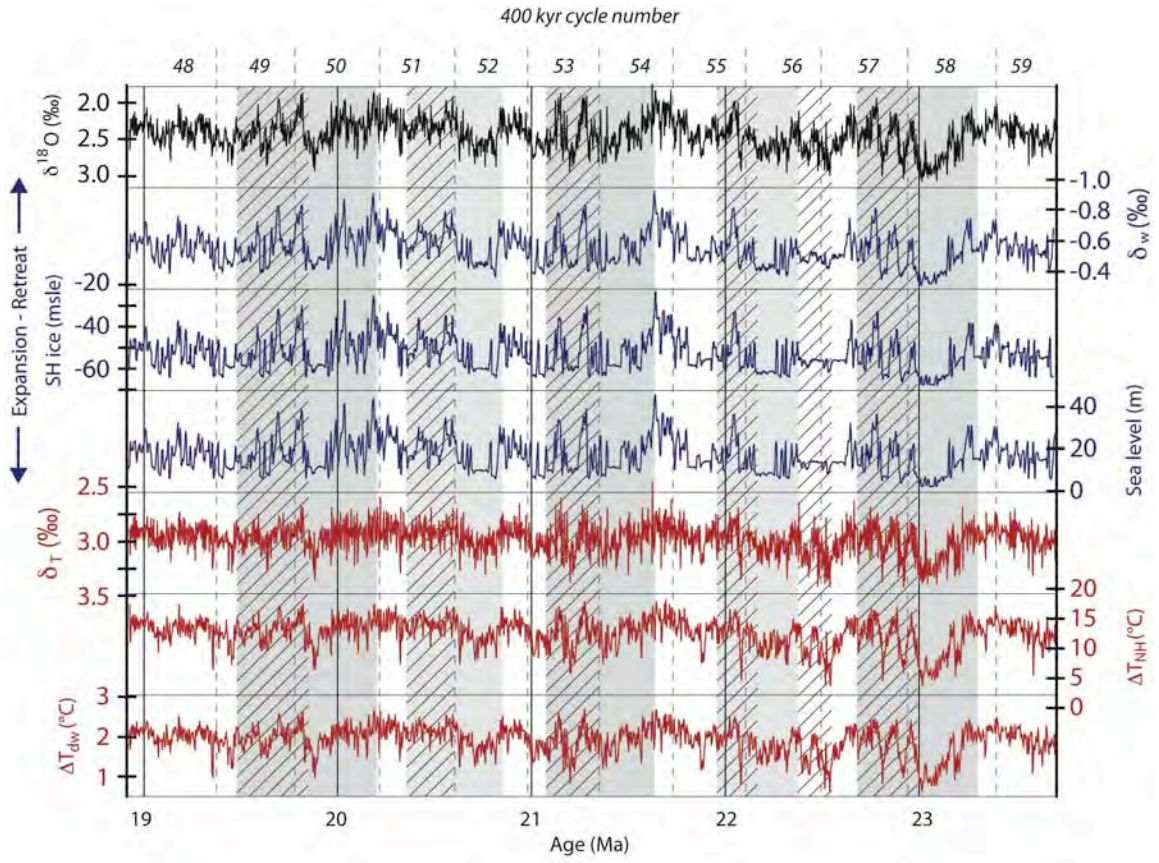

Supplementary Figure 2.12: *1-D inverse modelling output. The* $\delta^{18}O$ *record (as measured), calculated* δw *(seawater contribution, from ice volume, to* $\delta^{18}O$*), ice on Antarctica, eustatic sea level,* δ_T *(temperature contribution to* $\delta^{18}O$*), Northern Hemisphere (40-80° Latitude) annual average temperature (relative to present day) and deepwater temperature (relative to present day) calculated by the 1-D model [De Boer et al., 2010], are depicted. The* δ_w*,* δ_T*, and* ΔT_{dw} *values all represent oceans average values, because the model cannot resolve single water masses and/or oceans. Gray areas indicate cooling periods with reduced ~100-kyr power, gray and striped areas indicate ~100-kyr worlds, white areas are intermediate phases characterized by greater non-linear response to eccentricity modulated precession.*

CHAPTER 3:

ECCENTRICITY TUNED OLIGOCENE – MIOCENE CLIMATE PROXY RECORDS FROM THE WALVIS RIDGE (SOUTHEASTERN ATLANTIC OCEAN)

3.1 Abstract

Few astronomically calibrated high-resolution (≤ 5 kyr) Oligocene-Miocene climate proxy records exist and those available records show varying amplitude responses to frequencies of astronomical climate forcing. Therefore, the main pacemakers of global change remain debated. We present newly generated X-ray fluorescence core scanning and extended benthic foraminifer stable carbon and oxygen isotope records from ODP Site 1264 (Walvis Ridge, south-eastern Atlantic Ocean) that span a (near-) continuous Oligo-Miocene interval in high resolution (2.5 cm ≈ 3 kyr). Spectral analyses on the depth series indicate that the largest amplitude variability is associated with periodicities between 0.9 m and 3.7 m. Application of an initial bio-magnetostratigraphic age model indicates that this variability corresponds to ~100 to 405-kyr eccentricity periodicities. The strong expression of ~100 and 405-kyr cyclicity in our data guides the decision to develop an age model (30 – 19 Ma) in which the records are solely tuned to the stable eccentricity solution. The phase relation, on glacial-interglacial timescales, between our proxy records of global climate change to eccentricity is clear. All tuning target-curves used previously contained obliquity and climatic precession components because of the presence of higher frequency variability in the data. However, the stability of the ~40-kyr obliquity and ~20-kyr precession cycles in Earth-Moon models for ages >10 Ma is debated and the phase-relation between global climate and precession forcing had to be assumed. Long-term modulations of obliquity and precession are considered stable for the past 40 Myr. We compare our new records and the eccentricity tuned age model to previously tuned Oligo-Miocene climate proxy records to evaluate the astronomically pacing theories and calibrated (polarity) ages of *Billups et al*., [2004], *Pälike et al*., [2006a; 2006b], and *Tian et al*., [2008]. We find further support for the existing view [*Abels et al.*, 2005; *Holbourn et al.*, 2005; *Pälike et al.*, 2006a; *Pälike et al.*, 2006b; *Wade and Pälike*, 2004] and in contrast to earlier interpretations based on the early Miocene $\delta^{18}O$ record of Site 1264 [*Liebrand et al.*, 2011, Chapter 2], that the long-period eccentricity modulation (~2.4-Myr) caused greater sensitivity of the climate system to shorter-period (405 & ~100-kyr) eccentricity modulations of climatic precession. However, the relation between the

~1.2-Myr modulation of obliquity and climate/ice sheet dynamics on ~100-kyr time scales is more ambiguous for the Oligocene compared to the early Miocene.

3.2 Introduction

The dominance of either northern or southern hemisphere (summer) insolation forcing and pacing of global climate and Antarctic ice volume during Earth's pre-Pliocene (unipolar) Icehouse state is unknown [*Holbourn et al.*, 2007; *Pälike et al.*, 2006b; *Shackleton et al.*, 1999]. The phase relation between precession forcing and a possible Antarctic or global climate response during the Oligocene and Miocene is at present irresolvable because of limited age constraints and the limited (obliquity and precession) resolving capacities of proxy records of global change. Furthermore, the stability of both precession and obliquity throughout the Cenozoic Icehouse is unknown, because geologic interpretations and model studies have not come to conclusive values for climate friction yet. Climate friction (i.e. the combined effects of tidal dissipation and dynamical ellipticity) may have been (relatively) stable [*Levrard and Laskar*, 2003; *Pälike and Shackleton*, 2000], varying [*Hüsing et al.*, 2007; *Lourens et al.*, 2001; *Lourens et al.*, 2004; *Zeeden et al.*, 2013] or drifting [*Laskar et al.*, 2004] over geologic time, which would have resulted in constant, fluctuating or increased durations, respectively, of obliquity and precession cycles.

Yet, regardless of uncertainties in (1) the phase relation of global climatic response to precession forcing during the Oligocene through early Miocene and (2) the stability of climate friction (hence, obliquity and precession) over 10s to 100s of ice age cycles, all high-resolution deep marine Oligo-Miocene astrochronologies published to date have included precession and/or obliquity in their tuning target curves [*Billups et al.*, 2004; *Pälike et al.*, 2006a; *Pälike et al.*, 2006b; *Shackleton et al.*, 1999; *Shackleton et al.*, 2000; *Tian et al.*, 2008] (Supp. Table 3.1). This compromises accurate age control, although the accuracy of earlier tunings up to the ~100-kyr level is primarily constrained by independent spreading rate-based ages for the geomagnetic polarity timescale and tuning to the stable longer-period (eccentricity) amplitude modulations of obliquity and precession. This inaccuracy is also minimal compared to, for example, the Eocene astronomically tuned time scale where the tuning to the stable eccentricity solution is not yet (fully) completed. The uncertainties in precession phasing and obliquity/precession stability mainly hinder tuning, strictly defined as the unambiguous visual linkage of an obliquity-precession interference pattern in a tuning target-curve to a similar unmistakable pattern in a

proxy record, because no sole tuning-target curve can be selected *a priori* that will give accurate ages and is known to be the forcing mechanism. Hence, these uncertainties and unknowns limit our understanding of causal mechanisms between astronomical forcing agents and Earth's climate, cryosphere and carbon cycle response on a (obliquity and precession) cycle-to-cycle level.

We present newly generated high-resolution Oligo-Miocene (30 – 19 Ma) X-ray fluorescence (XRF) core scanning results and extended benthic $\delta^{13}C$ and $\delta^{18}O$ records from Site 1264 on the Walvis Ridge, located in the southeastern Atlantic Ocean. Time-frequency analyses, using an initial untuned age model, indicates that eccentricity is dominant [*Liebrand et al.*, 2011, Chapter 2]. We calibrate the records solely to the stable eccentricity solution and thereby avoid tuning complications arising from unknown phase relations and poorly constrained values for climate friction, tidal dissipation and dynamical ellipticity. Similar to earlier age calibration studies, we will not be able to tune "strictly" (i.e. link identical interference patterns in a signal to those in a target) to obliquity and precession and are merely able to construct a tuned age model by identifying the interference patterns resulting from different eccentricity periodicities (~95, ~125, 405-kyr, etc.) in signal and target curves, and their subsequent alignment. The latest numerical eccentricity solution is reliable back to ~50 Ma [*Laskar et al.*, 2011a; *Laskar et al.*, 2011b; *Westerhold et al.*, 2012]. We use our tuned astrochronology from Site 1264 to evaluate previously published astronomical climate forcing and pacing theories for the Oligo-Miocene that were based on records from Sites 926, 929, 1090, 1218 and 1148 [*Billups et al.*, 2004; *Pälike et al.*, 2006a; *Pälike et al.*, 2006b; *Tian et al.*, 2008; *Zachos et al.*, 2001a].

3.3 Site Descriptions

During ODP Leg 208 to the Walvis Ridge (southeastern Atlantic Ocean, Fig. 3.01), Neogene strata were recovered using the advanced piston corer (APC). At Site 1264 (2505 m water depth, 28°31.955'S, 2°50.730'E) the Oligocene and Miocene strata were relatively expanded compared to other Leg 208 sites. Palaeomagnetic results from Site 1265 (3059 m water depth, 28°50.101'S, 2°38.354'E) and Site 1266 (3798 m water depth, 28°32.550'S, 2°20.610'E) are correlated to Site 1264 because Site 1264 does not yield a clear primary palaeomagnetic record [*Bowles*, 2006; *Liebrand et al.*, 2011, Chapter 2; *Zachos et al.*, 2004].

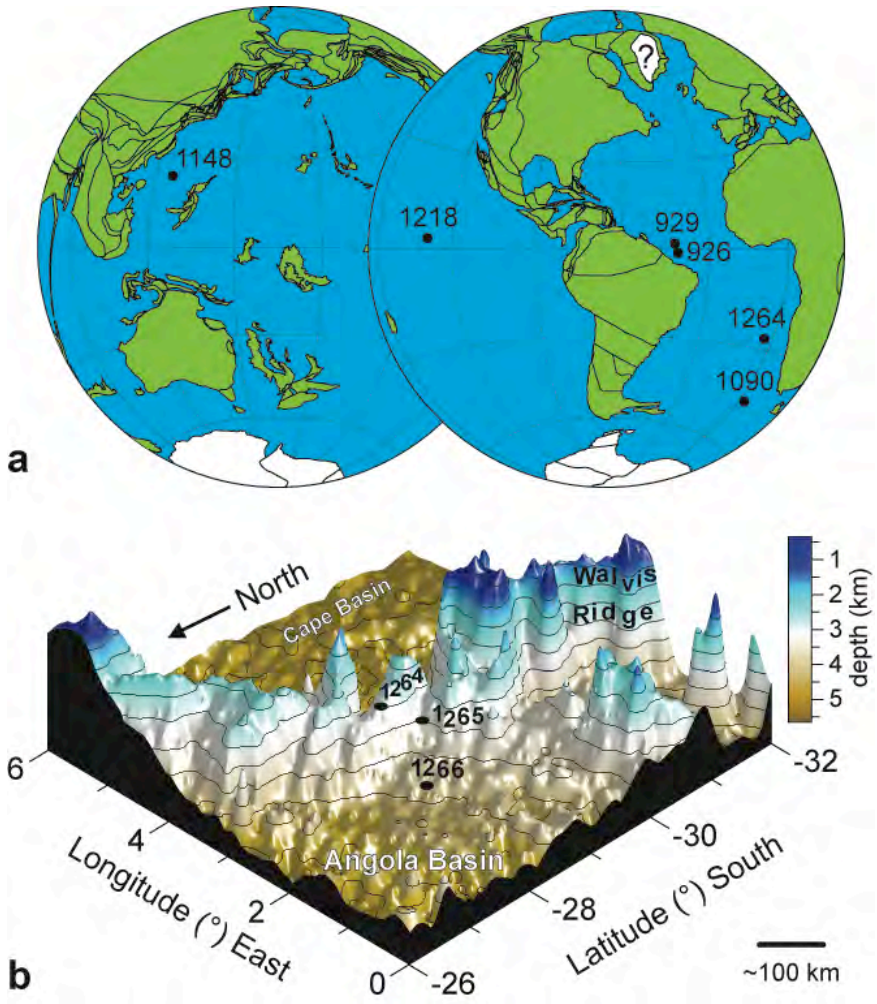

Figure 3.01: *Site locations.* ***a)*** *'Lambert azimuthal' palaeogeography map (~23 Ma, www.osdn.de) with approximate palaeopositions of ODP sites with mid-to-high resolution Oligo-Miocene stable-isotope chronologies that are discussed in this chapter. The presence of Northern Hemisphere ice during the Oligo-Miocene is unknown.* ***b)*** *Sites on the Walvis Ridge used to obtain stable-isotope, XRF and palaeomagnetic records. Bathymetry adapted from Smith and Sandwell [1997], site positions from Zachos et al. [2004]*

The astronomical age calibration, magnetostratigraphic and stable-isotope results obtained from the Walvis Ridge Sites 1264, 1265 and 1266 ([*Bowles*, 2006; *Liebrand et al.*, 2011, Chapter 2], this study) have been compared to those obtained from Ceara Rise Sites 926 and 929 (western equatorial Atlantic) [*Curry et al.*, 1995], Agulhas Ridge Site 1090 (Atlantic sector of Southern Ocean) [*Gersonde et al.*, 1999], Equatorial Pacific Site 1218 [*Lyle et al.*, 2002] and South China Sea Site 1148 [*Wang et al.*, 2000] (Supp. Table 3.01).

3.4 Methods

3.4.1 X-Ray Fluorescence Core Scanning

At Site 1264 we studied upper Oligocene and lower Miocene sediments (216 – 316 mcd), which consist of $CaCO_3$-rich foraminifer-bearing nannofossil ooze [*Zachos et al.*, 2004]. XRF element counts were generated at the MARUM XRF-laboratory, University of Bremen. For Site 1264 the entire study interval was scanned. Four splice gaps and/or uncertain tie-points were present in the Oligocene part of the shipboard splice of Site 1264 and therefore we also scanned the Oligocene and Oligocene-Miocene (climatic) transition (OMT) interval of Site 1265. Data were collected using an AVAATECH core scanner (Serial No. 12), installed with an Oxford Instruments 100W Neptune Rh X-ray tube and a Canberra X-PIPS Silicon Drift X-ray Detector (SDD; Model SXD 15C-150-500). A step size of 20 mm, down-core slit size of 10 mm and a cross-core slit size of 12 mm were applied. The X-ray tube was set at 10kV, 1500μA and measuring time was 20 sec. with a dead time of >20 sec. A 10kV-processing model that includes chlorine and rhodium was used to process the scanner output. Outliers resulting from section ends and cracks in the mud were selected by eye directly after scanning and removed. We use a calibration (r^2 = 0.85) between ln(Ca/Fe) and shipboard coulometric $CaCO_3$ measurements from Site 1264 [*Zachos et al.*, 2004] to estimate $CaCO_3$ ($CaCO_3$ est.) (Supp. Fig. 3.01). This calibration is also applied to calculate $CaCO_3$ est. for Site 1265. No direct calibration between ln(Ca/Fe) and $CaCO_3$ is calculated for Site 1265 because of the small set of coulometric $CaCO_3$ samples across the interval measured for XRF. For the purpose of time-series analyses we filled in the gaps of the $CaCO_3$ est. record from Site 1264 with data from Site 1265 into a composite record (not shown). The use of a log-ratio record was preferred over integrated elemental area or "count" records to avoid biases related to, for example, the closed sum effect (inherent to XRF core scanning) and aided the comparability between XRF data obtained from the different drill-sites [*Weltje and Tjallingii*, 2008].

3.4.2 Sample Processing and Stable-Isotope Analyses

For the Oligocene extension of the record 10 – 15 cm^3 samples were taken from Site 1264 at 2.5 cm resolution. After each step of sample processing, their weights were recorded. Discrete sample magnetic susceptibility (DS-MS) was measured on freeze-dried bulk samples in Utrecht on a Kappabridge KLY-2 and in Southampton on a Kappabridge KLY-4 magnetic susceptibility system. About 5 – 10 cm^3 of dry bulk sediment was archived at Utrecht for future analyses. Samples were washed over 38, 63 and 150 μm sieves with tap water and dried overnight in evaporation basins at 50°C. For the entire span of the record, the epifaunal benthic foraminifer species *Cibicidoides mundulus* [*Brady et al.*, 1888] was picked from the >150 μm fraction. Foraminiferal tests were not sonicated prior to measuring stable carbon and oxygen isotope ratios. Measurements were done preferably on single tests (the visually best specimen available per sample), however in rare cases two to four specimens were measured simultaneously, to reach the minimum (~20 μg) or ideal (30 – 50 μg) sample weight for the Kiel carbonate device. In Utrecht, the foraminiferal calcite was dissolved in a Finnigan MAT Kiel III automated preparation system. Purified CO_2 was analysed on a Finnigan MAT 253 mass spectrometer. The results were compared to an internal gas standard. Isotopic ratios were drift-corrected to nine individual NBS-19 values, measured along each sample run. Outliers in the stable-isotope records were removed arbitrarily by eye and were redefined in the previously published [*Liebrand et al.*, 2011, Chapter 2] early Miocene part of the records to obtain a visually cleaner result. Outliers defined in either carbon or oxygen, were removed from both records. If possible, repeat measurements were made for outlier-samples.

3.5 Results

3.5.1 Spliced Records and Site Correlations

The shipboard splices of Sites 1264 (between 206 – 316 mcd) (Fig. 3.02), 1265 (between 117 – 163 mcd) and 1266 (133 – 198 mcd) are adjusted using shipboard magnetic susceptibility and colour reflectance data and newly generated XRF data if available. For several splice tie-points, small corrections are made. The new composite depth scales are referred to as 'revised meters composite depth' (rmcd). Our terminology for the revised composite depth scale is different than that for Site 1218. *Pälike et al.* [2005; 2006b] used the acronym 'rmcd' to indicate the adjustment

of intervals that fall outside the splice to the mcd depth (i.e. stacking), where we use 'rmcd' to indicate changes in the original mcd depth scale. We do not present an adjusted-rmcd scale to correlate intervals outside the splices of the Walvis Ridge sites to the splice. All tables are presented in Appendix A.

The spliced records can be straightforwardly correlated between Walvis Ridge Sites 1264, 1265 and 1266 in the depth domain using visually selected MST-MS, CR or XRF tie-points and subsequent automated "matching" [*Lisiecki and Lisiecki*, 2002]. No major changes are made for the early Miocene correlation between Sites 1264 and 1265 previously published [*Liebrand et al.*, 2011, Chapter 2]. We estimate the maximum uncertainty in the depth correlations to be ~20 cm.

A magnetostratigraphic record is not available at Site 1264 [*Bowles*, 2006; *Zachos et al.*, 2004] and it has been substituted with palaeomagnetic records from Site 1265 (C5En(o) – C7n(y)) and Site 1266 (C6Cn.1n(y) – C11n.2n(o)). We reinterpret the labelling of chron names of one chron reversal at Site 1265 and of five chron reversals at Site 1266, after comparison with the Oligocene and Miocene GPTS [*Hilgen et al.*, 2012; *Vandenberghe et al.*, 2012] (see Table 3.01). The identified stratigraphic positions of the reversals remain unchanged [*Bowles*, 2006].

3.5.2 XRF and Stable-Isotopes

A steady upsection increase in the percentage of the 63 – 150 μm fraction is observed between 285 – 260 rmcd (late Oligocene warming) and a steady decrease between 255 – 220 rmcd (early Miocene). The >150 μm size fraction peaks around 253 rmcd (OMT interval) and the 216 – 253 rmcd interval (early Miocene) have higher values compared to the 253 – 317 rmcd interval ("mid" to late Oligocene) (Fig. 3.02).

The $CaCO_3$ est. record, which is derived from ln(Ca/Fe), broadly resembles the pattern in Fe-counts. Variability ranges between 88 and 100 % $CaCO_3$ of the dry sediment and is largest between 216 – 252 and 279 – 316 rmcd. Reduced variability is recorded during the late Oligocene interval, between 252 – 279 rmcd.

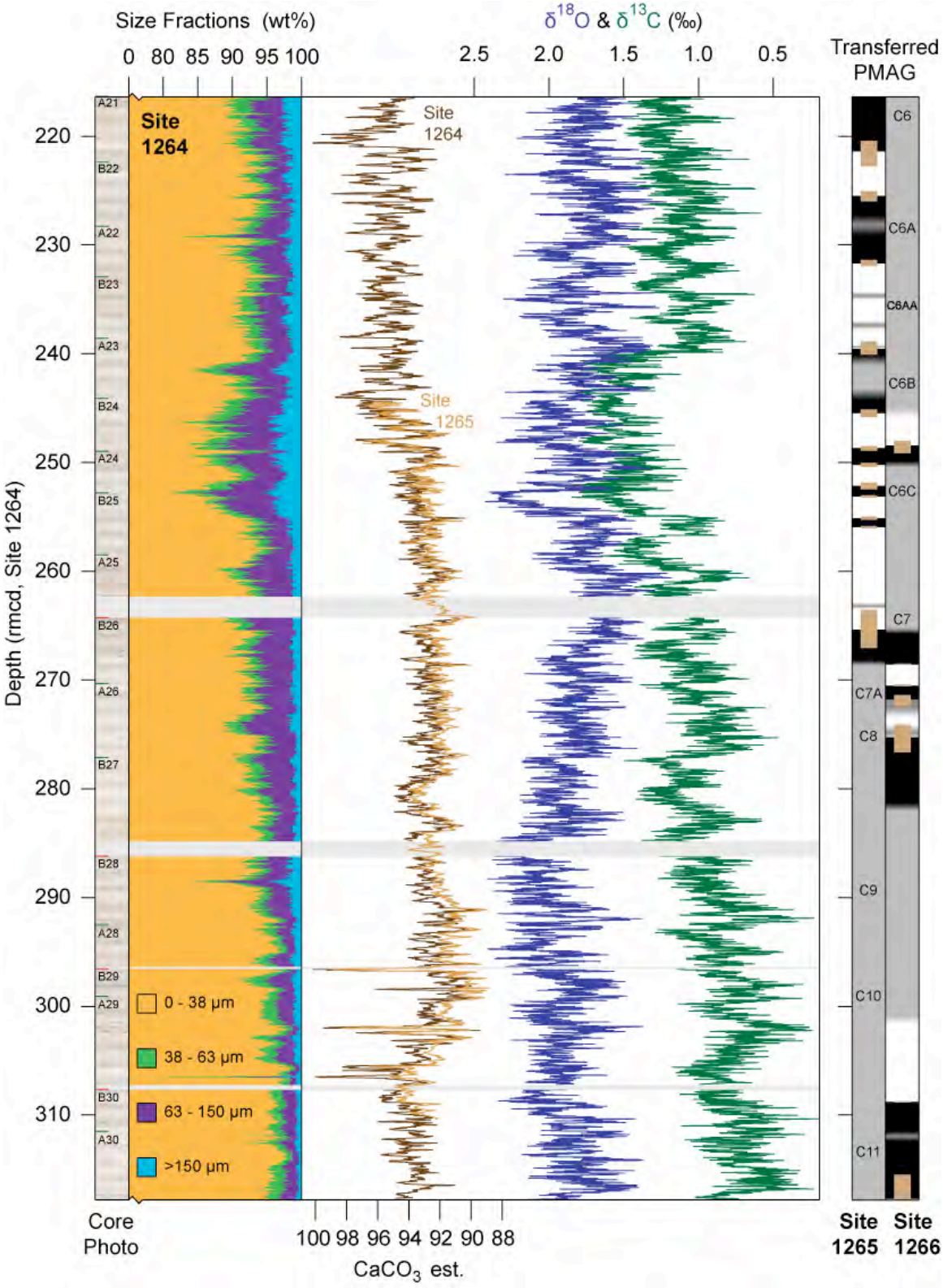
Size Fractions (wt%)
0 80 85 90 95 100
δ18O & δ13C (‰)
2.5 2.0 1.5 1.0 0.5
Transferred PMAG
Site 1264
Site 1264
Site 1265
Depth (rmcd, Site 1264)
220
230
240
250
260
270
280
290
300
310
A21
B22
A22
B23
A23
B24
A24
B25
A25
B26
A26
B27
B28
A28
B29
A29
B30
A30
0 - 38 µm
38 - 63 µm
63 - 150 µm
>150 µm
C6
C6A
C6AA
C6B
C6C
C7
C7A
C8
C9
C10
C11
Core Photo
100 98 96 94 92 90 88
CaCO3 est.
Site 1265
Site 1266

<< ***Figure 3.02:*** *Walvis Ridge Site 1264 core photographs and size fraction, $CaCO_3$ est., stable isotope, palaeomagnetic data presented in the depth domain (revised meters composite depth). $CaCO_3$ est. from Site 1265 and PMAG from Sites 1265 and 1266 have been transferred to Site 1264 rmcd via detailed correlations based on magnetic susceptibility, colour reflectance and XRF data (if available). Apparent cyclicity in the core photographs is biased by uneven lightening conditions when the photographs were taken.*

Benthic foraminifer stable carbon isotope ratio ($\delta^{13}C$) values range from ~0.20‰ to ~1.85‰ across the entire record. After removal of the long-term trends, the variability associated with orbital cycles and other causes of variability has a standard deviation of ~0.15‰ and a maximum of ~1.00‰ at 192 rmcd. A long-term increase in $\delta^{13}C$ is observed throughout the entire record, which is aberrated by a sudden step decrease at ~240 rmcd. Several $\delta^{13}C$ minima of ~0.2‰ are recorded between 290 – 316 rmcd. The $\delta^{13}C$ record peaks with 1.85‰ at ~253 rmcd, contemporaneous with maximum $\delta^{18}O$ values.

Benthic foraminiferal stable oxygen isotope ratios ($\delta^{18}O$) vary between ~1.25 – ~2.45 ‰, resulting in a 1.2 ‰ range of values for the study interval. The highest $\delta^{18}O$ values of 2.43 ‰ are reached at ~253 rmcd, characterising the maximum glacial conditions associated with the OMT. Low $\delta^{18}O$ values of 1.25‰ are recorded at several intervals throughout the latest Oligocene and early Miocene. After removal of long-term trends, variability is not evenly spread throughout the record, with a standard deviation of ~0.16‰ and a maximum variability of ~0.9‰ between 290 – 294 rmcd, 250 – 253 rmcd and between 234 – 236 rmcd. Similar to the $CaCO_3$ est. record, an interval with particularly reduced amplitude variability in $\delta^{18}O$ is recorded during the late Oligocene interval, between ~260 – ~280 rmcd.

3.5.3 Astronomical Tuning of Site 1264

A 405-kyr cycle count and preliminary tuning is derived from plotting the data on an initial bio-/magnetostratigraphic age model [*Bowles*, 2006; *Zachos et al.*, 2004] (Fig. 3.03). All data sets are considered to visually identify the individual ~100-kyr cycles. However, fine-tuning (i.e. selection of final depth-age tie-points) of the entire record to the La2011_ecc3L (i.e. nominal) eccentricity solution is solely based on a synchronisation of $CaCO_3$ est. maxima to ~100-kyr

eccentricity minima. At the ~100-kyr periodicity the phase relation between $CaCO_3$ est. and eccentricity stays constant throughout the study interval. For a more detailed discussion of the phase relation between ($CaCO_3$ est.) tuning signal and (eccentricity) tuning target-curve we refer to section 3.6.1.2. The La2011 solution is a revised and more accurate astronomical solution compared to the La2004 [*Laskar et al.*, 2004] and La2010 solutions [*Laskar et al.*, 2011a; *Laskar et al.*, 2011b], however differences between these solutions across our study interval are negligible (i.e. an exact in-phase relation is found on the 100 and 405-kyr periodicities between the La2004 and La2011 solution across the 20 – 30 Ma window). All tuning tie-points lie in ~100-kyr eccentricity minima, which reflect periods when Earth orbit around the sun was near circular. These minima are relatively short lasting 'events' in the eccentricity solution (compared to the maxima) and thereby form natural and precise age-calibration points. On the eccentricity-tuned age-model, linear sedimentation rates (LSR) for Site 1264 vary between 0.5 – 1.5 cm/kyr (Fig. 3.04). The LSR averages at ~1 cm/kyr, however they drop off towards the shallower end of the record. Increased LSR are recorded across the OMT (22.2 – 23.5 Ma, see Fig. 3.04).

Constrained by the 100-kyr-scale $CaCO_3$-tuned tie-points we then perform three "matching" [*Lisiecki and Lisiecki*, 2002] sensitivity tests. During each match the $CaCO_3$, $\delta^{18}O$ and $\delta^{13}C$ records are automatically and simultaneously aligned to a single (but varying between tests) astronomical template to test for the susceptibility of the data to record (higher) astronomical frequencies. We give a very high "penalty" on deviation from our manually selected ~100-kyr input age-depth tie-points (see Supp. Inf. for all settings). Our resulting four age models are referred to by their respective target curves (E = eccentricity, T = tilt/obliquity, P = precession, 2004 = La2004, 2011 = La2011) and age-calibration methods (tuned, matched). The first matching test is to the same target curve (E2011) as our original manual tuning was to. The two remaining matching tests, to ET2004 and ETP2004, use target curves that mimic 65°S caloric summer-half insolation (21 September – 21 March, plus an eccentricity component). The latter two matching targets were selected because the global climate during the Oligo-Miocene probably moved in phase with variability of the Antarctic ice sheet, which in turn, was most likely paced by southern hemisphere summer insolation. The matching targets that include precession and obliquity are calculated using present day values for tidal dissipation and dynamical ellipticity, despite the debated stability of these parameters. Variable phase-relations between proxy records and astronomical cycles are not considered in the matching tests. The best average fit of the data to a matching-target therefore determines the phase relationships. To calculate E2011, the La2011 eccentricity solution is normalised and for ET2004 and ETP2004 the

normalised La2004 eccentricity, obliquity (and precession) solutions were added in a ratio of 1:0.5(:0.85) and subsequently normalised again.

On our ~100-kyr fine-tuned age model, the stable-isotope records of Site 1264 span the interval between ~19 and ~30 Ma. This comprises a Rupelian – Burdigalian interval contemporaneous with ~2.4-Myr eccentricity cycles 13 – 9, ~1.2-Myr obliquity cycles 26 – 17, 405-kyr eccentricity cycles 74 – 48 and chrons C11 – C6 (Fig 3.05). The highest amplitude variability in $\delta^{18}O$ is on ~100-kyr time scales and is contemporaneous with 405-kyr and ~2.4-Myr maxima. Apart from the OMT, no clear relation between the ~1.2-Myr obliquity cycle and glacial expansions is observed. Long-term trends are observed in the $CaCO_3$ est., $\delta^{18}O$ and $\delta^{13}C$ chronologies (Fig. 3.05). $CaCO_3$ est. values are highest during the early Miocene. The benthic $\delta^{18}O$ record from Site 1264 shows the highest values during the mid Oligocene and OMT intervals, whereas the lowest values correspond to the late Oligocene. Our benthic $\delta^{13}C$ chronology shows a long-term trend of increasing values that is aberrated by a plateau of peak values associated with the Oligocene – Miocene Carbon Maximum (CM-OM) [*Hodell and Woodruff*, 1994].

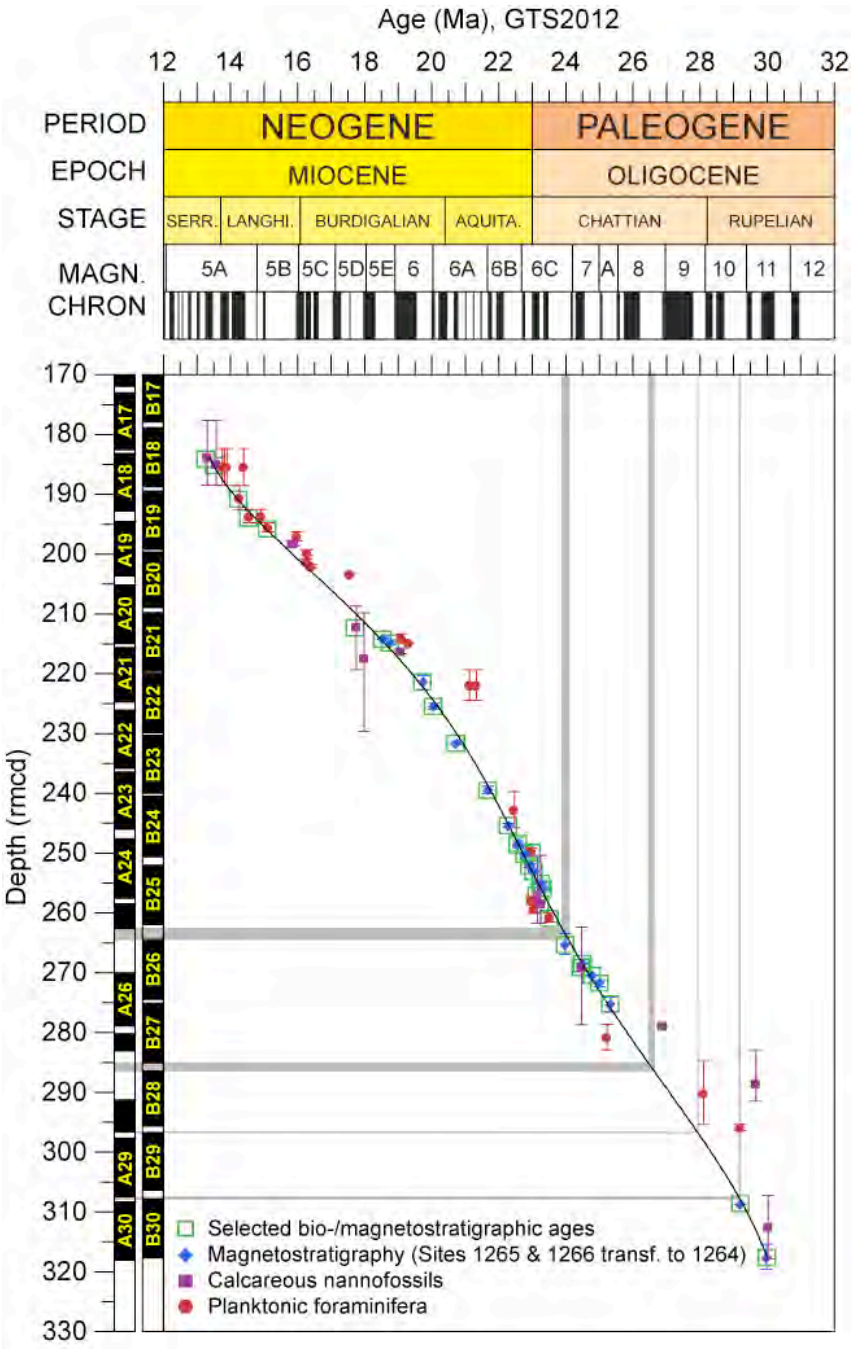

Figure 3.03: *Initial age model for Site 1264 based on a 6th order polynomial through selected shipboard bio-/magnetostratigraphic age control points [Bowles, 2006; Zachos et al., 2004]. Error bars were not considered for the fitting curve. A 405-kyr (and subsequent ~100-kyr) cycle interpretation is based on this initial age model. Top panel shows the periods, epochs, stages and magneto-chrons according to the GTS2012 [Hilgen et al., 2012; Vandenberghe et al., 2012].*

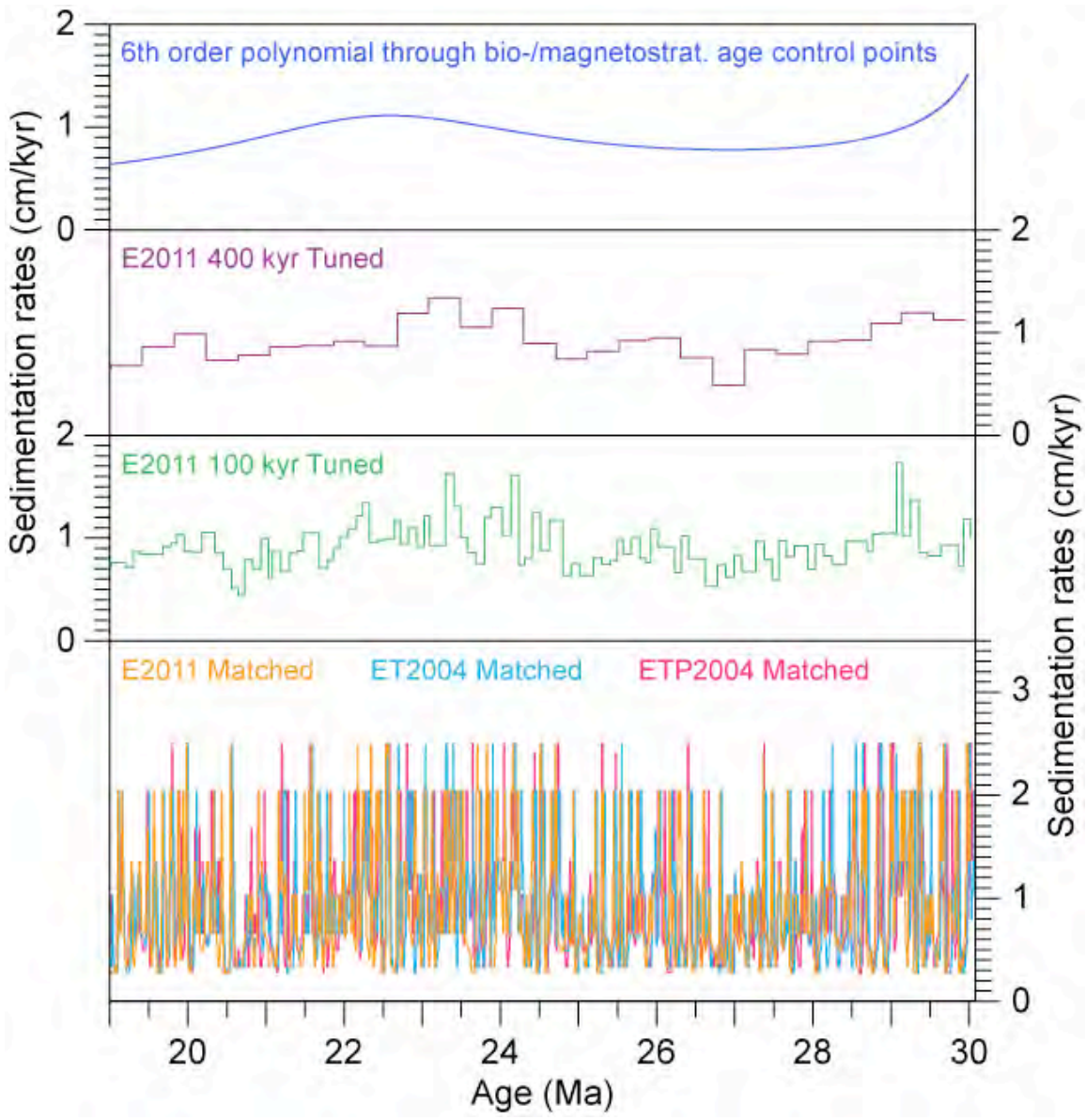

Figure 3.04: *Linear sedimentation rates of Site 1264 for subsequent steps (top to bottom) in age model refinements. Frequent small step-wise changes in sedimentation rates (bottom panel) characterize the algorithm-based (or "matched") age models.*

3.5.4 Spectral Analyses

Spectral power analyses on all depth-series ($CaCO_3$ est., $\delta^{13}C$, $\delta^{18}O$) show at least two (broad) spectral peaks: the first peak at 0.25 – 0.29 cycles/m, and a second peak at 0.63 – 1.25 cycles/m, most strongly recorded in $\delta^{13}C$ at ~0.71 cycles/m (Fig. 3.06). In general, the spectral power of the higher (>1 cycles/m) frequencies is much reduced compared to the power of the lower (<1 cycles/m) frequencies. The higher frequencies appear discontinuous throughout the record, but occur recurrently in short intervals of less than ~10 m in all depth-series (Fig. 3.06 left panel). Most distinct are the "ridges" with increased spectral power that are spaced ~20 m apart in the evolutive spectrum of $\delta^{13}C$ and, to a lesser degree, $\delta^{18}O$ (Fig. 3.06).

Power-spectral and evolutive analyses of the eccentricity tuned time-series ("E2011 tuned") of $CaCO_3$, $\delta^{18}O$ and $\delta^{13}C$ display a similar pattern, with dominant power at the lower (eccentricity) frequencies and reduced or absent power during shorter intervals at the higher (obliquity and precession) frequencies (Fig. 3.06 right panel). Similar as the depth series, short time intervals can be identified where the power of the higher frequency oscillations is enhanced, e.g., between 20.5 and 19.5 Ma in both the $\delta^{18}O$ and $\delta^{13}C$ records. An additional, non-eccentricity related, low frequency peak is recorded in the isotope time series. This (broad) spectral peak corresponds to periodicities of ~200 and ~160 kyr in $\delta^{18}O$ and $\delta^{13}C$ respectively. Time-frequency analyses of the matched time-series indicate variable responses of the different proxy records to higher frequency astronomical cycles (Figs. 3.08 – 3.10, Supp. Fig. 3.02).

>> *Figure 3.05:* *$CaCO_3$ and Cibicidoides mundulus $\delta^{18}O$ and $\delta^{13}C$ data from Site 1264 on the ~100-kyr eccentricity tuned age model (top three panels) is compared to the astronomical obliquity (La2004) and eccentricity (La2011) solutions (upper middle panel). We compare the transferred magnetostratigraphic results [Bowles, 2006] (lower middle panel) to the GPTS2012 [Hilgen et al., 2012; Vandenberghe et al., 2012] (bottom panel). The results from Site 1264 across Chrons C6, C6AA, C7, C7A, C8 and C11 are (partially) uncertain (brown) or unidentified (approximate position indicated in gray).*

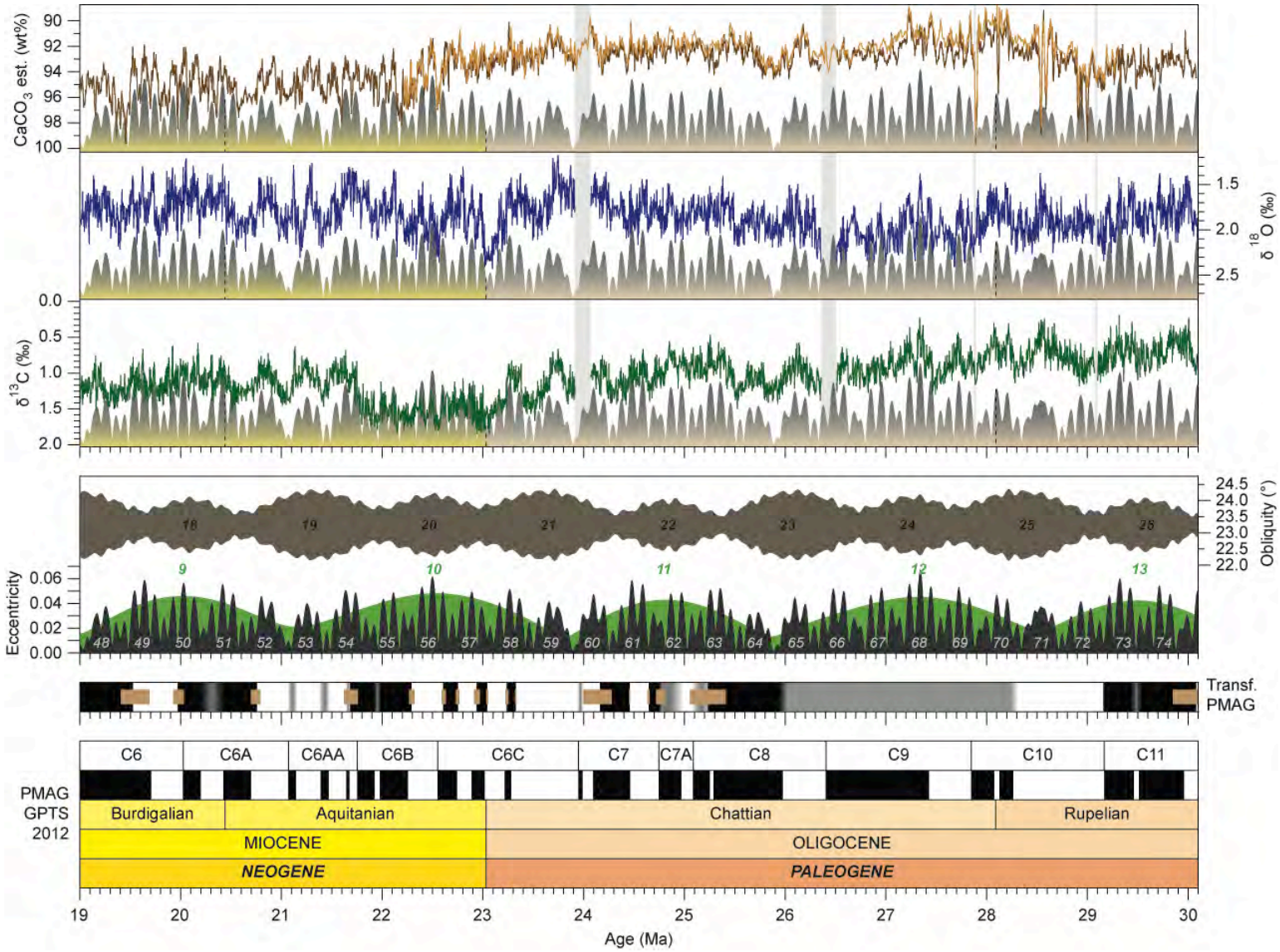
CaCO3 est. (wt%)
90
92
94
96
98
100
δ18O (‰)
1.5
2.0
2.5
δ13C (‰)
0.0
0.5
1.0
1.5
2.0
Obliquity (°)
24.5
24.0
23.5
23.0
22.5
22.0
18
19
20
21
22
23
24
25
26
Eccentricity
0.06
0.04
0.02
0.00
9
10
11
12
13
48
49
50
51
52
53
54
55
56
57
58
59
60
61
62
63
64
65
66
67
68
69
70
71
72
73
74
Transf.
PMAG
C6
C6A
C6AA
C6B
C6C
C7
C7A
C8
C9
C10
C11
PMAG
GPTS
2012
Burdigalian
Aquitanian
Chattian
Rupelian
MIOCENE
OLIGOCENE
NEOGENE
PALEOGENE
19
20
21
22
23
24
25
26
27
28
29
30
Age (Ma)

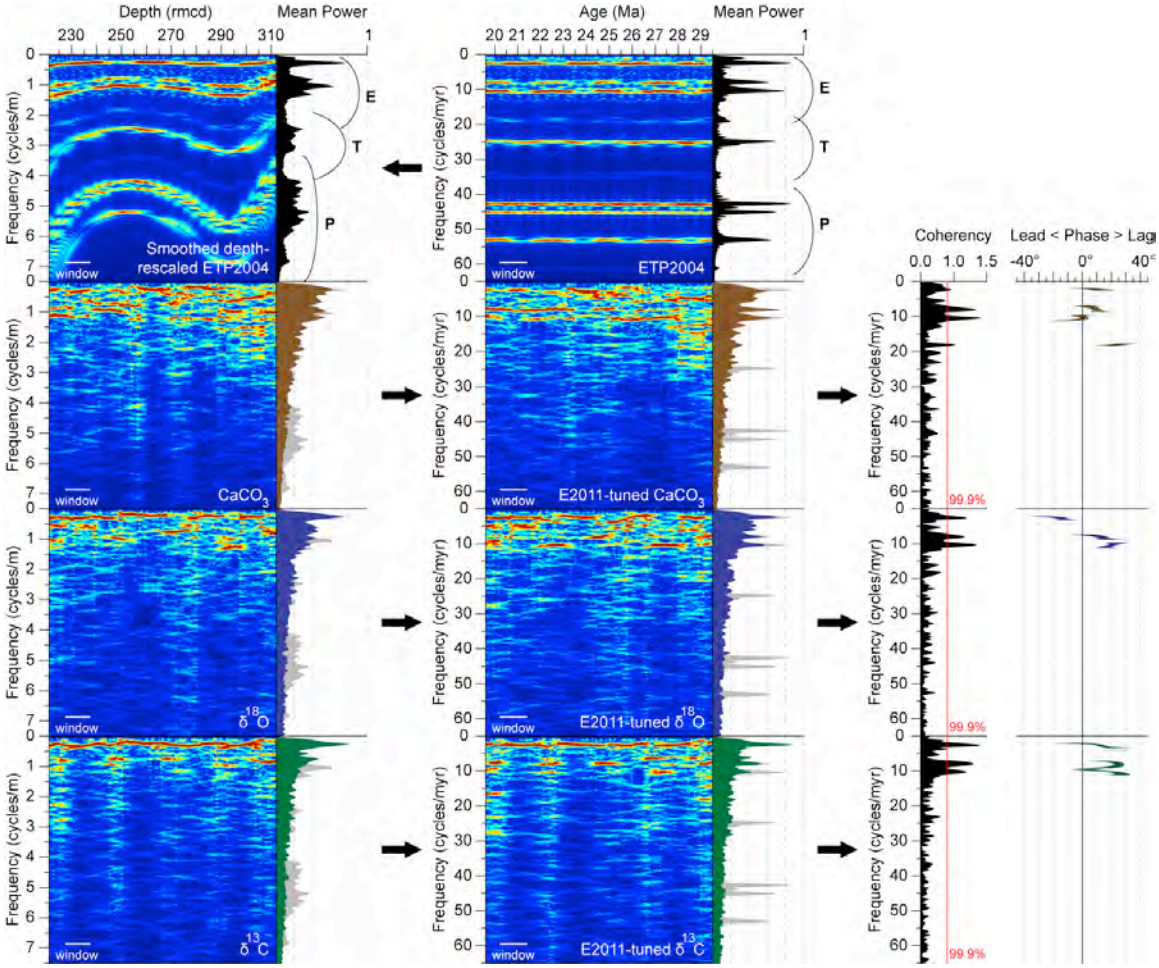

Figure 3.06: *Evolutive analyses on the depth and time series from Site 1264. Evolutive analyses results for a smoothed depth-rescaled ETP (La2004) curve (top left) are shown to show that the higher frequencies are more distorted by modest (i.e. 2-to-3 fold) changes in LSR, however, the La2011 eccentricity solution (not shown) is the sole tuning target used. Here, we compare the evolutive result of our tuned records with the ETP2004 matching target to indicate where the higher frequency astronomical frequencies are expected, if they had been (strongly) present in the data. Blackman-Tukey coherency with- and phase relations to- La2011 eccentricity are shown on the right.*

3.5.5 Coherency and Phase

On our original manually tuned time scale, all time-series are coherent (>99.9%) with eccentricity at the 405, 125 and 95 kyr periods and CaCO3 est. is also coherent on the (weak) ~50 kyr eccentricity periodicity (Fig. 3.06). Spectral power and coherency are variable throughout the records in close relation to modulation by the very long-term, i.e. the ~2.4-Myr eccentricity cycle. In particular, spectral power in the 405-kyr eccentricity band and associated coherency are generally larger during the ~2.4-Myr minima (especially for $\delta^{13}C$), while that of the shorter (i.e. <405-kyr) periods were more dominant during intervals of ~2.4-Myr-bound eccentricity maxima.

A strict interpretation of Blackman-Tukey phase estimates (Fig. 3.06) indicates a 3° – 13° (3 – 15 kyr) lag of $CaCO_3$ est., a -10° – -25° (11 – 28 kyr) lead of $\delta^{18}O$ and an 8° – 18° (9 – 20 kyr) lag of $\delta^{13}C$ to eccentricity at the 405-kyr period. At the 125-kyr period lags of 3° – 9° (1 – 3 kyr), 5° – 18° (2 – 6 kyr) and 22 – 25 (8 – 9 kyr) to eccentricity are found for $CaCO_3$ est., $\delta^{18}O$ and $\delta^{13}C$, respectively. A small lead to in-phase relation of -10° – 0° (3 – 0 kyr) is found at the 95 kyr eccentricity periodic for $CaCO_3$. This is a lag of 16° – 22° (4 – 6 kyr) and 15° – 26° (4 – 7 kyr) for $\delta^{18}O$ and $\delta^{13}C$, respectively. We note that these phase estimates are averages of the entire time-series. The phase-relations are not necessarily stable throughout and they are very sensitive to small changes in the age model. Phase relations to obliquity and precession are not calculated because they are excluded from the tuning target-curve.

3.5.6 Filtering and Amplitude Modulation

A Gaussian filter of the detrended data on the initial bio-/magnetostratigraphic age model, centred around the 405-kyr period, identifies 27 cycles indicating that the total duration of the time-series is 27 * 405-kyr = ~11 Myr. Notch-filtered and normalised time-series are filtered again using broad band-pass filters centred on the 1/405 and 1/110 (combined 1/125 and 1/95) eccentricity frequencies [*Paillard et al.*, 1996]. Their amplitude modulations are calculated in MATLAB using a Hilbert-transform (e.g. [*Shackleton et al.*, 1999]) (Fig 3.07). Amplitude demodulated $CaCO_3$ est. filters show a large response at the ~100-kyr periodicity between 22 and 19 Ma and between 28.5 – 26.5 Ma. Similar analyses on $\delta^{13}C$ show a strong ~100-kyr response between 28.0 – 27.0 Ma, however the 405-kyr cycle is dominant throughout. Notably, the amplitude of the 405-

kyr filtered $\delta^{13}C$ time-series is largest during ~2.4-Myr minima, thereby mimicking the amplitude modulation of the 405-kyr filtered eccentricity solution (albeit slightly amplified and lagged in certain intervals). Similar analyses on $\delta^{18}O$, show a ~100-kyr response of large amplitude between 30.0 – 26.5 and between 23.5 – 19.0 Ma, with some of the strongest responses during 405-kyr eccentricity cycles 73, 68, 57 and 49. A smaller amplitude response to the ~100-kyr cycle is found between 26.5 – 23.5 Ma (405-kyr cycles 64 – 59). A (weak) correlation is recognised between $\delta^{18}O$ and eccentricity in the ~2.4-Myr amplitude modulation of the 405-kyr cycle (not shown).

3.6 Interpretation and Discussion

3.6.1 Eccentricity Calibrated Age Model

3.6.1.1 Initial Age Model

We recognise clear bundling of three to four ~1 m cycles into ~3.6 m cycles in the best-preserved intervals of the $CaCO_3$ est. record (e.g. between 220 – 250 mcd, Fig. 3.02). This bundling pattern, taken together with the skewed shape of the ~1 m cycles (broad peaks and narrow troughs) is an expression (in the $CaCO_3$ est. depth-series) of the 95 and 125-kyr eccentricity interference patterns that result in bundles of three to four ~100-kyr cycles (~1 m) into 405-kyr cycles (~3.6 m). In conjunction with initial bio-/magnetostratigraphic age constraints, we confidently link the ~3.6 m and ~1 m cycles, present throughout nearly all depth-series, to the 405 and ~100-kyr eccentricity cycles respectively. Evolutive depth-frequency conversions show that we can track the ~3.6 m and ~1 m (weaker) cycles and that they vary in thickness throughout the records (Fig. 3.06).

Our initial age-model is simply based on a polynomial fitting through selected bio- and magnetostratigraphic age control points [*Bowles*, 2006; *Zachos et al.*, 2004] (Fig. 3.03). This polynomial age model is not affected by sudden changes in sedimentation rates or assumptions about astronomical climate forcing. To obtain an absolute 400-kyr age calibration, a rough 400-kyr tuned age model is derived from our initial age model by aligning 400-kyr data filters to the eccentricity solution. Our intermediate 400-kyr tuning forms the basis for subsequent, more detailed age calibration at the ~100-kyr level.

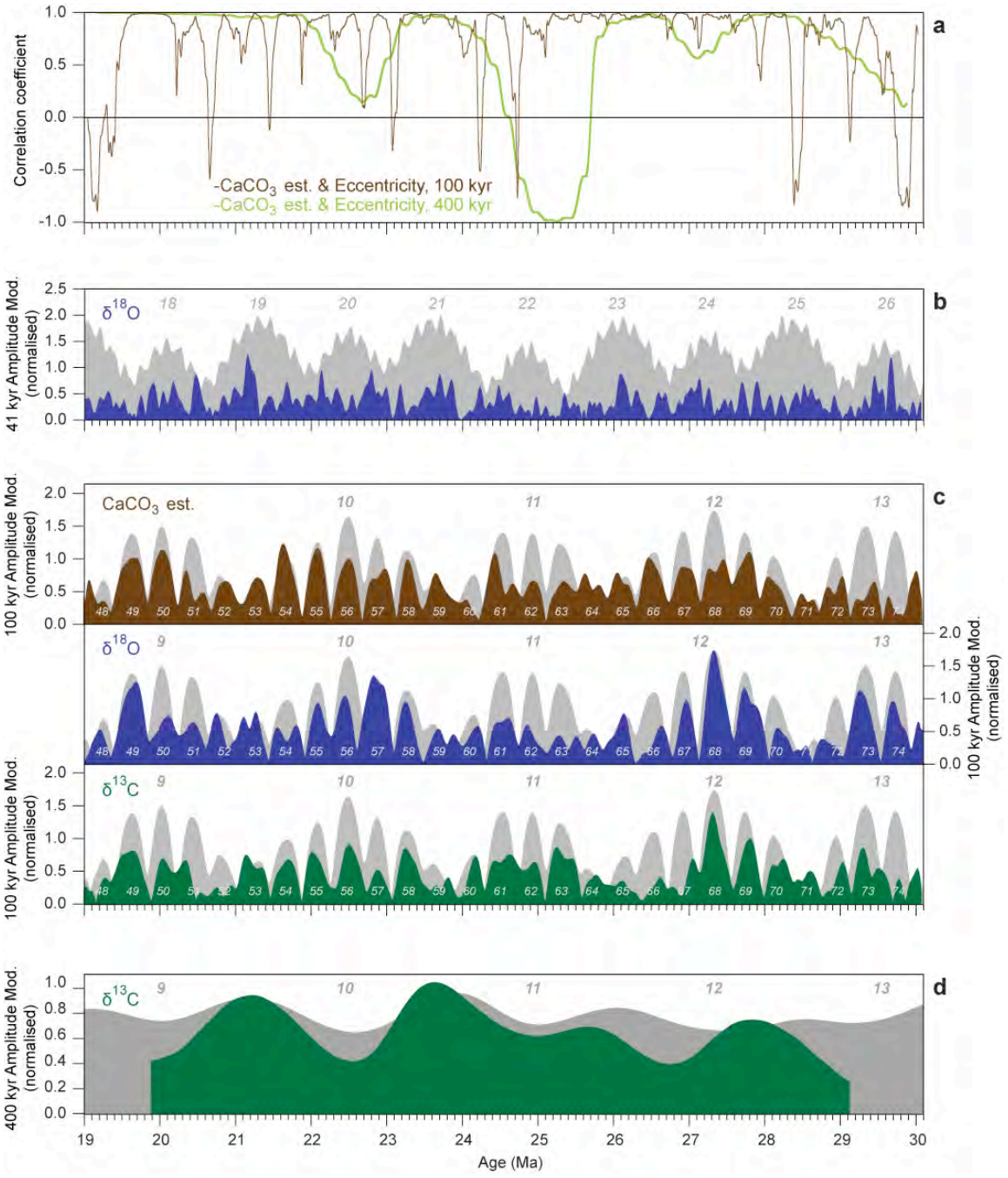

Figure 3.07: *Test of phase assumptions and amplitude modulation of Site 1264 data.* ***a)*** *Phase relations between 405 and ~100-kyr components of $CaCO_3$ est. (E2011 Tuned) and eccentricity as indicated by a moving r^2 (405 and 100-kyr windows, respectively) of the 405 and 100-kyr filtered $CaCO_3$ est. record and eccentricity solution.* ***b)*** *41 kyr amplitude modulation of filtered*

$\delta^{18}O$ (blue, ET2004 Matched) compared to 41 kyr amplitude modulation of obliquity (gray). A weak response is present, especially in the ~180 kyr band. ***c)*** *~100-kyr amplitude modulation of the filtered records (coloured, E2011 Tuned) compared to ~100-kyr amplitude modulation of the filtered eccentricity solution (gray backgrounds) revealing transient synchronisations of the proxy data to eccentricity. d) 405-kyr amplitude modulation of the filtered $\delta^{13}C$ record (E2011 Tuned) compared to 405-kyr amplitude modulation of the filtered eccentricity record (gray). The strongest 405-kyr cycles (generally) occur during ~2.4-Myr eccentricity minima and are often amplified and lagged in $\delta^{13}C$ (e.g. prior to the "mid" Oligocene cool phase and the OMT).*

3.6.1.2 Tuning Signal-Curve

We have selected the $CaCO_3$ est. record as our tuning signal because, compared to the isotope records, it appears the better recorder of eccentricity during most intervals, suggesting that the physical process(es) that link(s) $CaCO_3$ to eccentricity reacted most strongly to this forcing. Even though the amplitude response of $CaCO_3$ to eccentricity changes throughout our study interval (Fig. 3.07), we find that a near-linear response to the eccentricity modulation of precession (i.e. a quadratic non-linear response to precession forcing [*King*, 1996]) primarily controlled the $CaCO_3$ content of the sediment.

Keeping apart primary from secondary controls of carbonate accumulation, dissolution, dilution and bioturbation on our $CaCO_3$ tuning-signal can be complex. However, the cycle shape of the $CaCO_3$ est. record together with the size fraction data indicate that productivity is the most important variable. The record shows (very) skewed ~100-kyr cycle shapes, with narrow peaks and broad troughs. The peaks correspond to ~100-kyr eccentricity minima (glacials) and the troughs to eccentricity maxima (interglacials). If dissolution had been the primary control on $CaCO_3$ est. an inverse phase relation would have been expected with the most dissolution (and hence low $CaCO_3$) during glacial maxima [*Pälike et al.*, 2006a; *Zachos et al.*, 1997]. This is not found suggesting that productivity, perhaps underneath the South Atlantic gyre or associated with upwelling and nutrient availability caused by the Benguela current primarily controlled $CaCO_3$ at the relatively shallow Site 1264. Similar productivity control on $CaCO_3$ content of Oligo-Miocene sediments was found at the equatorial Pacific. These carbonates were deposited below the equatorial (Pacific) upwelling zone [*Pälike et al.*, 2010], and the CCD shows not major fluctuation during the Oligocene and early Miocene [*Pälike et al.*, 2012]. Similarly, our size

fraction data suggests that productivity increased during glacial maxima and no clear dissolution signal could be discerned. Bioturbation can be a mechanism to transfer power from higher astronomical frequencies to lower ones, especially at Site 1264, which is characterised by relatively low sedimentation rates.

We assume a complete (i.e. 180°) out-of-phase relation between XRF-based estimates of $CaCO_3$ and eccentricity on the ~100-kyr periodicity because of the striking similarity in the shape of the excursions between signal and target after this phase shift has been applied. This results in tying $CaCO_3$ maxima to eccentricity minima without introducing a lag. This phase-assumption does not hold for the 405-kyr periodicity (see negative r^2 values in Fig. 3.07) between 25.5 and 24.0 Ma where an in-phase relation is present. Detailed studies of phase relations between astronomical periodicities and deep-sea carbonate content during the Plio-Pleistocene indicates that they can be highly variable and that they can even switch sign (180°) [*Clemens*, 1999; *Sexton and Barker*, 2012]. Our resultant phasing between eccentricity and isotopes, in which isotope maxima fall together with eccentricity minima (ignoring lags between isotopes and eccentricity), supports our assumed phase-relation (at the ~100-kyr level) between $CaCO_3$ est. and eccentricity. For example, similar phase relations between isotope records and eccentricity forcing have been described for Oligo-Miocene records from the equatorial Pacific [*Pälike et al.*, 2006b; *Wade and Pälike*, 2004].

3.6.1.3 Tuning Target-Curve

Our choice of an eccentricity target-curve for tuning is primarily motivated by the strong expression of eccentricity in our records. Secondary reasons to restrict ourselves to a sole eccentricity target, and hence, exclude obliquity and precession are (1) the uncertainties in phase relations between proxy signals and precession-including targets and (2) the relatively unconstrained values for climate friction over 10s to 100s of glacial cycles that affect the durations of the obliquity and precession cycles and the precession-obliquity interference patterns (and thereby the exact age-positions of insolation extremes) [*Laskar et al.*, 1993; *Laskar et al.*, 2004; *Lourens et al.*, 2004].

The phase relation between globally integrated Oligo-Miocene climate proxy records (benthic $\delta^{13}C$ & $\delta^{18}O$, far-field sea level, etc.) and precession is unclear because no records have yet been generated that resolve a clear precession signal above noise levels (e.g. [*Proistosescu et al.*,

2012]). The relatively low sedimentation rates (average ~1 cm/kyr) of most deep-sea records compromise resolvability of the globally integrated proxy records and they are currently the main source of uncertainty for the precession phasing. Records with resolved precession cycles are present at, for example, the Ceara Rise [*Pälike et al.*, 2006a; *Shackleton and Crowhurst*, 1997; *Shackleton et al.*, 1999; *Zachos et al.*, 1997] and Monte dei Corvi land-based marine section in Italy [*Hüsing et al.*, 2007]. However, extrapolating precession phase interpretations to infer a dominant NH or SH precession control on global climate remains elusive because the derived precession phase-relations are critically based on the (assumed) stability of climate friction.

Climate friction, taken together with other contributing factors such as mantle convections, for example, affects values for tidal dissipation and dynamical ellipticity (TD and E_D). In turn, TD and E_D proportionally affect the frequencies of obliquity and precession over time [*Laskar et al.*, 1993], which taken together with the increasing uncertainty (with geologic time) in the (eccentricity) amplitude modulation of obliquity and precession results in alternative hypothetical obliquity-precession interference histories. Differences between solutions are generally well expressed during 2.4-Myr eccentricity minima. The uncertainties in values for climate friction can result in an error of up to ~3 obliquity and precession cycles (or anything in between) at ~23 Ma for realistic, but constant alternative values [*Lourens et al.*, 2004], supporting the view that the values of TD and E_D can drift over relatively short geologic time intervals [*Lourens et al.*, 2001]. However, astrophysical calculations suggest that (at least) obliquity has been very stable throughout Earth's Cenozoic (Icehouse) history and perhaps even into the far geologic past [*Levrard and Laskar*, 2003]. The stability of obliquity and precession is supported by the sedimentary records from the Ceara Rise, that cover the past 25 Ma [*Pälike and Shackleton*, 2000]. However, this finding is critically based on correct identification of precession phasing throughout the entire study interval and correctly spliced and tuned records [*Pälike and Shackleton*, 2000; *Shackleton and Crowhurst*, 1997; *Shackleton et al.*, 1999; *Weedon et al.*, 1997]. Both the original splice and tuning have been revised [*Pälike et al.*, 2006a; *Zeeden et al.*, 2013], thus challenging the sole geologic support for long-term climate friction stability. The latest geologic constraints on climate friction are currently available to ~10 Ma [*Hüsing et al.*, 2007; *Zeeden et al.*, 2013], tentatively supporting the view of stable obliquity [*Levrard and Laskar*, 2003] and stable obliquity and precession [*Pälike and Shackleton*, 2000] throughout the latest phase of the Cenozoic Icehouse. No Oligo-Miocene globally integrated climate proxy records exist that resolve an unambiguous obliquity-precession interference pattern. Absolute astronomical age control thus depends on the long-term (eccentricity) modulations of precession

and obliquity, which are stable in the astronomical solutions to 40 – 50 Ma [*Laskar et al.*, 2011a; *Laskar et al.*, 2011b; *Laskar et al.*, 2004; *Pälike et al.*, 2004; *Westerhold et al.*, 2012]. These modulations include the subtle ~180 kyr modulation of obliquity, which could prove a promising test for age model accuracy if the signal can be extracted from the geologic records [*Laskar*, 1999; *Shackleton et al.*, 1999; *Tian et al.*, 2008].

3.6.1.4 Eccentricity Tuning

Two unknowns currently affect progress in Oligo-Miocene age-calibration at the obliquity and precession levels; the phase relation of data records to precession has to be known to constrain values of climate friction, whereas realistic values of climate friction are needed to constrain the phase relation to precession. Therefore, also the understanding of causal relations between insolation forcing and climatic response is compromised. Our eccentricity tuning-approach is unaffected by these problems at the apparent cost of obliquity-precession age-precision. Supporting the findings of *Proistosescu et al.*, [2012], whom identified the eccentricity to be the only astronomical signal to be significantly present above noise in Oligo-Miocene isotope record from Site 1090, we argue that previously published Oligo-Miocene age calibration studies that incorporated obliquity and/or precession in their tuning-targets cannot guarantee absolute age-precision at this level. The accuracy of our ages is constrained by the stable eccentricity solution.

The general similarity between patterns identified in eccentricity and $CaCO_3$ est. is striking at Site 1264, especially during the early Miocene part of the record. Eccentricity pattern recognition in the $CaCO_3$ est. record becomes more difficult across intervals that correspond to strong ~2.4-Myr eccentricity minima, characterised by a weaker expression of the ~100-kyr beat for the duration of one or two 405-kyr cycles. In the ~2.4-Myr minima fewer tie-points are selected and only those that are certain on either side of the ~2.4-Myr eccentricity minimum are used. The Oligocene tuning is less precise in the vicinity of gaps in the isotope records from Site 1264, but the XRF core scanning records from Site 1265 that cover these gaps mitigate this.

On our tuned age model, eccentricity dominates the evolutive and mean power spectra, coherency and phase estimates of all data. Only a (very) weak obliquity component can be identified in certain intervals; an important result considering the exclusion of obliquity from our tuning target-curve. The presense of a weak obliquity signal is probably the result of the relatively low

sedimentation rates at Site 1264 and stands in stark contrast to Ceara Rise Sites 926 and 929 that show very strong obliquity imprint [*Pälike et al.*, 2006a]. The phase relations of the data to the 405-kyr and ~100-kyr eccentricity periodicities are in general agreement with those described for records from the Ceara Rise [*Pälike et al.*, 2006a; *Zachos et al.*, 2001a] and equatorial Pacific [*Pälike et al.*, 2006b], with the exception of the apparent ~20-kyr lead of Walvis Ridge's $\delta^{18}O$ record on the 405-kyr and ~20 and ~30-kyr lags of Ceara Rise's $\delta^{18}O$ and $\delta^{13}C$ isotope chronologies, respectively, on the ~100-kyr eccentricity periodicities (see [*Pälike et al.*, 2006a], their Fig. 3, panel c).

3.6.1.5 Matching Tests

Despite reasons to exclude obliquity and precession from our tuning targets, we test the sensitivity of the data to these higher frequency astronomical parameters because the obliquity and precession components explain almost 100% of the variance in insolation. Another reason to test for these higher astronomical frequencies is that our data are of sufficient resolution to resolve them, although the relatively low sedimentation rates (avg. ~1 cm/kyr) at Site 1264 could have preferentially distorted these signals. We now make a clear distinction between "tuning" and "matching". Tuning is the unambiguous identification of an interference pattern within or between different astronomical pace makers that can be aligned to a similar pattern in the data, whereas "matching" is the statistically optimal fit of the data to an astronomical template, given a set of input parameters (e.g. [*Lisiecki and Lisiecki*, 2002; *Pälike*, 2001]) and regardless of the uncertainties in the physical reality of that target or the signal in the source data. We perform three matching tests. The first matching test is to the La2011 eccentricity solution (E2011) that also forms our tuning target-curve, to see if we can improve the significance of higher frequency astronomical signals in the data by allowing relatively small age-model adjustments between ~100-kyr selected tie-points. For the 2nd and 3rd matching tests we selected the ET2004 and ETP2004 targets, both based on La2004 [*Laskar et al.*, 2004]. These matching-targets were made to mimic SH summer half insolation because the globally integrated isotope records probably predominantly responded to SH insolation forcing. During the Oligo-Miocene both the (sole and) largest ice cap and the main sources of deep-water formation were located in the SH [*Billups et al.*, 2002; *Zachos et al.*, 1997].

The "Match" algorithm is primarily designed to align records from different sites in the depth domain [*Lisiecki and Lisiecki*, 2002]. *Lisiecki and Lisiecki* [2002] argue that the program is not well suited for automated astronomical tuning. However, if we compare sedimentation rates based on our matching results to those based on a similar automated tuning method (i.e. dynamic time warping [*Pälike*, 2001]) used to align the isotope records from Sites 926/929 [*Pälike et al.*, 2006a] and Site 1218 [*Pälike et al.*, 2006b] to ETP target-curves, it becomes clear that our matching results are very comparable to these earlier algorithm-based age-calibrations (Supp. Fig. 3.03).

The three matching tests show that the data can be successfully aligned to target curves that contain higher frequency astronomical components (i.e. obliquity and precession). The success of the three matching tests is evaluated using evolutive analyses on the data (Figs. 3.08 – 3.10). The obliquity components in the $\delta^{18}O$ and $CaCO_3$ records can be significantly enhanced with the ET2004 match, in comparison to the E2011 tuning and match. Similar results are obtained on the precession frequencies in the $\delta^{13}C$ and (to a lesser amount) the $CaCO_3$ records. We note that the power on the obliquity frequency as found in the ET2004 matching results is often reduced in the ETP2004 matching results because power is shifted from the obliquity to the precession frequencies. Perhaps our precession frequency is too enhanced in our ETP2004 target curve, which makes that signal (and noise) are being redistributed across the different frequencies between matching options.

Despite the partial "success" of the matching sensitivity tests we have found no conclusive evidence that the higher frequencies (obliquity and precession) are truthfully recorded in the data. No clear ~1.2-Myr amplitude modulation has been identified, for example, in the ET2004 matched $\delta^{18}O$ record (see Fig. 3.07), suggesting that during the matching process noise and non-orbital variability is redistributed in the age domain. We advise to use the eccentricity tuned age model for future studies and correlation purposes.

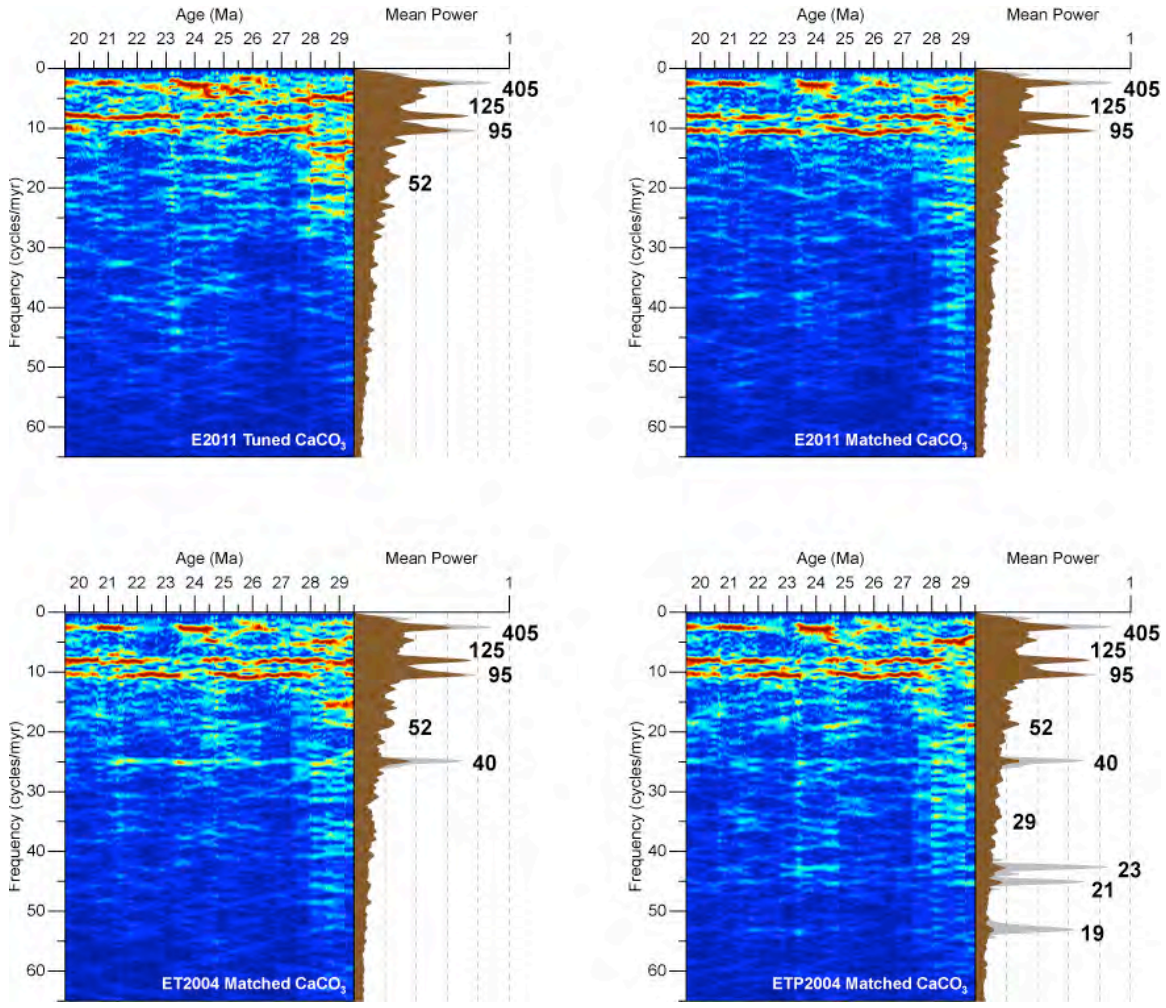

Figure 3.08: *Evolutive and spectral results of the composite $CaCO_3$ est. record from Sites 1264 and 1265 on the different tuned and matched age models. The grey power spectra in the background are calculated on the used tuning and matching targets and show the expected locations of the spectral peaks. Bold numbers refer to cycle periodicities in kyr. Note that when precession is included in the matching target (see ETP2004 Matched) then power in the obliquity band (see ET2004 Matched) is reduced.*

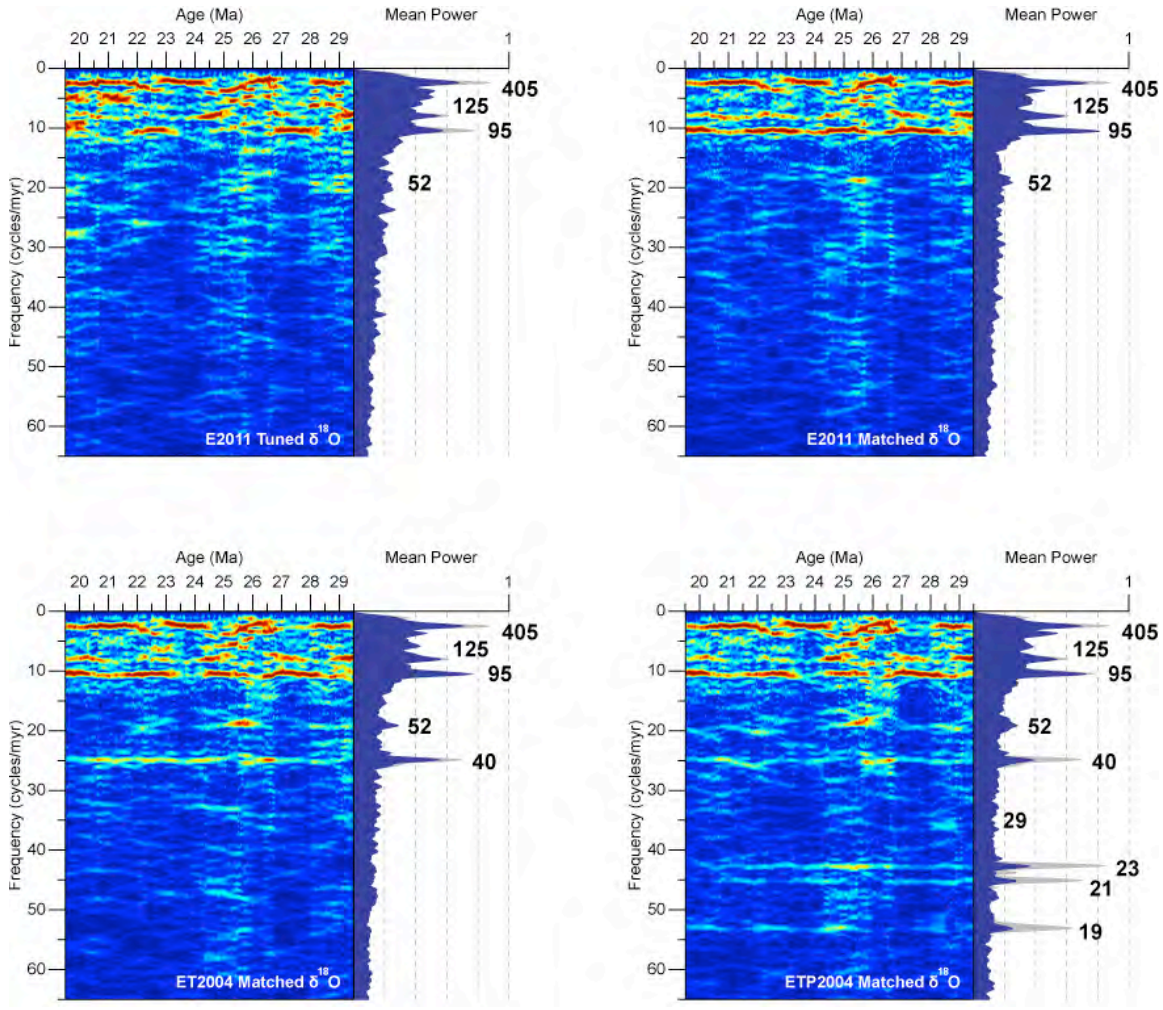

Figure 3.09: *Evolutive analyses results of the $\delta^{18}O$ record from Site 1264 on the different tuned and matched age models. The grey power spectra in the background are calculated on the used tuning and matching targets and show the expected locations of the spectral peaks. Bold numbers refer to cycle periodicities in kyr. Note that when precession is included in the matching target (see ETP2004 Matched) then power in the obliquity band (see ET2004 Matched) is reduced.*

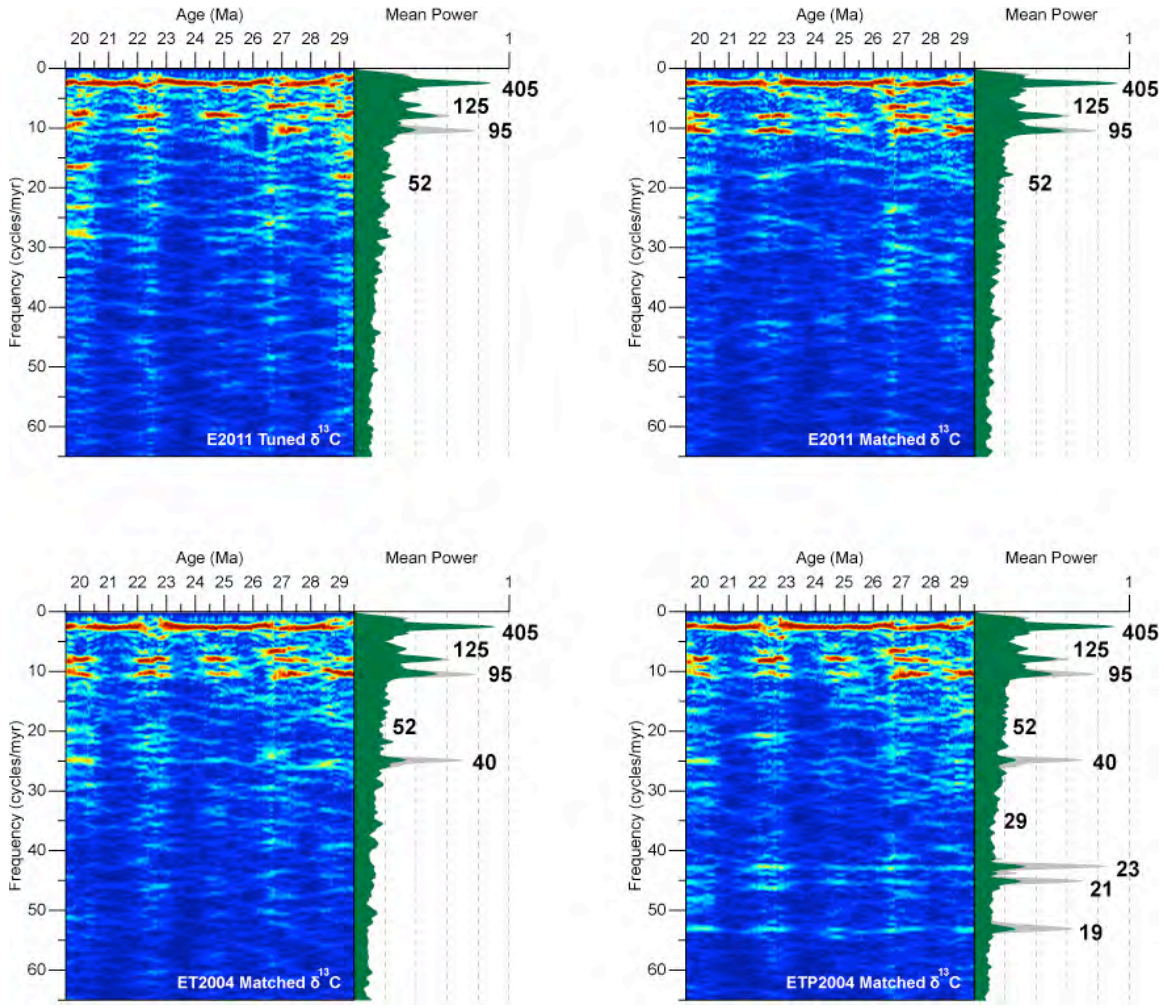

Figure 3.10: *Evolutive analyses results of the $\delta^{13}C$ record from Site 1264 on the different tuned and matched age models. The grey power spectra in the background are calculated on the used tuning and matching targets and show the expected locations of the spectral peaks. Bold numbers refer to cycle periodicities in kyr. Note that $\delta^{13}C$ is more susceptible to pick up a precession signal (see ETP2004 Matched) than an obliquity signal (see (ET2004 Matched).*

3.6.1.6 Sedimentation Rates and Size Fractions

The changes in linear sedimentation rates (LSR) of Site 1264 are typical for $CaCO_3$ dominated pelagic sites [*Zachos et al.*, 2004]. Peak LSRs are recorded across the OMT (Fig. 3.04), contemporaneous with a peak in %coarse fraction (predominantly size fractions 63 – 150 μm and >150 μm (Fig. 3.02). The 63 – 150 μm size fraction record shows a persistent increase between 27.5 – 23 Ma and a subsequent decrease between 23.0 – 21.5 Ma (not shown on age). We link these trends to changing climatic conditions and ecological circumstances contemporaneous with the late Oligocene warming trend and OMT that favoured the 63 – 150 μm sized microfossils over the 0 – 38 μm, 38 – 63 μm and >150 μm sized genera. Important to note is that the microfossil group size boundaries are arbitrarily selected, namely based on the mesh-size of the sieves, and that these results are not free from the closed-sum effect that can cause apparent variability in one size fraction resulting from changes in another (e.g. changes in the nannofossil dominated fine fraction). The increase in LSR across the OMB is synchronous with increased benthic foraminiferal accumulation rates at Site 1265 [*Diester-Haass et al.*, 2011] and may suggest (temporary) carbon burial in the deep sea as a contributing positive feedback to the transient OMT glaciation [*Diester-Haass et al.*, 2011; *Mawbey and Lear*, 2013].

3.6.1.7 Age Model Comparison

The palaeomagnetic records presented here [*Bowles*, 2006] on the tuned age model are probably not sufficiently resolved to further constrain the GPTS ages (Fig. 3.11, Table 3.01). Our ages generally support the ages of *Billups et al*. [2004], *Pälike et al.* [2006b] and the GTS2012 [*Hilgen et al.*, 2012; *Vandenberghe et al.*, 2012] between 30 – 19 Ma within the uncertainties related to site-to-site correlations (not shown), astronomical tuning (not known) and the exact position of the reversals in depth (see error bars Fig. 3.11). However our ages across Chron 7 (with the exception of C7n.2n(o)) appear anomalously young and do not compare well to the ages of the GTS2012 and *Cande and Kent* [1995]. These reversals are marked as "uncertain" by *Bowles* [2006]. Our tuned early Miocene ages between 23.5 – 20.5 Ma are consistently older by about 20 – 50 kyr.

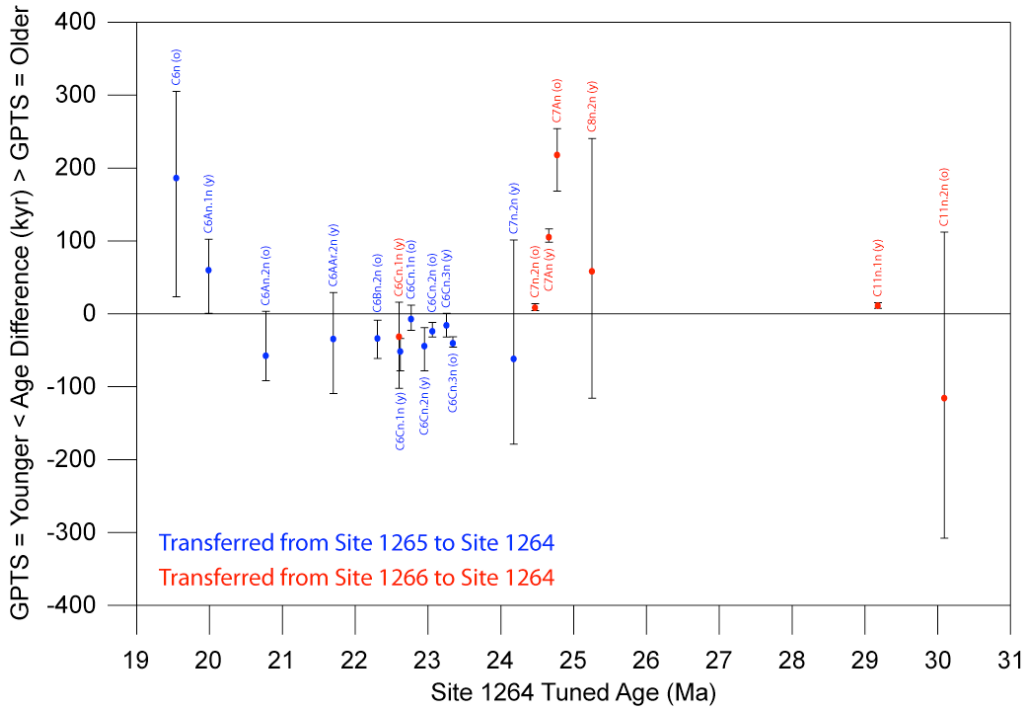

Figure 3.11: *Age differences between the tuned ages of Site 1264 and the Palaeogene and Neogene GTS ages between 31 and 19 Ma [Hilgen et al., 2012; Vandenberghe et al., 2012]. Error bars represent uncertainty of the exact position of the reversal in the depth domain, but they do not include the uncertainty resulting from the decimetre scale site-to-site correlations.*

Chron ID Bowles (2006)	Chron ID This Study	GTS2012 Age (Ma)	Top Depth (rmcd, Site 1264)	Mid Depth (rmcd, Site 1264)	Bottom Depth (rmcd, Site 1264)	Top Age (Ma)	Mid Age (Ma)	Bot Age (Ma)
Transferred from Site 1265								
C6n (o)	**C6n (o)**	19.722	220.45	221.44	222.80	19.416	19.534	19.698
C6An (y)	**C6An.1n (y)**	20.040	225.06	225.49	226.02	19.937	19.978	20.038
C6An (o)	**C6An.2n (o)**	20.709	231.40	231.71	231.98	20.705	20.765	20.800
C6Bn (y)	**C6AAr.2n (y)**	21.659	238.91	239.56	240.14	21.629	21.692	21.768
C6Bn (o)	**C6Bn.2n (o)**	22.268	245.14	245.47	245.85	22.276	22.300	22.328
C6Cn.1n (y)	**C6Cn.1n (y)**	22.564	248.52	248.68	248.95	22.597	22.614	22.641
C6Cn.1n (o)	**C6Cn.1n (o)**	22.754	250.07	250.26	250.41	22.741	22.759	22.776
C6Cn.2n (y)	**C6Cn.2n (y)**	22.902	251.88	252.15	252.48	22.920	22.944	22.979
C6Cn.2n (o)	**C6Cn.2n (o)**	23.030	253.04	253.14	253.25	23.041	23.052	23.061
C6Cn.3n (y)	**C6Cn.3n (y)**	23.233	254.99	255.13	255.29	23.231	23.247	23.264
C6Cn.3n (o)	**C6Cn.3n (o)**	23.295	255.85	255.97	256.07	23.325	23.334	23.340
C7n (y)	**C7n.2n (y)**	24.109	263.58	265.39	267.07	24.007	24.169	24.287
Transferred from Site 1266								
C6Cn (y)	**C6Cn.1n (y)**	22.564	248.03	248.48	249.19	22.547	22.594	22.665
C7n (o)	**C7n.2n (o)**	24.474	268.52	268.58	268.64	24.459	24.464	24.469
C7An (y)	**C7An (y)**	24.761	270.45	270.54	270.63	24.643	24.654	24.662
C7An (o)	**C7An (o)**	24.984	271.42	271.84	272.42	24.729	24.765	24.815
C8n (y)	**C8n.2n (y)**	25.304	274.15	275.34	276.68	25.063	25.244	25.419
C10n (y)	**C11n.1n (y)**	29.183	308.78	308.84	308.90	29.167	29.170	29.175
C10n (o)	**C11n.2n (o)**	29.970	315.55	317.77	319.69	29.857	30.084	30.277

Table 3.01: *Comparison between the astronomically tuned palaeomagnetic reversal ages (this study) and the ages of the GTS2012 [Hilgen et al., 2012; Vandenberghe et al., 2012].*

3.6.2 The Oligocene-Miocene Astronomical Forcing and Pacing Theory

3.6.2.1 Lack of Strong Precession and Obliquity Signals

The expression of eccentricity in al Site 1264 data sets is very strong, but eccentricity exerts almost no direct control on insolation quantities or distribution. Precession would instead be expected to be strongly present in the data as well, if a linear response-mechanism was involved. However, we only register a (very) weak precession imprint on our data. The resolution of the records (~3 kyr) is above the Nyquist frequency to resolve both precession and/or obliquity with average cycle thicknesses of ~20 and ~40 cm per cycle, respectively. With an estimated bioturbation depth of 7 to 10 cm, it could well be that these periodicities did influence our proxy records, but that their signals have been partially erased due to sediment mixing at the seafloor. Alternatively, diagenesis resulting from $CaCO_3$ dissolution and recrystallisation could have disturbed the higher frequency signals. Moderately preserved (i.e. "frosty") foraminifera at Site 1264 support some degree of diagenesis. Alternatively, the precession signal could have been cancelled out in the globally integrated proxy records, if an equal and out-of-phase NH and SH land-ice response to precession forcing was present during Oligo-Miocene, similar to what has been proposed for the dominant 40-kyr cyclicity during the early Pleistocene [*Raymo et al.*, 2006]. Finally, the two-to-three fold changes in LSRs (0.5 – 1.5 cm/kyr) may have distorted the higher frequencies in the depth domain, so that the precession, obliquity and eccentricity components begin to overlap in mean spectral power and especially the precession frequencies become harder to register (Fig. 3.06).

We speculate that the 160 – 200 kyr periodicity found in the power spectra of the isotope records from Site 1264 could represent a response to the ~180 kyr modulation of the 40-kyr obliquity or alternatively represent a harmonic response to two ~100-kyr eccentricity cycles. In either case, or a combination of the two, a non-linear climatic response mechanism must have been involved because no equally strong direct responses to obliquity or climatic precession are found. The ~180 kyr peak is also recognised in the amplitude modulation of spliced magnetic susceptibility records from Ceara Rise [*Shackleton et al.*, 1999] and in power spectra of an (obliquity-tuned) early Miocene benthic stable-isotope records from Site 1148 [*Tian et al.*, 2008], suggesting that it might indicate a global signal. At Walvis Ridge, however, the ~180 kyr peak in the power spectra of the ET2004 matched $\delta^{18}O$ record (Fig. 3.09) does not significantly increase compared to the power spectra of the same data on our manually E2011 tuned age model. Furthermore, only a

moderate ~180 kyr amplitude modulation of the 40-kyr filtered ET2004 matched $\delta^{18}O$ record is observed at Site 1264. Our data (from a site with relatively low sedimentation rates) thereby provides only weak support for a (non-linear) response to obliquity. If the 180 kyr modulation of obliquity could successfully be identified in other Meso- and Cenozoic records with a well resolved orbital imprint, taken together with the modulation of the 19 kyr precession component (or the 95 and 125 kyr eccentricity cycles), it has the potential to further constrain values for climate friction since it is not influenced by dynamics in the Earth-Moon system [*Laskar*, 1999].

No single record from a geological archive allows for a full estimation of causal relationships between higher frequency insolation parameters and global change. However, in spite of the weak(er) expression of (obliquity and) precession in the data from Site 1264, we tentatively explore the possibility that a linear control of climatic precession and obliquity on Oligo-Miocene global climate might have been smaller than previously thought [*Abels et al.*, 2007; *Pälike et al.*, 2006a; *Pälike et al.*, 2006b; *Tian et al.*, 2008]. Records from Sites 1090, 1218 and 926/929 record variable amounts of precession and obliquity influence [*Billups et al.*, 2004; *Pälike et al.*, 2006a; *Pälike et al.*, 2006b; *Tian et al.*, 2008]. These intervals with increased precession (and/or obliquity) power are not reproduced equally strong in this study. All earlier deep-sea astrochronologies have included precession and/or obliquity in their tuning-targets, which is a tuning-approach for the Oligo-Miocene that is debated and perhaps not suitable for all deep-sea records ([*Proistosescu et al.*, 2012], this study). The dominant expression of eccentricity in (most) benthic stable-isotope records appears difficult to reconcile with inferred early Oligocene glacio-eustatic sea level changes on the NW European continental shelf that are obliquity dominated [*Abels et al.*, 2007]. However power on ~100-kyr time scales could be resulting from a non-linear response to multiples of obliquity cycles, as has been suggested for the late Pleistocene ~100-kyr cycles [*Huybers and Wunsch*, 2005]. Such a view is only partially supported by our ET2004 matching results that show a stronger obliquity component in $\delta^{18}O$ (compared to the E2011 tuned $\delta^{18}O$ record), but show no clear ~1.2-Myr amplitude modulation of this cycle. The relatively low sedimentation rates at Site 1264 were probably not ideally suited to register and/or preserve obliquity cycles. At present no consensus exists on relative influences of higher frequency astronomical forcing on Oligo-Miocene globally integrated climate proxy records.

3.6.2.2 Eccentricity Dominance

The strong eccentricity signal in all Oligo-Miocene data from Site 1264 requires a non-linear mechanism to transfer power from the climatic precession band to eccentricity, just as the strong ~100-kyr cyclicity of the late Pleistocene glacial cycles does. For example NH summer insolation is regarded dominant in pacing glacial cycles during the late Pleistocene and the collapse of the Laurentide and Eurasian ice sheets is triggered by precession minima, obliquity maxima, or a combination of both [*Hays et al.*, 1976; *Huybers*, 2011]. The influence of the NH glaciations on globally integrated proxy records such as benthic $\delta^{13}C$, $\delta^{18}O$ and far-field (eustatic) sea level is so substantial that they can explain most of the variance in the records. During the Oligo-Miocene, the relatively long residence time of carbon in the oceans (10 – 100-kyr time scales [*Zachos et al.*, 2008]), the dissolution of deep-sea carbonates [*Pälike et al.*, 2006b], or the thermal inertia of large ice sheets [*Pollard and DeConto*, 2005] could have preferentially amplified longer and/or attenuated shorter periodicities. Oligo-Miocene atmospheric pCO_2 levels are reconstructed to be higher and more variable than those of the Pleistocene. [*Beerling and Royer*, 2011; *Pagani et al.*, 2005]. With values ranging between ~400 and ~1000 ppmv [*Pagani et al.*, 2005] the modelled instability thresholds of the Laurentide, Greenland and West-Antarctic ice-sheets would have been exceeded [*DeConto et al.*, 2008]. We argue that under these conditions large fluctuations in East Antarctic ice volume are needed to explain the ~1 ‰ variability in $\delta^{18}O$ on glacial-interglacial timescales. Data-constrained forward (i.e. inverse) modelling of the $\delta^{18}O$ signal from Site 1264 supports this view and suggest that between 20 – 80% of the $\delta^{18}O$ signal (depending on the phase of the glacial cycle) can be attributed to ice-volume changes on the East Antarctic ice sheet [*Liebrand et al.*, 2011, Chapter 2].

Given that a non-linear response mechanism must have been at play to explain the strong ~100 and 405-kyr eccentricity signals in $\delta^{13}C$ and $\delta^{18}O$, and that the Oligo-Miocene boundary conditions probably favoured a dynamic East Antarctic ice sheet, we speculate that a "proximal" (i.e. SH summer temperature) control on Antarctic land-ice accumulation and ablation is the most probable driver. We regard this as a more parsimonious explanation compared to the alternative; a "distal" NH summer temperature control, with the opposite phase of precession. The latter would require as of yet unknown teleconnections between hemispheres, unless a mechanism can be conceived that would make the pre-Plio-Pleistocene marine carbon cycle and/or Antarctic ice sheet more sensitive to extended SH summer duration (i.e. NH summer temperature = precession minima) than to SH summer temperature extremes (precession maxima) [*Huybers*, 2011]. Earlier

astronomical age-calibration studies in which $\delta^{18}O$ is aligned to a $La2004_{nominal}$ eccentricity-obliquity-precession mix inherently assume a response to NH summer temperature [*Billups et al.*, 2004; *Pälike et al.*, 2006a; *Pälike et al.*, 2006b]. We regard this option as less likely and favour a direct SH summer (extreme high) temperature control for the Oligo-Miocene. A SH summer temperature control on Oligo-Miocene Antarctic ice sheet expansion is similar to our fundamental understanding of the control that insolation exerts on Plio-Pleistocene glaciations on the Northern Hemisphere. Finally, the weaker expression of obliquity in our stable-isotope records could support a non-linear summer insolation control on Oligo-Miocene benthic isotope data because summer insolation is precession dominated, the eccentricity modulation of which we find in the data. However the low relative power of obliquity in our data could be compromised by the relatively low sedimentation rates and bioturbation.

3.6.2.3 Long-Period Climate Pacing

Sequences of increased amplitude responses of the data records to ~100-kyr eccentricity coincide 400-kyr maxima during ~2.4-Myr eccentricity maxima (Figs. 3.05 – 3.07). The ~2.4-Myr cycle is also expressed in the modulation of the 405-kyr filtered $\delta^{13}C$ record. When we place our data into a broader Meso-/Cenozoic context, by comparison with other high-resolution stratigraphies, this strongly suggests that the 405-kyr carbon cycle variability is persistently controlled by a ~2.4-Myr eccentricity pacing from the Cretaceous [*Sprovieri et al.*, 2013], through Palaeo-Eocene [*Littler et al.*, 2014; *Lourens et al.*, 2005] to (at least) the Oligo-Miocene ([*Boulila et al.*, 2012; *Pälike et al.*, 2006b], this study). However a temporary switch to the ~1.2-Myr modulation of obliquity remains a possibility resulting from scarcity of Mesozoic and early Cenozoic records. Our $\delta^{18}O$ data only partially supports the view that the power of ~100-kyr cycles increases during obliquity nodes [*Abels et al.*, 2005; *Holbourn et al.*, 2005; *Pälike et al.*, 2006a; *Pälike et al.*, 2006b; *Wade and Pälike*, 2004] (Fig. 3.05 and 3.07). Not all ~1.2-Myr obliquity nodes result in increased amplitude responses to the ~100-kyr eccentricity cycle and, because the ~1.2-Myr nodes of obliquity generally "saddle" the ~2.4-Myr eccentricity maxima, deconvolving the relative contributions of these very long-period cycles to global change is difficult. An increased ~100-kyr amplitude response may therefore be the result from the reduced amplitude of obliquity (during a ~1.2-Myr minimum) or the increased amplitude of eccentricity (during a ~2.4-Myr maximum). The identified ~2.4-Myr eccentricity cycle pacing of the major climatic events in the Oligocene and early Miocene partially conflicts with earlier pacing theories that suggested

stronger influence of the ~1.2-Myr obliquity cycle [*Pälike et al.*, 2006b] and 2 × to 4 × 400-kyr eccentricity cycles [*Liebrand et al.*, 2011, Chapter 2]. Our $\delta^{13}C$ record is too short to investigate the presence of a ~9 Myr cycle, however the amplitude modulation of the 405-kyr filtered $\delta^{13}C$ data (Fig 3.07) shows the strongest ~2.4-Myr cycles at ~23.6 Ma, contemporaneous with the (predicted) ~9 Myr eccentricity maximum, thereby perhaps giving some further support for this hypothesis [*Boulila et al.*, 2012; *Ikeda and Tada*, 2013; *Sprovieri et al.*, 2013].

3.7 Conclusions

We present high-resolution and near-continuous $\delta^{18}O$ and $\delta^{13}C$ chronologies from South Atlantic Site 1264. These benthic records are generated on a single species (*Cibicidoides mundulus*), and span the 30 – 19 Ma window. Our time-series are strongly eccentricity dominated. The weak expression of (obliquity and) climatic precession might be regarded as atypical for Oligo-Miocene high-resolution climate proxy records, but guides our decision to base the age model solely on the eccentricity solution. This age calibration approach is further strengthened by the unknown phase relation of the global climatic response to precession forcing and by the poorly constrained values for climate friction during Oligo-Miocene time, which affects both the stability of obliquity and precession in the ephemerides. Our eccentricity tuning is broadly in agreement with earlier astronomical age calibration studies and within error of GPTS2012 age calibrations of palaeomagnetic reversals.

Our records show variable amplitude responses to eccentricity and especially amplified ~100 and 405-kyr responses are found to be paced by the ~2.4-Myr eccentricity cycle. This view of phase locking of the global climate system to (predominantly) eccentricity during the early phase of the Cenozoic Icehouse revises previous Oligo-Miocene astronomical pacing and forcing theories that attributed stronger to almost sole linear control of obliquity (and precession) on global change. Our $\delta^{18}O$ data show that most of the sensitivities in the global (high-latitude) Oligo-Miocene ocean-atmosphere-cryosphere system lie on the 100-kyr timescales.

3.8 Acknowledgements

We thank Daniel Kelly for providing archived samples, Walter Hale, Alex Wülbers, David Naafs and Alice Lefebvre for help with additional sampling, Jan Drenth and Ian Croudace for help with freeze-drying the samples, Geert Ittman and Dominika Kasjaniuk, for help with washing samples, Anastasia Tsiola and Mischa Saes for help with washing and pre-picking samples, Thomas Westerhold and Ursula Röhl for their advise on XRF core scanning, Linda Hinnov for providing her evolutive analyses MATLAB-script, Christian Zeeden for help with the Hilbert-transform, and Samantha Gibbs and Isabella Raffi for their help with searching to *Sphenolithus delphix*. Discussion with Steven Bohaty, Paul Wilson, Sietske Batenburg, Frits Hilgen, Doug Wilson, and Eelco Rohling were particularly helpful. We used samples provided by the Ocean Drilling Program, sponsored by the US National Science Foundation and participating countries under the management of Joint Oceanographic Institutions. This research has been made possible by the European Community's Seventh Framework Programme (grant agreement number 215458).

3.9 Supplementary Information to Chapter 3

MID- TO HIGH-RESOLUTION OLIGOCENE-MIOCENE ASTRONOMICAL AGE CALIBRATION STUDIES					
Study	**Proxies**	**Age model**	**Age interval**	**GPTS age calibration**	**Selected references**
Ceara Rise Sites (925), 926, (928), 929 | XCB (some RCB) drilled | 3.6 - 4.4 km water depth | high-resolution					
[Shackleton et al., 1999] [Shackleton et al., 2000]	PMAG (Site 522), Phys. Prop., B: *C. mundulus*	**Initial:** Obliquity cycle count (floating) [Weedon et al., 1997] **Tuning signal:** Phys. Prop. **Tuning target:** Nominal La'93, T&P (T dominated)	34.0 - 14.0 Ma	Chron 7 - 6 (Along d13C correlation of Site 929 to Site 522)	[Berggren et al., 1995] [Cande & Kent, 1995] [Flower et al., 1997a] [Flower et al., 1997b] [Tauxe et al., 1984] [Tauxe and Hartl, 1997] [Weedon, 1997] [Weedon et al., 1997] [Zachos et al., 1997]
[Pälike et al., 2006a]	Phys. Prop., %CF, B: *C. mundulus, C. cresbi*	**Initial:** [Shackleton et al., 1999] **Tuning signal:** Phys. Prop. **Tuning target:** Nominal La'04, ETP (T dominated), 5 kyr lag on T	26.5 - 17.5 Ma	n/a (isotope correlation of Sites 926/929 to Site 1090 confirm results [Billups et al., 2004])	[Billups et al., 2004] [Pälike and Shackleton, 2000] [Paul et al., 2000] [Shackleton et al., 1999] [Shackleton et al., 2000] [Zachos et al., 2001]
Agulhas Ridge Site 1090 | APC drilled | 3.7 km water depth | high-resolution					
[Billups et al., 2004]	PMAG, B: *C. preamundulus, C. dickersoni, C. eocaenus, C. havanensis, C. mundulus, O. umbonatus*	**Initial:** [Cande & Kent 1995] [Shackleton et al., 2000] **Tuning signal:** d18O **Tuning target:** Nominal La'04, ETP (T dominated)	24.0 - 16.0 Ma	Chron 7 - 5	[Billups et al., 2002] [Channell et al., 2003] [Gersonde et al., 1999] [Shackleton et al., 1999] [Shackleton et al., 2000]
Equatorial Pacific Site 1218 | APC (late Oligo. - early Mio.), XCB (late Eo. - early Oligo.) | 4.8 km water depth | high-resolution					
[Pälike et al., 2006b]	PMAG, Phys. Prop., XRF, bulk, B: *Cibicidoides. spp, C. grimsdalei, C. havanensis, P: G. venezuelana*	**Initial:** PMAG and biostrat. ages from literature **Tuning signal:** d18O/d13C **Tuning target:** Nominal La'04, ETP (E dominated)	34.0 - 21.5 Ma	Chron 13- 6	[Coxall et al., 2005] [Flower et al., 2006] [Lanci et al., 2004] [Lanci et al., 2005] [Lear et al., 2004] [Lyle et al., 2002] [Pälike et al., 2005] [Wade and Pälike, 2004]
South China Sea Site 1148 | APC (Plio-Pleisto) & XCB (Oligo. - Mio.) drilled | 3.3 Km water depth | mid-resolution					
[Tian et al, 2008]	Phys. Prop., B: C. wuellerstorfi, C. kullenbergi (mundulus), Uvigerina sp. Cibicidoides spp. Oridorsalis sp.	**Initial:** [Lourens et al., 2004] **Tuning signal:** Phys. Prop. **Tuning target:** Nominal La'04, Obliquity (T) only	24.5 - 0.0 Ma	n/a	[Lourens et al. 2004] [Wang et al 2000]
Walvis Ridge Sites 1264, (1265), (1266) | APC drilled | 2.5 km water depth | high-resolution					
THIS STUDY	PMAG (Sites 1265/1266), Phys. Prop., XRF, B: *C. mundulus*	**Initial:** [Lourens et al., 2004], long eccentricity cycle count **Tuning signal:** XRF/d18O **Tuning target:** Nominal La'11, eccentricity (E) only	30.0 - 19.0 Ma	Chron 11 - 5 (Along Phys. Prop./XRF correlation of Sites 1265/1266 to Site 1264)	[Bowles et al., 2006] [Liebrand et al., 2011] [Lourens et al. 2004] [Zachos et al., 2004]

Supplementary Table 3.02: *Overview of Oligo-Miocene astronomical age calibration studies on ODP cores with benthic isotope chronologies.*

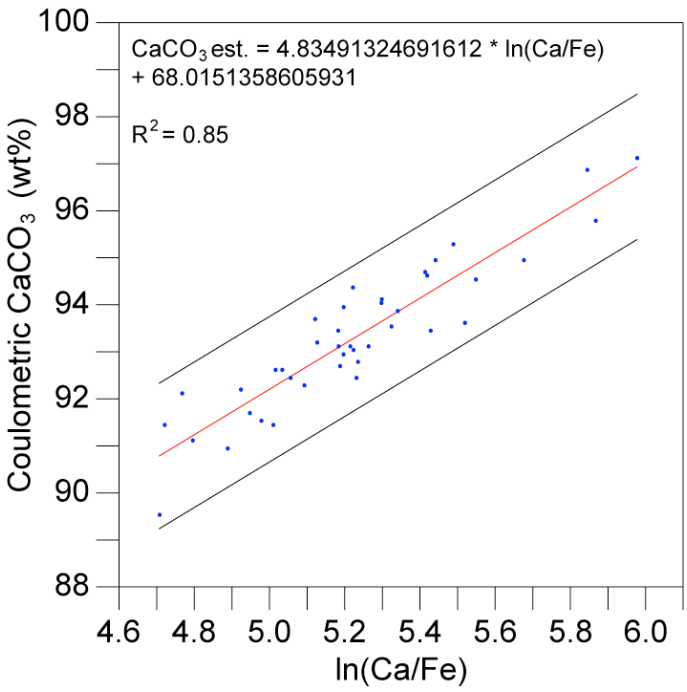

Supplementary Figure 3.12: *Calibration between ln(Ca/Fe) XRF data and shipboard coulometric $CaCO_3$ measurements from Site 1264. We removed one outlier. Red line is the calibration used. Black lines represent 1 standard deviation of the coulometric $CaCO_3$ data. This calibration is also used to calculate $CaCO_3$ estimates for Site 1265.*

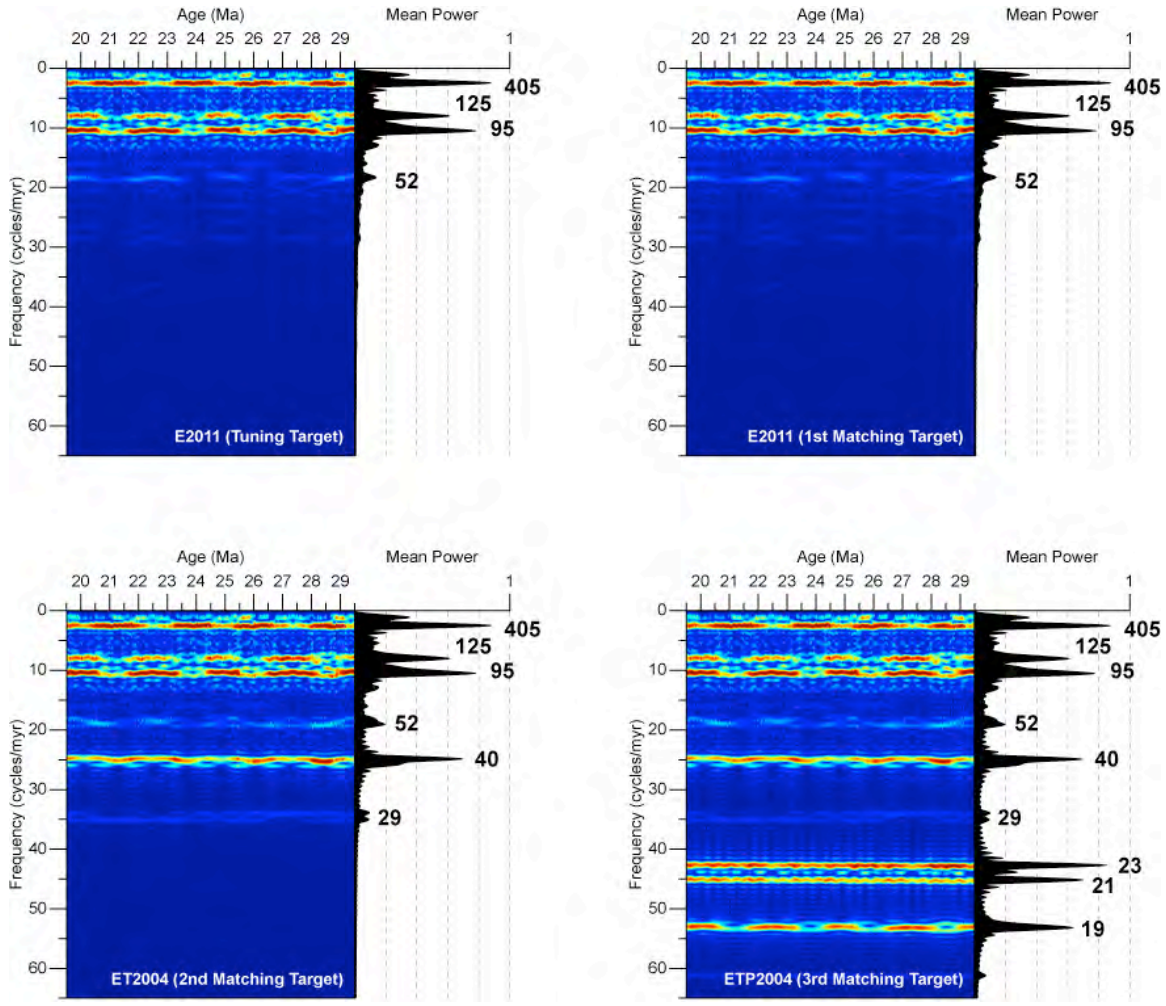

Supplementary figure 3.13: *Evolutive analyses results of the different tuning and matching targets. Bold numbers refer to cycle periodicities in kyr. Note that the ~52 kyr period is combination of eccentricity and obliquity components (compare E2011 with ET2004).*

Match 2.0 [*Lisiecki and Lisiecki*, 2002] Configurations:

Match between $CaCO_3$ est. (ln(Ca/Fe)), $\delta^{18}O$, $\delta^{13}C$ and eccentricity (E2011):
nomatch 15.2, speedchange 0.53, speedpenalty 0.71, gappenalty 70, gapsizemultiplier 0.122627, tiepenalty 100000, reversetiepenalty 0, begin1 198.75, end1 317.81, numintervals1 5954, begin2 15.5, end2 30.1, numintervals2 5954, normbegin1 NaN, normbegin2 NaN, normend1 NaN, normend2 NaN, tiefile autotune.tie, #series1gaps is not set., #series2gaps is not set., matchfile autotune.match, #matrixfile is not set., logfile autotune.log, #mean1 is not set., #mean2 is not set., #stddev1 is not set., #stddev2 is not set., series1 lnCaFeISO.txt d18O.txt d13C.txt, series2 e2011short.txt e2011short.txt e2011short.txt, speeds 3:1 5:2 2:1 5:3 3:2 4:3 5:4 1:1 4:5 3:4 2:3 3:5 1:2 2:5 1:3, targetspeed 1:1

Match between $CaCO_3$ est. (ln(Ca/Fe)), $\delta^{18}O$, $\delta^{13}C$ and eccentricity + obliquity (ET2004):
nomatch 15.1, speedchange 0.53, speedpenalty 0.71, gappenalty 69, gapsizemultiplier 0.122627, tiepenalty 100000, reversetiepenalty 0, begin1 198.75, end1 317.81, numintervals1 5954, begin2 15.5, end2 30.1, numintervals2 5954, normbegin1 NaN, normbegin2 NaN, normend1 NaN, normend2 NaN, tiefile autotune.tie, #series1gaps is not set., #series2gaps is not set., matchfile autotune.match, #matrixfile is not set., logfile autotune.log, #mean1 is not set., #mean2 is not set., #stddev1 is not set., #stddev2 is not set., series1 lnCaFeISO.txt d18O.txt d13C.txt, series2 ET2004short.txt ET2004short.txt ET2004short.txt, speeds 3:1 5:2 2:1 5:3 3:2 4:3 5:4 1:1 4:5 3:4 2:3 3:5 1:2 2:5 1:3, targetspeed 1:1

Match between $CaCO_3$ est. (ln(Ca/Fe)), $\delta^{18}O$, $\delta^{13}C$ and eccentricity + obliquity + precession (ETP2004):
nomatch 15.1, speedchange 0.53, speedpenalty 0.7, gappenalty 69, gapsizemultiplier 0.122627, tiepenalty 100000, reversetiepenalty 0, begin1 198.75, end1 317.81, numintervals1 5954, begin2 15.5, end2 30.1, numintervals2 5954, normbegin1 NaN, normbegin2 NaN, normend1 NaN, normend2 NaN, tiefile autotune.tie, #series1gaps is not set., #series2gaps is not set., matchfile autotune.match, #matrixfile is not set., logfile autotune.log, #mean1 is not set., #mean2 is not set., #stddev1 is not set., #stddev2 is not set., series1 lnCaFeISO.txt d18O.txt d13C.txt, series2 ETP2004short.txt ETP2004short.txt ETP2004short.txt, speeds 3:1 5:2 2:1 5:3 3:2 4:3 5:4 1:1 4:5 3:4 2:3 3:5 1:2 2:5 1:3, targetspeed 1:1

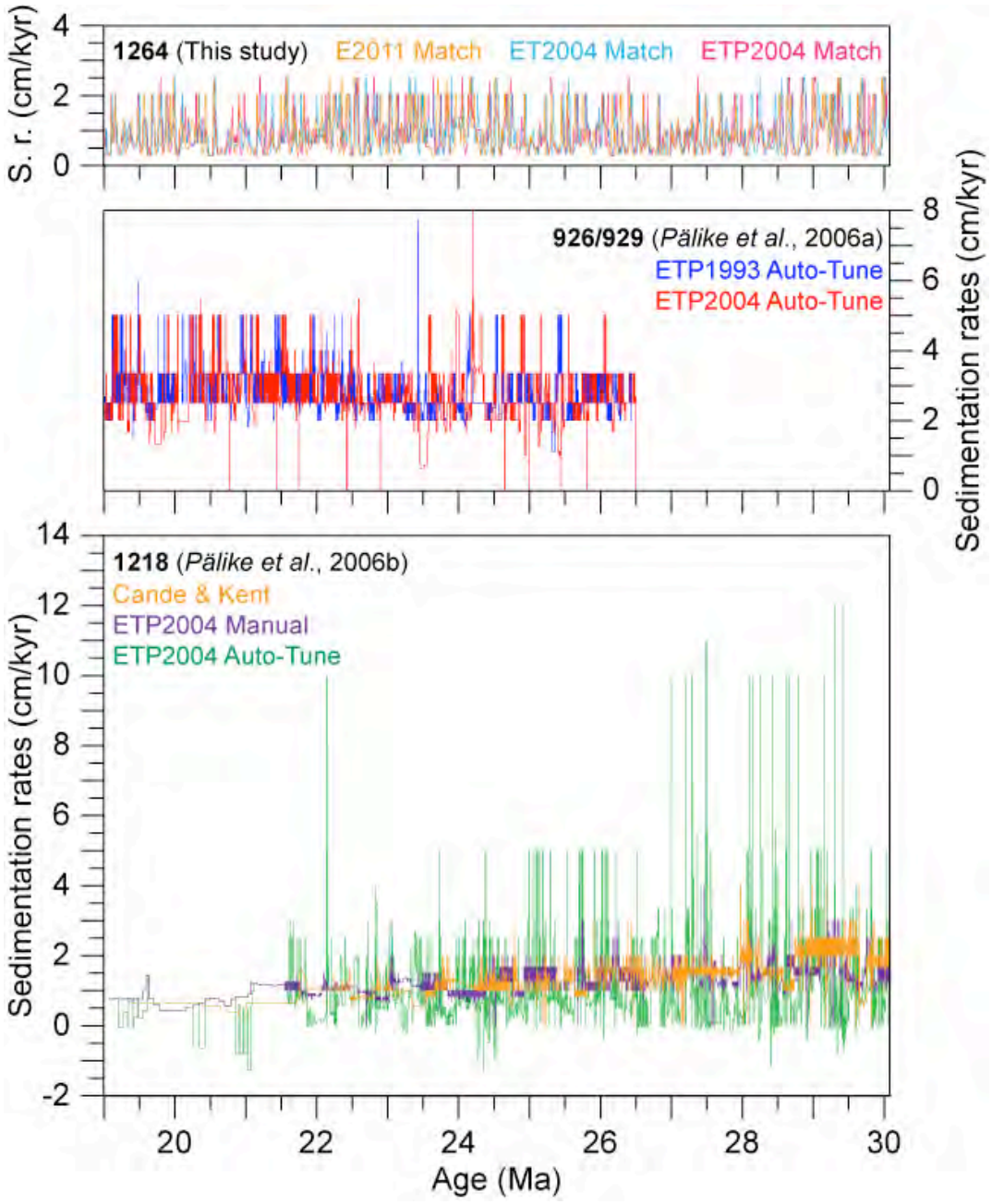

Supplementary Figure 3.14: *"Automated tuning" [Pälike, 2001] and "matching" [Lisiecki and Lisiecki, 2002] age-calibration approaches compared through sedimentation rates (1st derivative of the age-depth relation) between 30 – 19 Ma. The sedimentation rates based on the matched age models presented in this study compare well to those previously published [Pälike et al., 2006a; Pälike et al., 2006b] that were based on an alternative automated tuning method. Similar rapid step-wise changes in sedimentation rates are present (to various degrees) in all age models to optimise the correlation between the geologic data and an astronomical template of choice.*

CHAPTER 4:

TRANSIENT SYNCHRONISATIONS OF OLIGO-MIOCENE CLIMATE AND ICE SHEETS TO ECCENTRICITY

4.1 Abstract

Deconvolving linear from non-linear response mechanisms of Earth's climate to astronomical forcing is key in understanding internal dynamics, response times and thresholds. No investigations into the evolution of (non-) linearity in the climate system, on astronomical timescales, for the Oligo-Miocene have taken place to date. We present climate proxy records, from Walvis Ridge, southeastern Atlantic Ocean that resolve the high-latitude temperature and global ice volume evolution on astronomical time scales. Our near-continuous 11 million-year-long records span a key interval in Earth history, across the "mid" Oligocene and Oligo-Miocene. We find recurrent episodes of high-amplitude ~100-kyr cycles in benthic foraminiferal $\delta^{18}O$ that are phase-locked to changes in the eccentricity of Earth's orbit, notwithstanding an increasing phase lag through time. This suggests transient and recurrent rapid responses (synchronisations) of Earth's climate system, deep-sea temperatures and large ice sheets to astronomical climate forcing. Furthermore, it indicates an evolution through the Oligo-Miocene interval in the climatic/cryospheric response time and threshold respond-mechanism. We speculate that this increasing response time and the evolution of a threshold can be linked to the development of non-linear ice sheet response mechanisms in the early Miocene and suggest that it could be related to the evolving topography on East Antarctica and its effect on the carrying capacity of the ice sheet. Alternatively long-term trends in pCO_2 could have caused changes in the cryospheric response to astronomical climate forcing. Our data suggests that the early EAIS was very sensitive to astronomically controlled changes in radiation balance throughout the Oligo-Miocene, but started to show stronger hysteresis towards the end of the early Miocene (~ 19 Ma). Exceptionally high $\delta^{18}O$ values across the Oligocene – Miocene Transition suggests an additional, significant land-ice contribution, probably on Greenland or West Antarctica.

4.2 Introduction

The East Antarctic Ice Sheet (EAIS) is one of the slowest responding physical components in Earth's climate system and requires 100s – 1000s of years to fully equilibrate to changes in radiative forcing [*Imbrie and Imbrie*, 1980]. In light of continuously increasing anthropogenic greenhouse gas (GHG) emissions that have reached Oligo-Miocene-equivalent atmospheric CO_2 levels of ≥ 400 ppmv [*ESRL/NOAA*], investigations of past climates characterised by a (predominantly) unipolar Icehouse state, under similar to present and future GHG conditions, are crucial to better constrain the natural variability, rates of change and dynamics of the EAIS.

The major glaciation events during the early phase of Earth's Cenozoic glaciated history are generally thought to be contemporaneous with periods of reduced seasonal insolation extremes resulting from ~1.2-Myr obliquity "nodes" [*Miller et al.*, 1991; *Pälike et al.*, 2006b; *Wright and Miller*, 1992]. Support for obliquity as the dominant pacemaker of high-latitude (and global) climates and glacio-eustacy has come from high-resolution proxy records spanning different parts of the Oligo-Miocene interval [*Abels et al.*, 2007; *Billups et al.*, 2004; *Pälike et al.*, 2006a; *Tian et al.*, 2008; *Zachos et al.*, 2001a]. Intervals with more dominant responses to ~100 and 405-kyr eccentricity-modulated-precession have also been described [*Holbourn et al.*, 2013; *Holbourn et al.*, 2014; *Pälike et al.*, 2006b], Identification of dominant pacemakers of changes in global climate and cryosphere are crucial to constrain response times and to understand where internal sensitivities lie. Well resolved globally integrated climate proxy records are needed. Our 11-Myr long records shows that, during most of the "mid" Oligocene (informal stage name) through early Miocene, the Earth system predominantly responded to ~100-kyr, 405-kyr and ~2.4-Myr eccentricity cycles. The congruence between glaciations and ~1.2-Myr obliquity nodes were less frequent than previously thought [*Pälike et al.*, 2006b]. Furthermore, our extended record no longer supports a non-linear response to multiples of the ~400-kyr eccentricity cycle [*Liebrand et al.*, 2011, Chapter 2], but rather supports non-linear phase-locking of the climate system to intervals (often ~400-kyr in duration) with strong ~100-kyr cycles during ~2.4-Myr eccentricity maxima. We refer to these recurrent sequences of events as as "transient synchronisations".

Younger Icehouse records, although good analogues to study ice sheet dynamics under boundary conditions more similar to present-day, display a complex interaction of Northern and Southern Hemisphere ice ages [*De Boer et al.*, 2012; *Raymo et al.*, 2006]. The Oligocene and early Miocene (between 34 and 17 Ma) represents the earliest phase of Cenozoic glaciated history with

evidence of land-ice on Antarctica [*Naish et al.*, 2001], whereas the presence of significant ice sheets on the Northern Hemisphere at this time is unclear [*Eldrett et al.*, 2007; *Moran et al.*, 2006]. This (inferred) persevering unipolar Icehouse state makes that ice mass effects imprinted on benthic $\delta^{18}O$ effectively represent changes in the mass of the combined West and East Antarctic ice sheets, probably without the additional obscuring contributions of other significant land-ice masses elsewhere. The current reconstructions of atmospheric pCO_2 for the Oligocene range between 400 and 1000 ppmv [*Beerling and Royer*, 2011; *Pagani et al.*, 2005; *Zhang et al.*, 2013]. A sharp drop at 24 Ma, roughly 1 Myr prior to the Oligocene Miocene transition (OMT) brings the range of values for the early Miocene to broadly vary (± 100) around 400 ppmv [*Beerling and Royer*, 2011; *Pagani et al.*, 2005; *Zhang et al.*, 2013] – values which have already been reached [*ESRL/NOAA*] by current GHG emission [*IPPC*, 2013].

4.3 Site description and Methods

We present extended [*Liebrand et al.*, 2011, Chapter 2] high-resolution (2.5 cm, ~3 kyr) single-species benthic foraminifer (*Cibicidoides mundulus*) stable oxygen and carbon isotope records from Walvis Ridge Site 1264 (28°31.955'S, 2°50.730'E, 2505 m water depth), drilled during Ocean Drilling Program Leg 208 [*Zachos et al.*, 2004], with near-continuous sediments spanning the mid Oligocene – early Miocene (30 – 17 Ma) interval. In addition we present high-resolution X-ray fluorescence (XRF) core scanning records that have been used to verify the shipboard composite depth scale of our study interval. The natural logarithm of Ca over Fe counts is calibrated to $CaCO_3$ estimates (est.). Spectral, evolutive and wavelet analyses indicate that the data have recurrent power on frequencies ranging from 0.25 – 1 cyc/m. On an initial, untuned age model [*Liebrand et al.*, 2011, Chapter 2] the XRF and isotope records are eccentricity dominated and show spectral power on frequencies ranging from 2.5 – 10 cyc/Myr.

At the distal and relatively shallow Site 1264, the XRF-based $CaCO_3$ estimates are a primarily a measure of productivity. Benthic $\delta^{13}C$ values are offset to other Atlantic $\delta^{13}C$ chronologies [*Billups et al.*, 2004; *Pälike et al.*, 2006a] by ~0.5‰, reflecting a more ^{12}C-depleted water mass that probably results from Site 1264's shallower position. Benthic $\delta^{18}O$ visually resolves glacial-interglacial cycles at an unprecedented level, making it a reference record for future high-resolution studies.

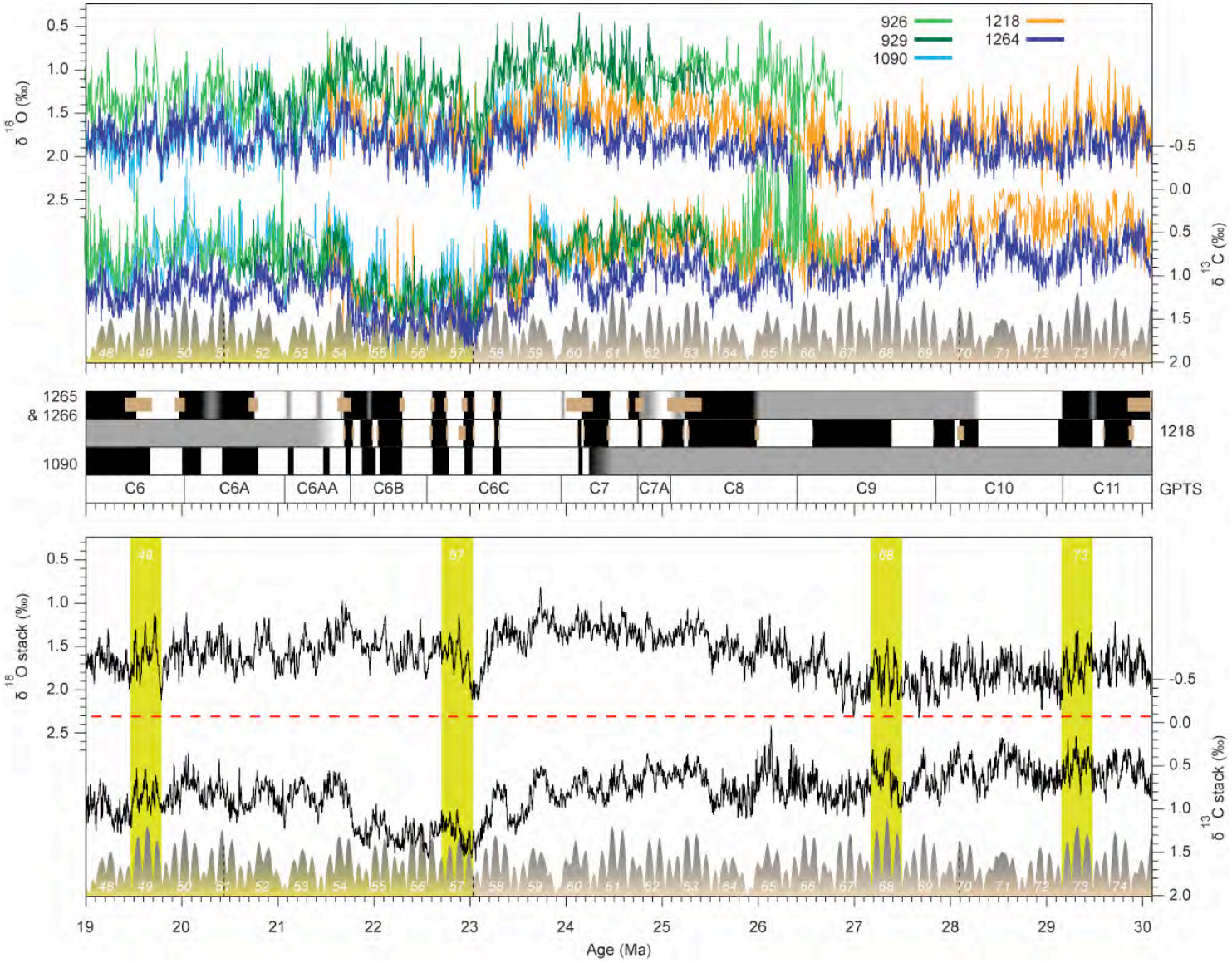
926
929
1090
1218
1264
δ 18O (‰)
δ 13C (‰)
1265
& 1266
1090
1218
C6
C6A
C6AA
C6B
C6C
C7
C7A
C8
C9
C10
C11
GPTS
δ 18O stack (‰)
δ 13C stack (‰)
Age (Ma)

*<< **Figure 4.01:** Overview of high-resolution benthic foraminiferal $\delta^{18}O$ and $\delta^{13}C$ stratigraphies across the Oligo-Miocene study interval. Top panel shows high-resolution records that have been correlated to Site 1264 and subsequently plotted on the ~100-kyr eccentricity tuned age model. The middle panel indicates how well the different magnetostratigraphic records compare to the GPTS. Around Chrons 7 and 9 (near coring gaps in the record from Site 1264) the correlation needs improvement. The bottom panel shows the stacked $\delta^{18}O$ and $\delta^{13}C$ records. For different intervals, the stack consists out of the equally weighted averages of 2 – 5 records. Higher $\delta^{18}O$ values across the mid Oligocene (compared to the OMT, see red dashed line), also noted at Site 1218 [Pälike et al., 2006b], are probably resulting from diagenesis and isotopic 'drifting' at the deeper Sites 1218, 926, 929 and 1090. At Site 1264 the OMT has the heaviest $\delta^{18}O$ values. The stack represents the average of 2 – 5 isotope records and the offsets in absolute values also explain the heavier $\delta^{18}O$ values during the mid Oligocene, compared to the OMT. The intervals (green bars) with strong variability on ~100-kyr timescales are also present in the stacked records and correspond to 2.4-Myr maxima.*

We explore the dual effects of temperature and ice volume on benthic $\delta^{18}O$ by direct comparison with other Atlantic and Pacific high-resolution chronologies. A stack is generated through equal weighing between records (Fig. 4.1). The stack represents the "global" (i.e. deep water/high latitude temperature and ice volume) consensus. The remaining variance in the individual $\delta^{18}O$ chronologies is resulting from variable temperature effects, diagenetic histories, noise and/or laboratory techniques. Varying sample processing procedures followed, inter-laboratory offsets in $\delta^{18}O$ determinations [*Ostermann and Curry*, 2000], benthic foraminifer species offsets from equilibrium [*Shackleton*, 1974] and/or taxonomic definitions can explain up to an estimated 0.4‰. The recurrent intervals with strong variability on ~100-kyr time scales, as identified at Site 1264 are also present in $\delta^{18}O$ records from Sites 926 and 929 [*Pälike et al.*, 2006a; *Zachos et al.*, 1997; *Zachos et al.*, 2001a], Site 1218 [*Pälike et al.*, 2006b] and Site 1090 [*Billups et al.*, 2004]. No other site, however, registers these episodes at the achieved clarity of Site 1264. Inverse modelling also accounts for a relatively large Antarctic contribution [*Liebrand et al.*, 2011, Chapter 2] to $\delta^{18}O$ (~0.5‰ of the signal on average on the ~100 and 405-kyr periodicities). These data comparisons and mass-balance/isotope fractionation calculations support the view that cycle geometry as identified at Site 1264 is a truthful recorder of, and proxy for, Antarctic ice sheet dynamics.

The Site 1264 records are age-calibrated to the stable $La2011_{(nominal)}$ [*Laskar et al.*, 2011a; *Laskar et al.*, 2011b] eccentricity solution, to which the phase relation on glacial-interglacial time scales is clear (e.g. [*Pälike et al.*, 2006a; *Pälike et al.*, 2006b]). The eccentricity solution is free from uncertainties related to climate friction [*Laskar et al.*, 2004]. Our initial age model was based on limited bio-/magnetostratigraphic age control points [*Bowles*, 2006] and subsequent 405-kyr (~3.7 m) cycle counts. The ~100-kyr (i.e. 95, 99, 124 & 131-kyr) eccentricity interference patterns were identified in tuning-target (eccentricity) and signals ($CaCO_3$ est., $\delta^{18}O$ and $\delta^{13}C$) and subsequently aligned, in which the final tie-point assignment for the entire record is solely based on the alignment of $CaCO_3$ maxima to eccentricity minima.

4.4 Results and Discussion

The Site 1264 eccentricity calibrated records span an 11-Myr long mid Oligocene – early Miocene interval (30 – 19 Ma, Fig. 4.01). Amplitude variability is observed on 10^3 – 10^6 year time-scales and is present on all major eccentricity periodicities. Multi-Myr trends in $CaCO_3$ (est.) indicate deepening of the lysocline in the early Miocene (22.6 – 19.3 Ma) in the mid-latitude South Atlantic. Trends and patterns in our single-species (*Cibicidoides mundulus*) stable-isotope records are comparable to equivalent (often multi-species) Pacific [*Pälike et al.*, 2006b] and Atlantic [*Billups et al.*, 2004; *Pälike et al.*, 2006a] chronologies, suggesting that a significant part of the variance in our data reflects global processes. Multiple episodes with enhanced ~100-kyr cyclicity are identified in the amplitude modulation of the filtered time series. These intervals correspond to 405 and ~2.4-Myr eccentricity maxima. The evolving glacial-interglacial cycle shape shows increasing asymmetry (i.e. sawtooth patterns) that indicates the origination of an increased threshold response mechanism of the Antarctic ice sheet(s).

The largest $\delta^{18}O$ variability of ~1‰ present in the Site 1264 record is predominantly in response to astronomical forcing on short (~100-kyr) eccentricity time scales. This conflicts with the prevailing paradigm and accompanying Oi and Mi naming scheme [*Miller et al.*, 1991; *Wright and Miller*, 1992] that the largest 'glaciations' are spaced ~1.2-Myr apart and paced by minima in the amplitude modulation of obliquity during which seasonal extremes (i.e. very warm summers) are reduced for substantial periods of time. We implement a 405-kyr cycle numbering scheme.

Unlike other $\delta^{18}O$ records that span the OMT, Site 1264 shows a two-step increase across the event, spaced 405-kyr apart (Fig. 4.01), reminiscent of the two steps across the Eocene – Oligocene transition (EOT) [*Coxall and Wilson*, 2011]. Similar to the EOT, a positive correlation with $\delta^{13}C$ is present in both instances, suggestive of strong coupling(s) between Earths carbon cycle, global climate and ice mass [*Diester-Haass et al.*, 2011; *Mawbey and Lear*, 2013]. A eustatic sea level lowering could explain this observed coupling, as has been suggested for the EOT [*Merico et al.*, 2008]. The first, step at 23.6 Ma, together with the drop in pCO_2 [*Beerling and Royer*, 2011; *Pagani et al.*, 2005; *Zhang et al.*, 2013] at ~24.0 Ma are contemporaneous with a strong ~2.4-Myr eccentricity minimum and these astronomically forced carbon cycle events most likely preconditioned the climate system for the major transient glaciation between 23.2 – 22.8 Ma. Our record is too short to evaluate the pacing of the Oligo-Miocene carbon maxima on 10^7 year time scales [*Boulila et al.*, 2012]. The rapid onsets and terminations of the 'carbon maxima' [*Hodell and Woodruff*, 1994] suggest threshold response mechanisms resulting from positive feedbacks such as increased primary and export productivity and organic carbon burial [*Mawbey and Lear*, 2013]. We speculate that the a nonlinear response of the carbon cycle is controlled by sea level thresholds, perhaps in a similar manner as to the mechanism proposed for the EOT [*Merico et al.*, 2008], whereby a lowering of the sea level results in exposure and carbonate weathering of shelf sea carbonates. Benthic $\delta^{18}O$ values reach their maximum values during a ~100-kyr plateau (23.1 – 23.0 Ma) contemporaneous with a 405-kyr eccentricity minimum and a ~1.2-Myr obliquity node. This plateau represents a 'missing' response to a low amplitude ~100 eccentricity cycle. Values are an additional 0.1 – 0.3 ‰ heavier in comparison to other glaciation events, suggesting the presence of additional land ice on not-previously glaciated highlands (e.g. Greenland or West Antarctica). This view is tentatively supported by numerical- [*DeConto et al.*, 2008] and data constrained forward-modelling [*Liebrand et al.*, 2011, Chapter 2]. The deepening of the CCD and lysocline in the Angola basin followed 0.5 Myr after maximum glaciated conditions, a signal that is also recorded in the North Atlantic Ocean [*Norris et al.*, 2014].

Our $\delta^{18}O$ record from Site 1264 shows that the OMT is not a unique event during the early phase of Earth Cenozoic glaciated history. Episodes with similar glaciation histories are found in early and late Oligocene and early Miocene (Figs. 4.02 and 4.03). These episodes have similar durations compared to the events across the OMT and also show sensitivity of the climate system to ~100-kyr forcing (Fig. 4.03.). We speculate that these episodes represent glacial expansion (during the early Miocene) and subsequent high-amplitude ~100-kyr variability of the Antarctic

ice sheet(s) and global climate system. They can be perceived as natural experiments, or "repeating" glaciation histories, under changing initial and boundary conditions, which makes comparison of these events across our 11-Myr long record the tool to identify when (and perhaps why and how) these conditions changed.

The 'first' strong ~100-kyr $\delta^{18}O$ cycle of each 405-kyr window appears to shows the largest lag compared to the subsequent cycles, which are more in-phase with eccentricity (Fig. 4.3). It is however not possible to test for this observation using Blackman-Tukey cross-spectral analyses because the length of the individual windows is too short. The absolute strength of the 'later' ~100-kyr cycles (per window) appear to be more attenuated relative to the earlier cycles, thereby only partially mimicking the eccentricity solution (Fig. 4.3). This results in (apparent) ~200 kyr cycles post mid Oligocene and post OMT. The two transient synchronisations during the early Miocene were preceded by large glaciations, however this is not (as strongly) present in the Oligocene part of the record.

With eccentricity-modulated-precession identified as the main pacemaker, we expect that larger amplitude ~100-kyr forcing would have resulted in larger responses, something that is only partly supported by the amplitude modulation of the ~100-kyr filtered $\delta^{18}O$ data (Fig. 4.02). All the recurrent intervals with strong 100-kyr variability correspond with 405-kyr and ~2.4-Myr maxima, however not all 405-kyr maxima resulted in strong responses, indicating that non-linear response mechanisms were involved. The phase-locking between eccentricity forcing on 100-kyr time-scales and the response of the climate system is stable and continuous. The relation between $\delta^{18}O$ maxima (and subsequent intervals with high amplitude ~100-kyr variability) to the ~1.2-Myr obliquity nodes is more ambiguous and only the maximum glacial conditions across the OMT fall exactly together with an obliquity node.

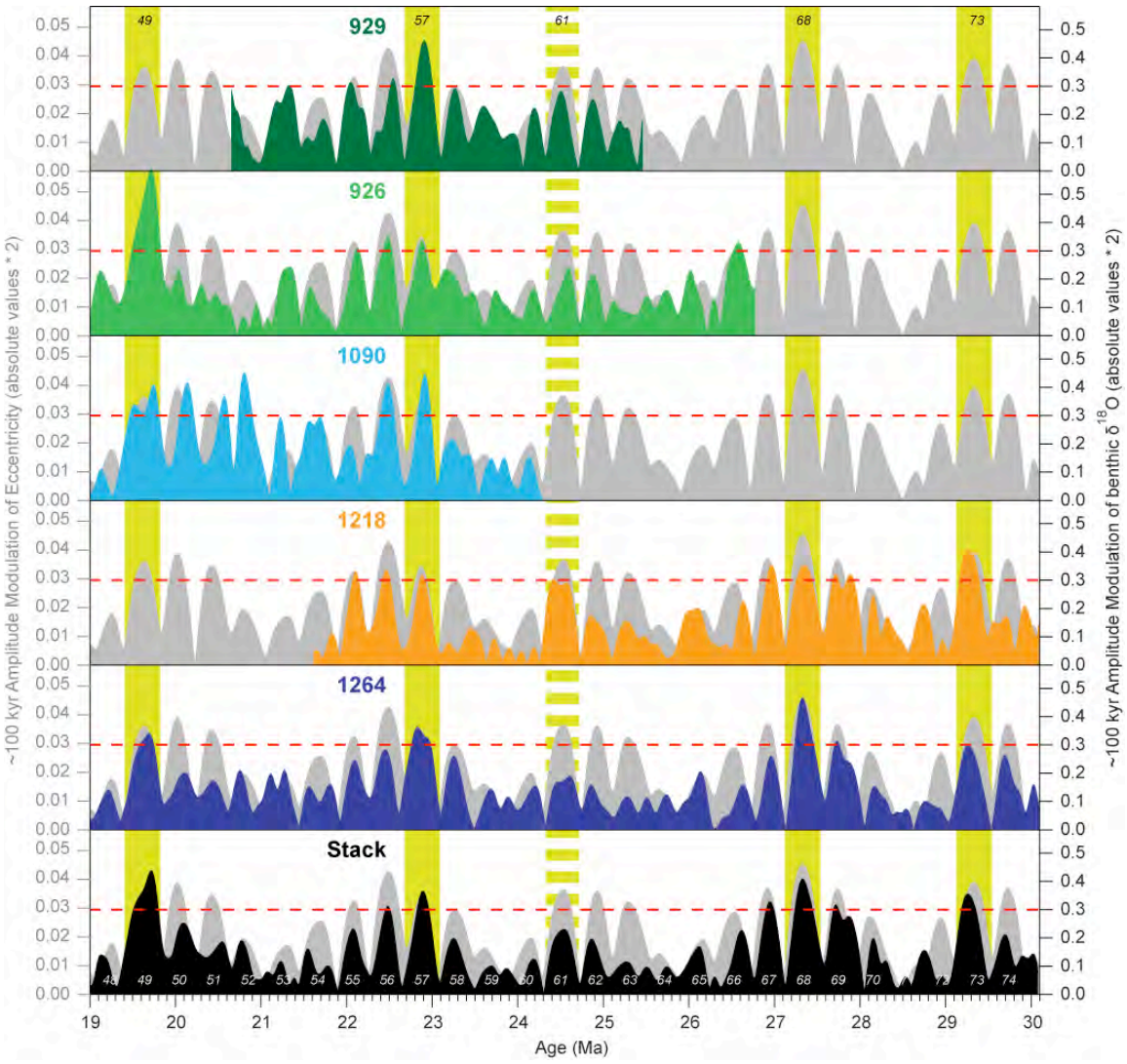

Figure 4.02: *Comparison of ~100-kyr amplitude modulation of high-resolution Oligo-Miocene benthic* $\delta^{18}O$ *stratigraphies. We argue that the similarities in the ~100-kyr response between these records support the global nature of the transient synchronisations of Earth's climate and ice sheets to eccentricity as identified in the record from Site 1264.*

To understand changing glacial dynamics we quantify the geometry of the ~100-kyr cycles in $\delta^{18}O$ and track their skewness and (a)symmetry. We interpret this as a measure of threshold response or (non-) linearity in the response of system Earth to astronomical climate forcing [*King*, 1996]. On 100-kyr time scales the $\delta^{18}O$ record displays increasing asymmetry through the mid Oligocene and early Miocene (Figs 4.03 and 4.04), in response to (symmetrical) eccentricity forcing, indicating the origination of a threshold response mechanism. The sudden terminations of the 100-kyr cycles in the early Miocene are also recognised in other benthic isotope chronologies (Fig. 4.01). This suggests that a globally integrated (e.g. ice sheet) mechanism is a more likely explanation for this observed change in cycle geometry than regional or local mechanisms, such as a threshold response in bottom water overturning circulation (e.g. [*Ganopolski and Rahmstorf*, 2001]). We suggest that the evolving threshold response can be directly linked to changing boundary conditions of the EAIS.

*>> **Figure 4.03:** Selection of recurrent glacial episodes and subsequent transient synchronisations of variability in Earth's Oligo-Miocene Antarctic ice volume to eccentricity, compared to ~100-kyr cycles in a Pleistocene stack [Lisiecki and Raymo, 2005]. The green horizontal band represents the broad "full" Antarctic base level. Absolute values of the base level are different between the Pleistocene stack and the $\delta^{18}O$ record from Walvis Ridge, because no correction (of +0.64 ‰) has been made to the latter record. However they do represent the same fixed 'base level' in all panels.*

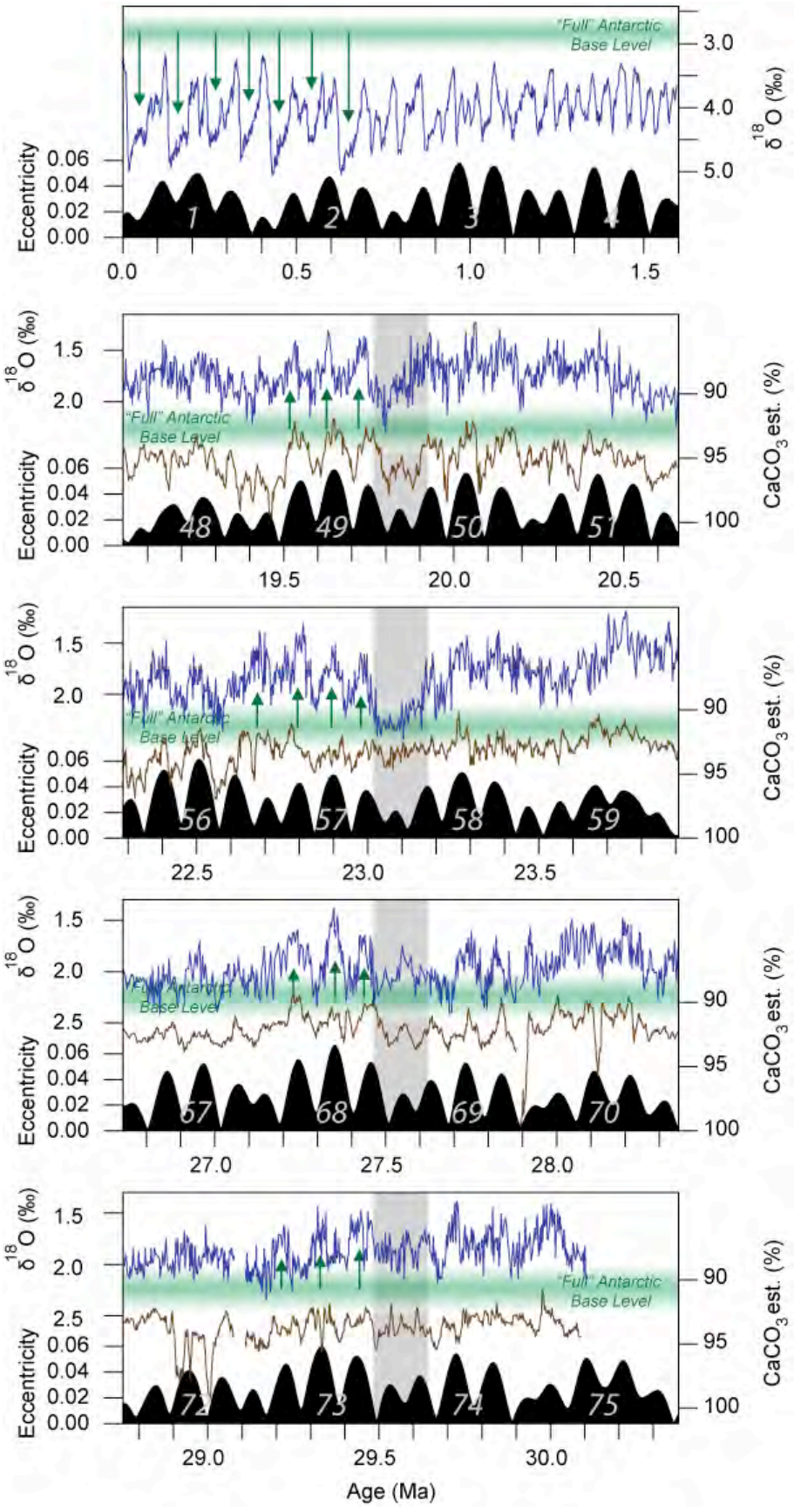
"Full" Antarctic Base Level
Eccentricity
δ18O (‰)
CaCO3 est. (%)
Age (Ma)

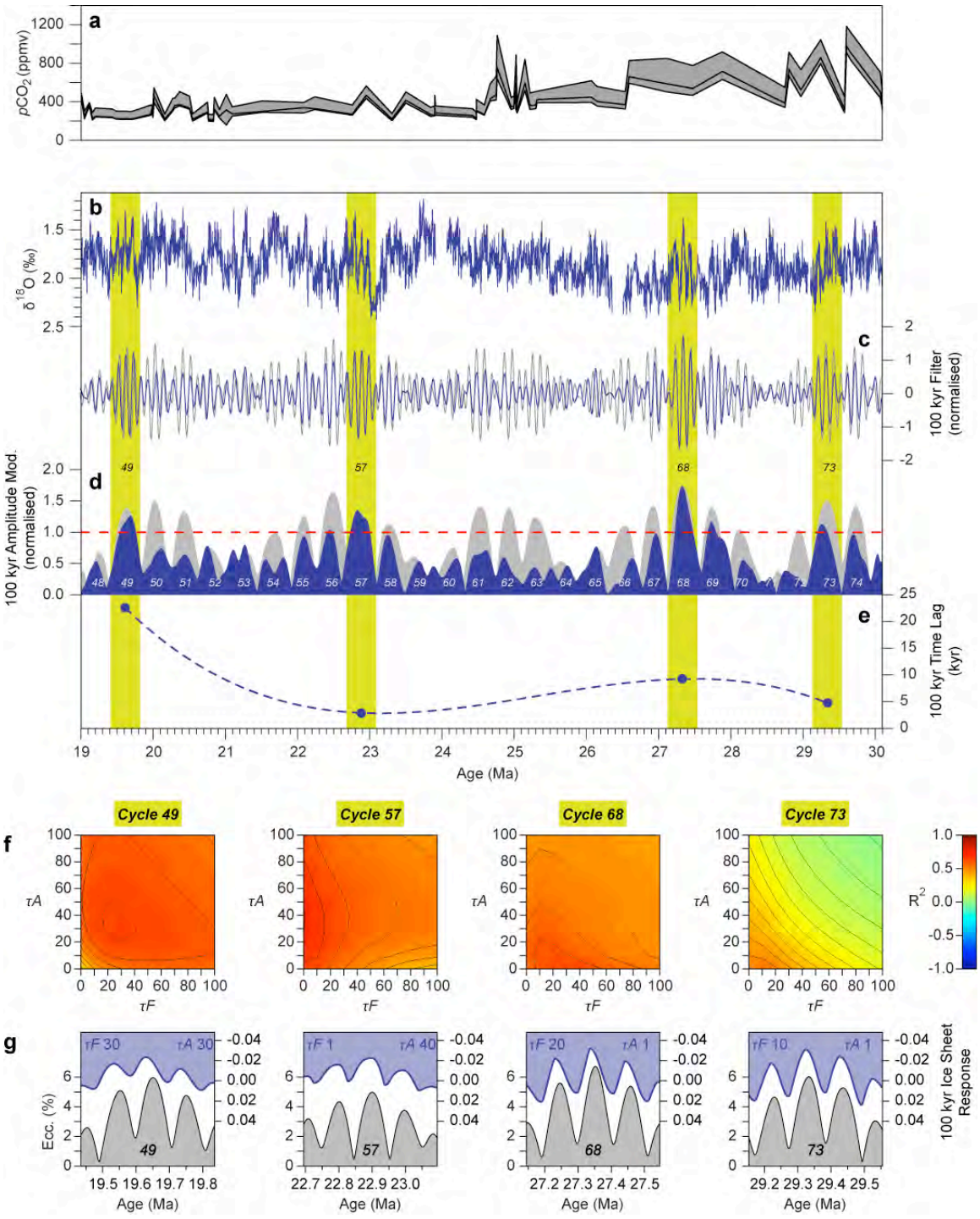
a
pCO_2 (ppmv)
1200
800
400
0
b
$\delta^{18}O$ (‰)
1.5
2.0
2.5
c
100 kyr Filter (normalised)
d
100 kyr Amplitude Mod. (normalised)
e
100 kyr Time Lag (kyr)
49
57
68
73
Age (Ma)
f
Cycle 49
Cycle 57
Cycle 68
Cycle 73
τA
τF
R^2
g
τF 30
τA 30
τF 1
τA 40
τF 20
τA 1
τF 10
τA 1
Ecc. (%)
100 kyr Ice Sheet Response
Age (Ma)

*<< **Figure 4.04:** Evolving ~100-kyr response time and cycle geometry across the four main transient synchronisations of Earth's climate and cryosphere to eccentricity during the Oligo-Miocene. **(a)** Reconstructed pCO_2 for the Oligo-Miocene (data of [Beerling and Royer, 2011; Pagani et al., 2005; Zhang et al., 2013]). **(b)** Raw $\delta^{18}O$ data from ODP Site 1264. **(c)** Gaussian filter of the combined 95 kyr and 125 kyr periodicities (centred around ~110 kyr) of the eccentricity solution and notch filtered (high-pass) $\delta^{18}O$ data. **(d)** Amplitude modulation of the filters in panel b. Red line represents arbitrary cut-off value for the transient synchronisations that are analysed further. **(e)** Results of cross-spectral analyses across the four intervals with strongest ~100-kyr variability in $\delta^{18}O$. Dashed line represents a 3rd order polynomial fit and suggests the possible evolution of ~100-kyr time lag (of $\delta^{18}O$ to eccentricity) if the synchronisations had not been transient. **(f)** Correlation test between the Imbrie and Imbrie model [1980] (calculated using analyseries [Paillard et al., 1996]) and the notch-filtered benthic $\delta^{18}O$ across the four main transient synchronisations (405-kyr duration) of Earth's cryosphere to ~100-kyr eccentricity. Eccentricity was inserted in the model and fusion time scale (τF) and accumulation time scale (τA) were set to cover values between 0 - 100. The R^2 landscape indicates for which values of τF and τA the correlation to $\delta^{18}O$ across a 405-kyr window is best. In other words: the imbrie model output splits the time lag (panel d) into a lag in warming and a lag in cooling. τF and τA can be expressed (back calculated) in lag in kyr (to the combined 95 and 125 kyr ecc cycles) through an arctangent relation. **(g)** The ice sheet response functions with the highest R^2 compared to eccentricity (top left: τF value, top right: τA value, bottom: 405-kyr cycle number).*

Using the model of *Imbrie and Imbrie* [1980] we calculate [*Paillard et al.*, 1996] 121 ice-sheet response curves (based on the eccentricity solution) by gradually changing the fusion (τF) and accumulation (τA) time scales. We take the correlation coefficient between $\delta^{18}O$ and the model output over a 400-kyr window across the intervals with the transient synchronisations as a measure of asymmetry (panel f in Fig. 4.04) and plot the curves with the highest r^2 values (panel g in Fig. 4.04). An increase in both τF and τA is observed suggesting that the response of the global climate system/ice sheets was more sluggish during the early Miocene in comparison to the late Oligocene. We speculate that this is suggestive of greater thermal inertia of the Antarctic ice sheet, or more dampened pCO_2 fluctuations (radiative forcing and air temperatures) on astronomical time scales during the early Miocene.

$CaCO_3$ dissolution in the deep-sea could possible influence observed cycle geometry. Our $CaCO_3$ est. record tracks the lysocline migration, indicating that the Oligocene and late early Miocene were relatively more affected by dissolution than the early Miocene. However $CaCO_3$ values have remained high (>90%) and Site 1264 was well above the calcite compensation depth (CCD) during the entire late Palaeogene and Neogene [*Zachos et al.*, 2004]. No unidirectional distortion of cycle geometry has been discerned (Fig 4.04).

Palaeotopographic reconstructions of West Antarctica indicate that tectonic evolution and glacial erosion affected boundary conditions drastically over the past 34 Myrs [*Wilson and Luyendyk*, 2009]. We cannot distinguish between relative contributions of West and East Antarctica, however, it is likely that glacial erosion, both on West and East Antarctica removed large quantities of sediment, during the 170 or so ~100-kyr glacial cycles that occurred during the early unipolar Icehouse phase (34 – 17 Ma). This would have continuously altered the topographic landscape and the background conditions for glaciations and most likely affected the carrying capacity of the EAIS over time [*Gasson et al.*, 2012; *Jamieson and Sugden*, 2008; *Jamieson et al.*, 2008; *Jamieson et al.*, 2010; *Pollard and DeConto*, 2003]. This could have culminated in a more dome-shaped EAIS during the early Miocene compared to a more flattened one during the mid Oligocene. Although volume- (or mass-) wise, land-ice quantities on East Antarctica were probably similar, as inferred from absolute $\delta^{18}O$ values, we speculate that the more dome-shaped early Miocene ice-cap had a greater thermal inertia and this resulted in an increased threshold response with more sudden deglaciations.

Alternatively the main control on the evolution of a threshold response mechanism is not ice sheet shape, but atmospheric pCO_2 (panel a in Fig. 4.04). No astronomically resolved Oligo-Miocene pCO_2 reconstructions have been published to date, however the long-term trends suggest a significant lowering, from ~800 to ~400 ppmv [*Beerling and Royer*, 2011; *Pagani et al.*, 2005; *Zhang et al.*, 2013], at around ~24 Ma. Air temperature has the main control on the line between ablation and accumulation of snow on the ice sheets, and because pCO_2 has a direct effect on radiative forcing (and hence air temperature) a change in pCO_2 could also explain the change in ~100-kyr cycle geometry that we observe.

Regardless of the main control on global climate/ice sheet response times during the Oligo-Miocene, our data suggests that the ice sheets were much more dynamic on ~100-kyr time scales than state-of-the-art coupled climate/ice sheet models would suggest [*DeConto and Pollard*,

2003a]. This could have profound implications for the hysteresis properties currently present in those models. Alternatively atmospheric pCO_2 was variable, on astronomical time scales, to an extent that has no Quaternary equivalent, especially during the Oligocene.

Our $\delta^{18}O$ data show that the ~100-kyr cyclicity is dominating climate and EAIS variability during the early unipolar Icehouse. Similar periodicities have been found to pace early Eocene hyperthermals and late Pleistocene variability of the Laurentide and Eurasian ice sheets, suggesting that regardless of climate state (i.e. Greenhouse, unipolar Icehouse or bipolar Icehouse) several and widely varying components of Earth's climate system expose a tendency to phase lock with eccentricity.

CHAPTER 5:

CONCLUSIONS, SOCIETAL SIGNIFICANCE AND FUTURE WORK

The preceding chapters of this thesis are based on Oligo-Miocene XRF and benthic stable-isotope records from ODP Site 1264 (30 – 17 Ma). The benthic foraminiferal oxygen and carbon stable-isotope chronologies from Site 1264 represent the highest-resolution near-continuous records to date. In this time interval they are unique in the fact that they are generated on a single-species, the benthic epifaunal foraminifer *Cibicidoides mundulus*. All records show an exceptionally strong imprint of eccentricity and, surprisingly, very attenuated obliquity and precession signals. The response of the Oligo-Miocene climate and ice sheets to the ~100-kyr eccentricity forcing (through the amplitude modulation of precession) reveals a highly non-linear relation, whereby certain intervals, generally spanning one or two 405-kyr cycles, show a much amplified response. These transient synchronisations of global climate to ~100-kyr eccentricity, always fall together with relatively stronger ~100 kyr cycles (and weaker 405-kyr cycles) during ~2.4-Myr eccentricity maxima and are often preceded by strong glaciations, such as the glaciations associated with the mid Oligocene and OMT intervals. Detailed correlations to other high-resolution chronologies reveals that the $\delta^{18}O$ signal from Walvis Ridge carries a strong global signal, perhaps more so than that it carries signals of (local) bottom water temperatures or (regional) South Atlantic or high-latitude climate variability. In this final chapter the research objectives outlined in Chapter 1 and the study methodologies, results and discussions of Chapters 2 – 4 are evaluated and summarised, to identify the key conclusions. The implications of this research for society are discussed and an outlook on future work that can be undertaken to further our understanding of the Oligo-Miocene is given.

5.1 Conclusions

5.1.1 Astronomical Pacemakers of Global Significance

One purpose of generating a new high-resolution benthic stable-isotope chronology for the Oligo-Miocene is to test the reproducibility of previously published mid to high-resolution records [*Billups et al.*, 2004; *Pälike et al.*, 2006a; *Pälike et al.*, 2006b; *Tian et al.*, 2008; *Zachos et al.*, 1997]. Most of these records show the imprint of (precession,) obliquity and ~100 and 405-kyr

eccentricity, with the greatest variance found on the obliquity frequencies in the Ceara Rise, Agulhas Ridge and South China Sea records [*Billups et al.*, 2004; *Pälike et al.*, 2006a; *Tian et al.*, 2008]. Only at the equatorial Pacific most variance in the data is found on the eccentricity periodicities [*Pälike et al.*, 2006a]. This is an enigma, since benthic stable oxygen and carbon isotope records are generally thought to predominantly record and reflect global (or high-latitude in the case of oxygen) processes. Our new, unprecedentedly high-resolution, single-species chronology from a shallower site is the least noisy available to date and is only partially compromised by the low-to-average pelagic sedimentation rates. Despite this compromising factor it is evident that the dominant pacemakers of the Oligo-Miocene have successfully been identified; namely ~100-kyr eccentricity in case of $\delta^{18}O$ and 405-kyr eccentricity in case of $\delta^{13}C$. These findings in part conflict with earlier astronomical pacing theories that attributed (more) dominant variability to obliquity (and precession). We argue that the selection of suitable astronomical tuning target curves is crucial in obtaining an unbiased view of the true variability in the marine climate archives.

5.1.2 Global Climate and Oceanographic Change

A second objective of the research presented here is to track global change throughout the Oligo-Miocene on time scales ranging from the astronomic to the tectonic. To achieve this goal, detailed correlations between all (new and previously published) high-resolution chronologies are constructed. To accurately quantify changing isotopic gradients between sites, water depths and basins, the correlations need to be precise and accurate to (at least) the ~100-kyr level. We have achieved such detailed correlations (with the exception of two short intervals near gaps in the Site 1264 record that need further improvement) and show that the gradients, levels of variability, trends and absolute isotope values are highly variable in the Oligo-Miocene. No clear, single explanation has been found for the differences between the records. However it is most likely that prevailing climatic Icehouse conditions resulted in multiple localities for deep-water formation. It is also suggested that increased pole to equator temperature gradients resulted in enhanced wind-driven circulation patterns which could have resulted in different isotopic signatures for different ocean basins. A possible bias in absolute $\delta^{18}O$ and $\delta^{13}C$ values, the gradients between sites and the slope of the trends, resulting from diagenetic overprinting, variable burial depth, the benthic species used and alternative laboratory techniques can also not be ruled out.

Our data lends further support to the observation that long-period astronomical cycles, in combination with trends on tectonic time-scales, set the 'landscape' for climatic aberrations on astronomical timescales. The clearest examples of such events are the global cooling events that are followed by high amplitude climate variability on ~100-kyr timescales, such as for example the mid Oligocene cool phase/event and the OMT. The amplified ~2.4-Myr amplitude modulation of the 405-kyr cycle in $\delta^{13}C$ is unmistakable and this fact, taken in combination with the long-period eccentricity pacing of $\delta^{18}O$ events points towards the intricate relations between Earth's carbon cycle and global climate on (long-period) astronomical timescales.

5.1.3 Hysteresis and Antarctic ice sheet stability

The combined data and modelling output presented in this thesis further indicates that the strong hysteresis in state-of-the-art coupled climate-ice sheet models probably underestimates the true variability of the Oligo-Miocene Antarctic ice sheets. Depending on the phase and duration of the glacial cycle, between 20% and 80% (averaging at ~50%) of the Site 1264 $\delta^{18}O$ variance can be attributed to changes in Antarctic ice volume. This is the equivalent to the melt and re-accumulation of approximately half the modern-day EAIS. This finding is not reconcilable with 3D models that generally show strong hysteresis (i.e. large thermal inertia of the Antarctic ice sheets), even if relatively 'extreme' pCO_2 scenarios are considered. The implication of the absolute $\delta^{18}O$ amplitude on ~100-kyr timescales (~1‰) and the attributed Antarctic ice volume component (based on mass-balance equations using a 1D forward modelling approach), is that the 3D coupled climate-ice sheet models do not accurately approximate the true physical reality of the (Antarctic) ice sheets and/or that other components than ice-volume (e.g. temperature, diagenesis) affected absolute $\delta^{18}O$ values and variability significantly.

5.2 Earth's Climate System as a Complex System

Recently, complexity theory has been applied to qualitatively describe characteristics of palaeoclimate records [*Lenton*, 2009; *Scheffer*, 2009]. In this conclusion chapter we give two examples, based on the data presented in this thesis, where complex system science helps to direct the understanding of climate mechanisms and processes through simplified visual representations of steps and patterns in the data.

Firstly we show the $\delta^{13}C$ record of Site 1264 (Fig. 5.01), before, during and after the Oligocene Miocene Carbon Maximum and indicate that during the Oligo-Miocene at least two stable dynamic-equilibrium states in the carbon cycle evolved. The long durations (multi-Myr) of the stable phases indicate that a hysteresis loop prevented frequent switches between states. This qualitative behaviour can be better understood, without knowing the exact geographic settings, sea levels etc. that might have favoured organic carbon burial in Florida during the CM-OM [*Compton et al.*, 1993]. Future studies may be directed at constraining the thresholds associated with the onset and end of the CM-OM.

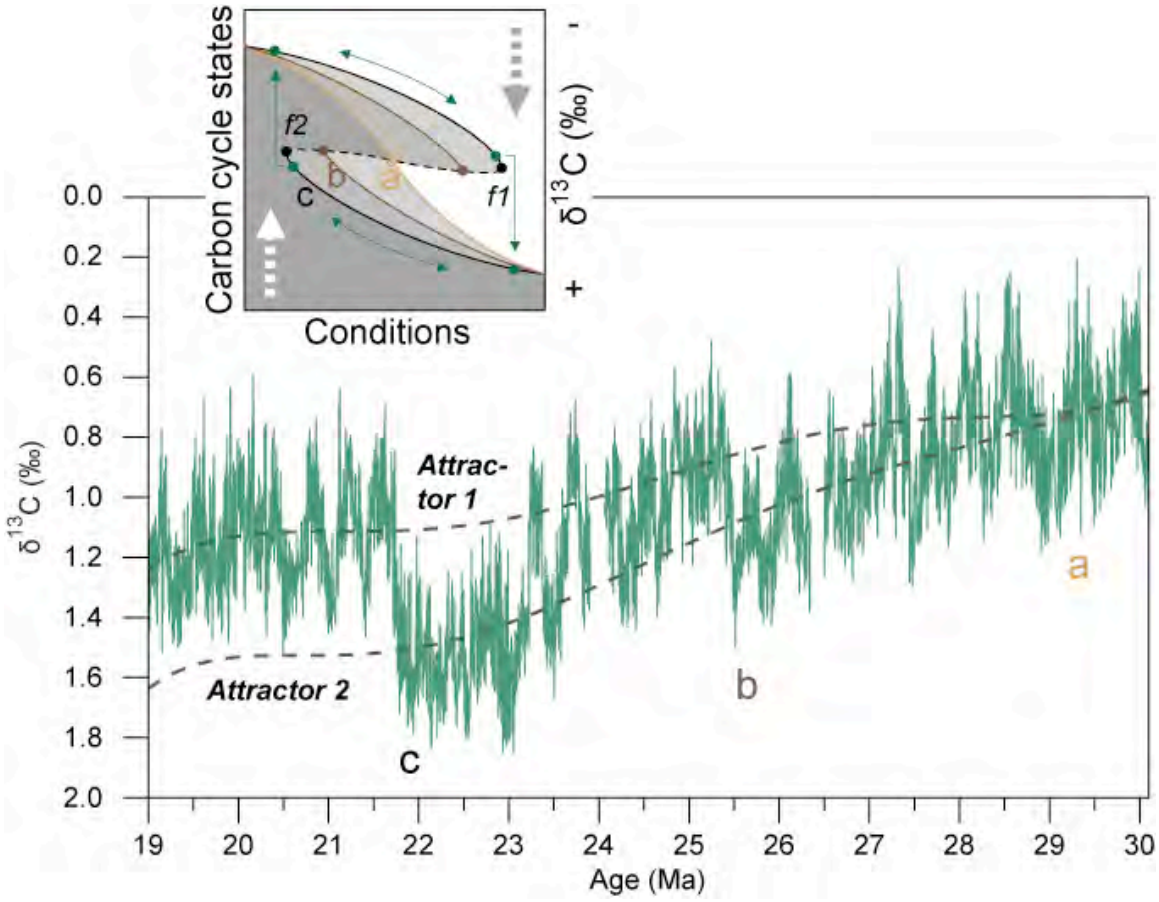

Figure 5.01: *Graphical representation of the possible evolution of two alternative stable states in Earth's carbon cycle throughout the Oligo-Miocene. The dashed lines represent mean $\delta^{13}C$ values from Site 1264 that correspond to alternative attractors. A hysteresis loop and threshold responses were involved to jump from one dynamic-equilibrium to the alternative one (see inset).*

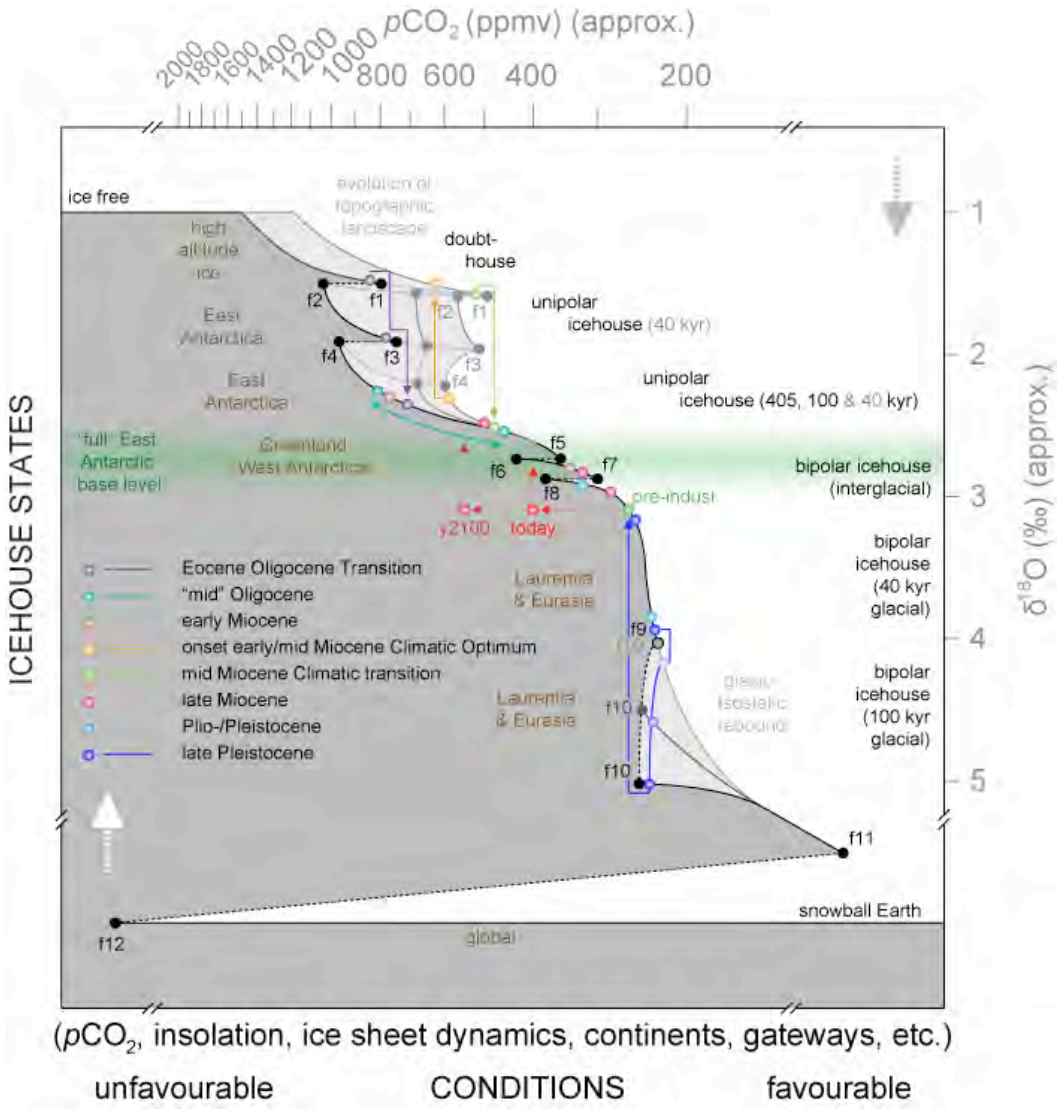

Figure 5.02: *Graphical depiction of the possible long-term evolution of equilibrium Icehouse states during the Cenozoic Icehouse (34 – 0 Ma). This conceptual model is an attempt to reconcile benthic $\delta^{18}O$ values and inferred Icehouse states (also based on other proxy data) with the long-term evolution of atmospheric pCO_2. Equilibrium states as drawn are inspired by [Abe-Ouchi et al., 2013; De Boer et al., 2014; De Boer et al., 2012; De Boer et al., 2010; DeConto and Pollard, 2003b; Foster and Rohling, 2013; Gasson et al., 2012; Paillard, 1998; Pollard and DeConto, 2005; Rohling et al., 2013; Scheffer, 2009; Van de Wal et al., 2011]. In this model gradual change and critical transitions result from positive feedbacks where, for example, an initial perturbation (i.e. small change of state) or change in (boundary) conditions is amplified by 'runaway' processes until a new equilibrium is encountered. (f-numbers depict bifurcation points associated with catastrophe folds).*

Our second example, for which complexity theory may provide the visual tool to (re)consider Earth's climate system, is the relation between glacial cycle shape, period and amplitude during the Icehouse state of the past 34 Myr. In figure 5.02 we show a simplified graphical overview of evolving equilibrium states in Icehouse Earth, in an attempt to reconcile benthic $\delta^{18}O$ values with pCO_2 estimates, both on tectonic and astronomic time scales. To achieve a good fit between the data across the (unipolar) Icehouse, the EAIS must have become much more instable during its earliest phase of significant Cenozoic glaciation. The increasing steepness of the slope of the equilibrium line, which represents long-term climate sensitivity according to the definition of *Rohling et al.* [2013], indicates that at present a much smaller change in radiative forcing is needed to destabilize the EAIS compared to the Oligocene and early Miocene. Reconstructions of Pliocene EAIS dynamics support this view and show for example that the Wilkes subglacial basin retreated [*Cook et al.*, 2013] in response to radiative forcings associated with pCO_2 values of ~400 ppmv, likely in conjunction with an unfavourable orbit. Figure 5.02 also visualises that under 'moderate' (from a Cenozoic perspective, i.e. unipolar Icehouse) pCO_2 values the Antarctic ice sheet will grow and the NH ice sheets will eventually collapse, both resulting from positive feedbacks. The land-based ice sheets therefore form a long-term 'base level' from which unipolar (i.e. SH) interglacials and bipolar (i.e. SH and NH) glacials depart from and return to. This conceptual model with broad full East Antarctic base level qualitatively 'explains' or visualises the difference in geometry of SH-sources and NH-source ~100-kyr cycles as recorded in benthic $\delta^{18}O$, as their periodicities. It also suggest a similar (ice-sheet or pCO_2) threshold was passed during Mi-3b as was passed across the EOT, linking these two events together through a similar causal mechanism. The symmetrical glacial cycles in the Oligocene of Site 1264 suggest that no clear threshold was present and suggest that pCO_2 may have been highly variable.

5.3 Societal Significance

In the past two decades a much better understanding of the Cenozoic climate and climate change has been achieved. Improved recovery of deep marine sedimentary climate archives through ocean drilling has proved crucial to this success. The science presented in this thesis is testimony to the potential of the marine archives and it contributes to the understanding of climate change on astronomical to tectonic time scales. However there are also implications for our understanding of climate dynamics on shorter, centennial – millennial, time scales. Our ice volume estimates, taken together with reconstructed pCO_2 values for the Oligocene and early

Miocene (~350 – ~800 ppmv), indicate that Northern Hemispheric ice volume was much reduced compared to present day. Therefore, if the Oligo-Miocene serves as an appropriate natural analogue, global warming, sea-level rise and land ice loss is to be expected, until the present day ice caps have reached long-term equilibrium with atmospheric CO_2.

Some of the questions that (palaeo-) climatologists are currently trying to address are: How fast will the globe warm in response to anthropogenic carbon dioxide emissions? (What is climate sensitivity?) Which regions are most susceptible to climate change? What can be expected for the coming 10 years or 100 years? Studying Cenozoic climate analogues can also play a pivotal role in answering these questions and especially studies into the unipolar Icehouse phase, a relatively understudied interval with similar to present radiative forcing conditions can shed light on the dynamics of global climate and SH ice sheets. Questions such as: What set of boundary conditions caused the Antarctic ice sheet to be so dynamic? And what is their relative importance on (palaeo-) climate sensitivity? What are past maximum rates of global change? And how do they compare to present rates of change? These are just some of the questions in need of further research before we will be able to answer them.

5.4 Future Work

The Oligo-Miocene interval as defined in the introduction spans around a 17 Myr interval of which 11 Myr are studied here in detail. A logical next step might be to extend the records to include the earliest Oligocene and the EOT (30 – 34 Ma window) on the older end of the record, and the later part of the early Miocene and the onset of the early/mid Miocene climatic optimum (17 – 19 Ma window), on the younger end. Site 1264 can only be extended upwards, so a jump to Site 1265 (or Site 1266) is needed to extend the record downwards. An extended record will give a more complete picture of the evolution of Oligo-Miocene (i.e. early Icehouse) climate and ice sheet dynamics. Alternative statistical methods of quantifying cycle geometry need to be explored to properly estimate the significance of (a)symmetry found in the $\delta^{18}O$ record from Walvis Ridge. Calculation of the 3rd order spectra (i.e. bispectra) could prove to be a statistical-technique to better-quantify cycle geometry. However, the relatively low sample resolution of palaeoclimate records may compromise the significance levels of these statistical analyses.

To further test reproducibility of the findings presented in this thesis and to better resolve certain events or time intervals, benthic chronologies can be constructed on sites with higher sedimentation rates and preferably better-preserved foraminifera. Such sediments were recently drilled off-coast Newfoundland [*Norris et al.*, 2014]. Consisting of a combination of clay and carbonates, these drift sediments were deposited underneath the intersection of the palaeo-Gulf stream and Labrador Sea Current and are characterised by exceptionally well-preserved microfossils, ideal for accurate palaeoclimate studies. The high sedimentation rates associated with drift deposits will enable rates of change to be better constrained and therefore to better understand how dynamic the Antarctic ice sheet exactly was in the past. These higher resolution records are most likely less noisy and can be used to obtain a clearer view on evolving cycle geometry. Some intervals are characterised by such high sedimentation rates that even studies of sub-orbital climate dynamics are within reach. This can have profound implications for our understanding of the millennial scale dynamics of the Antarctic ice sheet and North Atlantic palaeoceanography.

In addition to extended and new benthic stable-isotope stratigraphies a suite of other organic and inorganic geochemical proxy techniques could be applied to the sediments of Walvis Ridge or time-equivalent sites, to answer a broad spectrum of questions. Planktic stable-isotope stratigraphies across this time interval are still extremely sparse, limiting our understanding of surface water temperatures, temperature gradients and other conditions. High-resolution stable strontium isotopes and other weathering proxies (lithium, osmium) can perhaps be applied to disentangle the influence of continental weathering (on tectonic time scales) and physical and chemical erosion resulting from higher-frequency climate change (on astronomical time scales) on atmospheric pCO_2, and thereby further our understanding of causality in Cenozoic climate change. However, this would need to be accompanied by detailed pCO_2 reconstructions (boron and/or alkenones), also on astronomical time scales.

References

Abe-Ouchi, A., F. Saito, K. Kawamura, M. E. Raymo, J. Okuno, K. Takahashi, and H. Blatter (2013), Insolation-driven 100,000-year glacial cycles and hysteresis of ice-sheet volume, *Nature*, *500*, 190-194.

Abels, H. A., S. Van Simaeys, F. Hilgen, E. De Man, and N. Vandenberghe (2007), Obliquity-dominated glacio-eustatic sea level change in the early Oligocene: evidence from the shallow marine siliciclastic Rupelian stratotype (Boom Formation, Belgium), *Terra Nova*, *19*, 65-73.

Abels, H. A., F. J. Hilgen, W. Krijgsman, R. W. Kruk, I. Raffi, E. Turco, and W. J. Zachariasse (2005), Long-period orbital control on middle Miocene global cooling: Integrated stratigraphy and astronomical tuning of the Blue Clay Formation on Malta, *Paleoceanography*, *20*.

Beaufort, L. (1994), Climatic importance of the modulation of the 100 kyr cycle inferred from 16 m.y. long Miocene records, *Paleoceanography*, *9*(6), 821-834.

Beerling, D. J., and D. L. Royer (2011), Convergent Cenozoic CO2 history, *Nature Geoscience*, *4*, 418 - 420.

Berggren, W. A., D. V. Kent, C. C. Swisher, and M. Aubry (1995), A Revised Cenozoic Geochronology and Chronostratigraphy, *Geochronology, Time Scales and Global Stratigraphic Correlation.*, *54*, 129-212.

Bijl, P. K., et al. (2013), Eocene cooling linked to early flow across the Tasmanian Gateway, *Proceedings of the National Academy of Sciences of the USA*, *110*(24), 9645 - 9650.

Billups, K., J. E. T. Channell, and J. Zachos (2002), Late Oligocene to early Miocene geochronology and paleoceanography from the subantarctic South Atlantic, *Paleoceanography*, *17*(1).

Billups, K., H. Pälike, J. E. T. Channell, J. Zachos, and N. J. Shackleton (2004), Astronomic calibration of the late Oligocene through early Miocene geomagnetic polarity time scale, *Earth and Planetary Science Letters*, *224*, 33-44.

Bintanja, R., and R. S. W. Van de Wal (2008), North American ice-sheet dynamics and the onset of 100,000-year glacial cycles, *Nature*, *454*, 869-872.

Bintanja, R., R. S. W. Van de Wal, and J. Oerlemans (2005), Modelled atmospheric temperatures and global sea levels over the past million years, *Nature*, *437*, 125-128.

Bohaty, S., J. C. Zachos, and M. L. Delaney (2012), Foraminiferal Mg/Ca evidence for Southern Ocean cooling across the Eocene-Oligocene transition, *Earth and Planetary Science Letters*, *317 - 318*, 251 - 261.

Boulila, S., B. Galbrun, J. Laskar, and H. Pälike (2012), A ~9 myr cycle in Cenozoic δ13C record and long-term orbital eccentricitiy modulation: Is there a link?, *Earth and Planetary Science Letters*, *317-318*, 273-281.

Bowles, J. (2006), Data report: revised magnetostratigraphy and magnetic mineralogy of sediments from Walvis Ridge, Leg 208*Rep.*, Ocean Drilling Program, College Station, TX.

Brady, H. B., W. K. Parker, and T. R. Jones (1888), On some foraminifera from the Abrolhas Bank, *Transactions of the Zoological Society, London*, *12*, 40-47.

Broecker, W. S. (2002), *The Glacial World According to Wally*, Eldigio, Palisades, N. Y.

Campbell Jr, K. E., D. R. Prothero, L. Romero-Pittman, F. Hertel, and N. Rivera (2010), Amazonian magnetostratigraphy: Dating the first pulse of the Great American Faunal Interchange, *Journal of South American Earth Sciences*, *29*, 619 - 626.

Cande, S. C., and D. V. Kent (1995), Revised calibration of the geomagnetic polarity timescale for the Late Cretaceous and Cenozoic, *Journal of Geophysical Research*, *100*(B4), 6093-6095.

Channell, J. E. T., S. Galeotti, E. E. Martin, K. Billups, H. D. Scher, and J. S. Stoner (2003), Eocene to Miocene magnetostratigraphy, biostratigraphy, and chemostratigraphy at ODP Site 1090 (sub-Antarctic South Atlantic), *GSA bulletin*, *115*(5), 607-623.

Clemens, S. (1999), An astronomical tuning strategy for Pliocene sections: implications for global-scale correlation and phase relationships, *Phil. Trans. R. Soc. Lond.*, *357*, 1949-1973.

Compton, J. S., S. W. Snyder, and D. A. Hodell (1990), Phosphogenesis and weathering of shelf sediments from the southeastern United States: Implications for Miocene $\delta^{13}C$ excursions and global cooling, *Geology*, *18*, 1227-1230.

Compton, J. S., D. A. Hodell, J. R. Garrido, and D. J. Mallinson (1993), Origin and age of phophorite from the south-central Florida Platform: Relation of phosphogenesis to sea-level fluctuations and $\delta^{13}C$ excursions, *Geochimica et Cosmochimica Acta*, *57*, 131-146.

Cook, C. P., et al. (2013), Dynamic behaviour of the East Antarctic ice sheet during Pliocene warmth, *Nature Geoscience*, *6*, 765 - 769.

Coxall, H. K., and P. A. Wilson (2011), Early Oligocene glaciation and productivity in the eastern equatorial Pacific: Insights into global carbon cycling, *Paleoceanography*, *26*(PA2221).

Coxall, H. K., P. A. Wilson, H. Pälike, C. H. Lear, and J. Backman (2005), Rapid stepwise onset of Antarctic glaciation and deeper calcite compensation in the Pacific Ocean, *Nature*, *433*(7021), 53-57.

Cramer, B. S., J. R. Toggweiler, J. D. Wright, M. E. Katz, and K. G. Miller (2009), Ocean overturning since the late Cretaceous: Inferences from a new benthic foramniniferal isotope compilation, *Paleoceanography*, *24*.

Curry, W. B., N. J. Shackleton, C. Richter, and e. al. (1995), Initial Report: Leg 154*Rep.*, Ocean Drilling Program.

De Boer, B., L. J. Lourens, and R. S. W. Van de Wal (2014), Persistent 400,.000-year variability of Antarctic ice volume and the carbon cycle is revealed throughout the Plio-Pleistocene, *Nature Communications*, *5:2999*.

De Boer, B., R. S. W. Van de Wal, L. J. Lourens, and R. Bintanja (2012), Transient nature of the Earth's climate and the implications for the interpretation of benthic δ18O records, *Palaeogeography, Palaeoclimatology, Palaeoecology*, *335-336*, 4-11.

De Boer, B., R. S. W. Van de Wal, R. Bintanja, L. J. Lourens, and E. Tuenter (2010), Cenozoic global ice-volume and temperature simulations with 1-D ice-sheet models forced by benthic δ18O records, *Annals of Glaciology*, *51*(55), 23-33.

DeConto, R. M., and D. Pollard (2003a), A coupled climate-ice sheet modeling approach to the Early Cenozoic history of the Antarctic ice sheet, *Palaeogeography, Palaeoclimatology, Palaeoecology*, *198*, 39-52.

DeConto, R. M., and D. Pollard (2003b), Rapid Cenozoic glaciation of Antarctica induced by declining atmospheric CO2, *Nature*, *421*(6920), 245-249.

DeConto, R. M., D. Pollard, P. A. Wilson, H. Pälike, C. H. Lear, and M. Pagani (2008), Thresholds for Cenozoic bipolar glaciation, *Nature*, *455*, 652-656.

Diester-Haass, L., K. Billups, and K. Emeis (2011), Enhanced paleoproductivity across the Oligocene/Miocene boundary as evidenced by benthic foraminiferal accumulation rates, *Palaeogeography, Palaeoclimatology, Palaeoecology*, *302*, 464 - 473.

Edinger, E. N., and M. J. Risk (1994), Oligocene-Miocene Extinction and Geographic Restriction of Caribbean Corals: Roles of Turbidity, Temperature, and Nutrients, *Palaios*, *9*(6), 576-598.

Eldrett, J. S., I. C. Harding, P. A. Wilson, E. Butler, and A. P. Roberts (2007), Continental ice in Greenland during the Eocene and Oligocene, *Nature*, *446*.

ESRL/NOAA Mauna Loa CO2, edited.

Flower, B. P., and K. E. Chrisholm (2006), Magnetostratigraphic Calibration of the Late Oligocene Climate Transition*Rep.*

Flower, B. P., J. C. Zachos, and H. Paul (1997a), Milankovitch-scale climate variability recorded near the Oligocene/Miocene boundary, in *Proceedings of the Ocean Drilling Program, Scientific Results.*, edited by N. J. Shackleton, W. B. Curry, C. Richter and T. J. Bralower, pp. 433 - 439.

Flower, B. P., J. C. Zachos, and E. Martin (1997b), Latest Oligocene through early Miocene isotopic stratigraphy and deep-water paleoceanography of the Western Equatorial Atlantic: Sites 926 and 929, in *Proceedings of the Ocean Drilling Program, Scientific Results.*, edited by N. J. Shackleton, W. B. Curry, C. Richter and T. J. Bralower, pp. 451 - 461.

Flower, B. P., J. C. zachos, and P. N. Pearson (2006), Astronomic and Oceanographic Influences on Global Carbon Cycling across the Oligocene/Miocene Boundary, in *Micropaleontology Application in Stratigraphy and Paleoceanography*, edited by D. K. Sinha, Narosa Publishing House, New Delhi, Chennai, Mumbai, Kolkata.

Foster, G. L., and E. J. Rohling (2013), Relationship between sea level and climate forcing by CO2 on geological timescales, *Proceedings of the National Academy of Sciences of the USA*, *110*(4), 1209 - 1214.

Ganopolski, A., and S. Rahmstorf (2001), Rapid changes of glacial climate simulated in a coupled climate model, *Nature*, *409*, 153 - 158.

Gasson, E., M. Siddall, D. J. Lunt, O. J. Rackham, C. H. Lear, and D. Pollard (2012), Exploring uncertainties in the relationship between temperature, ice volume, and sea level ove the past 50 million years, *Reviews of Geophysics*, *50*.

Gersonde, R., D. A. Hodell, P. Blum, and e. al. (1999), Initial Report: Leg 177*Rep.*, Ocean Drilling Program.

Grinsted, A., J. C. Moore, and S. Jevrejeva (2004), Application of the cross wavelet transform and wavelet coherence to geophysical time series, *Nonlinear Processes in Geophysics*, *11*, 561-566.

Hays, J. D., J. Imbrie, and N. J. Shackleton (1976), Variations in the Earth's Orbit: Pacemaker of the Ice Ages, *Science*, *194*(4270), 1121-1132.

Hilgen, F. J., L. J. Lourens, and J. A. van Dam (Eds.) (2012), *The Neogene Period*, Elsevier.

Hodell, D. A., and F. Woodruff (1994), Variations in the strontium isotopic ratio of seawater during the Miocene: Stratigraphic and geochemical implications, *Paleoceanography*, *9*(3), 405-426.

Hohbein, M. W., P. F. Sexton, and J. A. Cartwright (2012), Onset of North Atlantic Deep Water production coincident with inception of the Cenozoic global cooling trend, *Geology*, *40*(3), 255 - 258.

Holbourn, A., W. Kuhnt, M. Schulz, and H. Erlenkeuser (2005), Impacts of orbital forcing and atmospheric carbon dioxide on Miocene ice-sheet expansion, *Nature*, *438*(24).

Holbourn, A., W. Kuhnt, M. Schulz, J.-A. Flores, and N. Andersen (2007), Orbitally-paced climate evolution during the middle Miocene "Monterey" carbon-isotope excursion, *Earth and Planetary Science Letters*, *261*, 534-550.

Holbourn, A., W. Kuhnt, S. Clemens, W. Prell, and N. Andersen (2013), Middle to late Miocene stepwise climate cooling: Evidence from a high-resolution deep-water isotope curve spanning 8 million years.

Holbourn, A., W. Kuhnt, M. Lyle, L. Schneider, O. Romero, and N. Andersen (2014), Middle Miocene climate cooling linked to intensification of eastern equatorial Pacific upwelling, *Geology*, *42*(1), 19 - 22.

Hüsing, S. K., F. J. HIlgen, H. Abdul Aziz, and W. Krijgsman (2007), Completing the Neogene geological time scale between 8.5 and 12.5 Ma, *Earth and Planetary Science Letters*, *253*, 340-358.

Hüsing, S. K., K. F. Kuiper, W. Link, F. J. Hilgen, and W. Krijgsman (2009), The upper Tortonian-lower Messinian at Monte dei Corvi (Northern Apennines, Italy): Completing

a Mediterranean reference section for the Tortonian Stage, *Earth and Planetary Science Letters*, *282*, 140 - 157.
Huybers, P. (2011), Combined obliquity and precession pacing of late Pleistocene deglaciations, *Nature*, *480*, 229-232.
Huybers, P., and C. Wunsch (2005), Obliquity pacing of the late Pleistocene glacial terminations, *Nature*, *434*, 491-494.
Ikeda, M., and R. Tada (2013), Long period astronomical cycles from the Triasic to Jurassic bedded chert sequence (inuyama, Japan): Geologic evidences for the chaotic behavior of solar planets, *Earth Planets Space, *, *65*, 1-10.
Imbrie, J., and J. Z. Imbrie (1980), Modelling the climatic response to orbital variations, *Science*, *207*, 943 - 953.
IPPC (2013), AR5.
Jamieson, S. S. R., and D. E. Sugden (2008), Landscape Evolution of Antarctica, in *Antarctica: A Keystone in a Changing World*, edited by A. K. Cooper, P. Barrett, H. Stagg, B. Storey, E. Stump, W. Wise and t. I. e. team, The National Academies Press, Washington, DC.
Jamieson, S. S. R., N. R. J. Hulton, and M. Hagdorn (2008), Modelling landscape evolution under ice sheets, *Geomorphology*, *97*, 91 - 108.
Jamieson, S. S. R., D. E. Sugden, and N. R. J. Hulton (2010), The evolution of the subglacial landscape of Antarctica, *Earth and Planetary Science Letters*, *293*, 1 - 27.
Katz, M. E., B. S. Cramer, J. R. Toggweiler, G. Esmay, C. Liu, K. G. Miller, Y. Rosenthal, B. S. Wade, and J. D. Wright (2011), Impact of Antarctic Circumpolar Current development on late Paleogene ocean structure, *Science*, *332*.
King, T. (1996), Quantifying nonlinearity and geometry in time series of climate, *Quaternary Science Reviews*, *15*, 247 - 266.
Köppen, V. P., and A. Wegener (1924), Die Klimate der Geologischen Vorzeit.
Kürschner, W. M., Z. Kvacek, and D. L. Dilcher (2008), The impact of Miocene atmospheric carbon dioxide fluctuations on climate and the evolution of terrestrial ecosystems, *Proceedings of the National Academy of Sciences of the USA*, *105*(2), 449-453.
Lanci, L., J. M. Parés, J. E. T. Channell, and D. V. Kent (2004), Miocene magnetostratigraphy from Equatorial Pacific sediments (ODP Site 1218, Leg 199), *Earth and Planetary Science Letters*, *226*, 207-224.
Lanci, L., J. M. Parés, J. E. T. Channell, and D. V. Kent (2005), Oligocene magnetostratigraphy from Equatorial Pacific sediments (ODP Sites 1218 and 1219, Leg 199), *Earth and Planetary Science Letters*, *237*, 617-634.
Laskar, J. (1999), The limits of Earth orbital calculations for geological time-scale use, *Phil. Trans. R. Soc. A*, *357*, 1735 - 1759.
Laskar, J., F. Joutel, and F. Boudin (1993), Orbital, precessional, and insolation quantities for the Earth from -20 Myr to +10 Myr, *Astronomy and Astrophysics*, *270*, 522-533.
Laskar, J., A. Fienga, M. Gastineau, and H. Manche (2011a), La2010: A new orbital solution for the long term motion of the Earth, *Astronomy and Astrophysics*, *532*(A89).
Laskar, J., M. Gastineau, J.-B. Delisle, A. Farrés, and A. Fienga (2011b), Strong chaos induced by close encounters with Ceres and Vesta, *Astronomy and Astrophysics*, *532*(L4), 1-4.
Laskar, J., P. Robutel, F. Joutel, M. Gastineau, A. C. M. Correia, and B. Levrard (2004), A long-term numerical solution for the insolation quantities of the Earth, *Astronomy and Astrophysics*, *428*, 261-285.
Lear, C. H., H. Elderfield, and P. A. Wilson (2000), Cenozoic Deep-Sea Temperatures and Global Ice Volumes from Mg/Ca in Benthic Foraminiferal Calcite, *Science*, *287*.
Lear, C. H., Y. Rosenthal, H. K. Coxall, and P. A. Wilson (2004), Late Eocene to early Miocene ice sheet dynamics and the global carbon cycle, *Paleoceanography*, *19*.
Lenton, T. M. (2009), Early warning of climate tipping points, *Nature Climate Change*, *1*, 201 - 209.

Levrard, B., and J. Laskar (2003), Climate friction and the Earth's obliquity, *Geophysical Journal International*, *154*, 970-990.

Liebrand, D., L. J. Lourens, D. A. Hodell, B. De Boer, R. S. W. Van de Wal, and H. Pälike (2011, Chapter 2), Antarctic ice sheet and oceanographic response to eccentricity forcing during the early MIocene, *Climate of the Past*, *7*, 869-880.

Lisiecki, L. E., and P. A. Lisiecki (2002), Application of dynamic programming to the correlation of paleoclimate records, *Paleoceanography*, *17*(4).

Lisiecki, L. E., and M. E. Raymo (2005), A Pliocene-Pleistocene stack of 57 globally distributed benthic $\delta^{18}O$ records, *Paleoceanography*, *20*.

Littler, K., U. Röhl, T. Westerhold, and J. C. zachos (2014), A high-resolution benthic stable-isotope record for the South Atlantic: Implications for orbital-scale changes in Late Paleocene-Early Eocene climate and carbon cycling, *Earth and Planetary Science Letters*, *401*, 18 - 30.

Lourens, L. J., and F. J. Hilgen (1997), Long-periodic variations in the earth's obliquity and their relation to third-order eustatic cycles and late Neogene glaciations, *Quaternary International*, *40*, 43-52.

Lourens, L. J., R. Wehausen, and H. J. Brumsack (2001), Geological constraints on tidal dissipation and dynamical ellipticity of the Earth over the past three million years, *Nature*, *409*(6823), 1029-1033.

Lourens, L. J., F. J. Hilgen, N. J. Shackleton, J. Laskar, and D. Wilson (2004), The Neogene Period, in *A Geologic Time Scale 2004*, edited by F. Gradstein, J. Ogg and A. Smith, Cambridge University Press.

Lourens, L. J., A. Sluijs, D. Kroon, J. C. Zachos, E. Thomas, U. Röhl, J. Bowles, and I. Raffi (2005), Astronomical pacing of late Palaeocene to early Eocene global warming events, *Nature*, *435*, 1083-1087.

Lyle, M., P. A. Wilson, and T. R. Janecek (2002), Initial Reports: Leg 199*Rep.*

Mawbey, E. M., and C. H. Lear (2013), Carbon cycle feedbacks during the Oligocene-Miocene transient glaciation, *Geology*.

Merico, A., T. Tyrell, and P. A. Wilson (2008), Eocene/Oligocene ocean de-acidification linked to Antarctic glaciation by sea-level fall, *Nature*, *452*, 979-983.

Milankovitch, M. (1941), *Canon of Insolation and the Ice-Age Problem*, 1st ed., Zavod za udžbenike i nastavna sredstva & Muzej nauke i tehnike Srpske akademije nauka i umetnosti, Beograd.

Miller, K. G., and R. G. Fairbanks (1983), Evidence for Oligocene-Middle Miocene abyssal circulation changes in the western North Atlantic, *Nature*, *306*(17), 250 - 253.

Miller, K. G., J. D. Wright, and A. N. Brower (1989), Oligocene to Miocene stable isotope stratigraphy and planktonic foraminifer biostratigraphy of the Sierra Leone Rise (DSDP Site 366 and ODP Site 667), *Proceedings of the Ocean Drilling Program, Scientific Results.*, *108*, 279 - 294.

Miller, K. G., J. D. Wright, and R. G. Fairbanks (1991), Unlocking the Ice House: Oligocene-Miocene Oxygen Isotopes, Eustacy and Margin Erosion, *Journal of Geophysical Research*, *96*(B4), 6829-6848.

Moran, K., et al. (2006), The Cenozoic palaeoenvironment of the Arctic Ocean, *Nature*, *441*.

Naafs, B. D. A. (2011), Unpublished data, edited.

Naish, T. R., et al. (2001), Orbitally induced oscillations in the East Antarctic ice sheet at the Oligocene/Miocene boundary, *Nature*, *413*, 719-723.

Newkirk, D. R., and E. E. Martin (2009), Circulation through the Central American Seaway during the Miocene carbonate crash, *Geology*, *37*(1), 87 - 90.

Norris, R. D., S. Kirtland Turner, P. M. Hull, and A. Ridgwell (2013), Marine ecosystem responses to Cenozoic global change, *Science*, *341*.

Norris, R. D., P. A. Wilson, P. Blum, and Expedition_342_Scientists (2014), Expedition Reports*Rep.*, Integrated Ocean Drilling Program, College Station.

Omta, A. W., and H. A. Dijkstra (2003), A physical mechanism for the Atlantic-Pacific flow reversal in the early Miocene, *Global and Planetary Change*, *36*, 265 - 276.

Oslick, J. S., K. G. Miller, M. D. Feigenson, and J. D. Wright (1994), Oligocene-Miocene strontium isotopes: Stratigraphy revisions and correlations to an inferred glacioeustatic record, *Paleoceanography*, *9*(3), 427-443.

Ostermann, D. R., and W. B. Curry (2000), Calibration of stable isotopic data: An enriched $\delta^{18}O$ standard used for source gas mixing detection and correction, *Paleoceanography*, *15*(3), 353-360.

Pagani, M., M. A. Arthur, and K. H. Freeman (1999), Miocene evolution of atmospheric carbon dioxide, *Paleoceanography*, *14*(3), 273-292.

Pagani, M., J. C. Zachos, K. H. Freeman, B. Tipple, and S. Bohaty (2005), Marked decline in atmospheric carbon dioxide concentrations during the paleogene, *Science*, *309*.

Paillard, D. (1998), The timing of Pleistocene glaciations from a simple multiple-state climate model, *Nature*, *391*, 378 - 381.

Paillard, D., L. Labeyrie, and P. Yiou (1996), Analyseries, Macintosh program performs time-series analysis, *EOS Transactions AGU*, *77*(39), 379.

Pälike, H. (2001), Extending the astronomical calibration of the geological time scale, 226 pp, University of Cambridge, Cambridge.

Pälike, H., and N. J. Shackleton (2000), Constraints on astronomical parameters from the geological record for the last 25 Myr, *Earth and Planetary Science Letters*, *182*(1), 1-14.

Pälike, H., J. Laskar, and N. J. Shackleton (2004), Geologic constraints on the chaotic diffusion of the solar system, *Geology*, *32*(11), 929-932.

Pälike, H., J. Frazier, and J. C. zachos (2006a), Extended orbitally forced palaeoclimatic records from the equatorial Atlantic Ceara Rise, *Quaternary Science Reviews*, *25*(23-24), 3138-3149.

Pälike, H., M. W. Lyle, H. Nishi, and e. al. (2012), A Cenozoic record of the equatorial Pacific carbonate compenstion depth, *Nature*, *488*, 609 - 615.

Pälike, H., T. Moore, J. Backman, I. Raffi, L. Lanci, J. M. Pares, and T. Janecek (2005), Integrated stratigraphic correlation and improved composite depth scales for ODP Sites 1218 and 1219*Rep.*, Texas A&M Univerisity, College Station.

Pälike, H., H. Nishi, M. Lyle, I. Raffi, K. Gamage, A. Klaus, and E. Scientists (2010), Expedition 320/321 summary*Rep.*, Tokyo.

Pälike, H., R. D. Norris, J. O. Herrle, P. A. Wilson, H. K. Coxall, C. H. Lear, N. J. Shackleton, A. K. Tripati, and B. S. Wade (2006b), The Heartbeat of the Oligocene Climate System, *Science*, *314*, 1894-1898.

Patterson, M. O., R. McKay, T. Naish, C. Escutia, F. J. Jiménez-Espejo, M. E. Raymo, S. R. Meyers, L. Tauxe, H. Brinkhuis, and I. E. Scientists (2014), Orbital forcing of the East Antarctic ice sheet during the Pliocene and Early Pleistocene, *Nature Geoscience*, *7*, 841 - 847.

Paul, H. A., J. C. Zachos, B. P. Flower, and A. Tripati (2000), Orbitally induced climate and geochemical variability across the Oligocene/Miocene boundary, *Paleoceanography*, *15*(5), 471-485.

Pearson, P. N., N. J. Shackleton, G. P. Weedon, and M. A. Hall (1997), Multispecies planktonic foraminifer stable isotope stratigraphy through Oligocene/Miocene boundary climatic cycles, Site 926, in *Proceedings of the Ocean Drilling Program, Scientific Results.*, edited by N. J. Shackleton, W. B. Curry, C. Richter and T. J. Bralower, College Station, Texas.

Pekar, S. F., and R. M. DeConto (2006), High-resolution ice-volume estimates for the early Miocene: Evidence for a dynamic ice sheet in Antarctica, *Palaeogeography, Palaeoclimatology, Palaeoecology*, *231*, 101 - 109.

Pollard, D., and R. M. DeConto (2003), Antarctic ice and sediment flux in the Oligocene simulated by a climate-ice sheet-sediment model, *Palaeogeography, Palaeoclimatology, Palaeoecology*, *198*, 53 - 67.

Pollard, D., and R. M. DeConto (2005), Hysteresis in Cenozoic Antarctic ice-sheet variations, *Global and Planetary Change*, *45*(1-3), 9-21.

Proistosescu, C., P. Huybers, and A. C. Maloof (2012), To tune or not to tune: Detecting orbital variability in Oligo-Miocene climate records, *Earth and Planetary Science Letters*, *325-326*, 100-107.

Raymo, M. E., W. F. Ruddiman, and P. N. Froelich (1988), Influence of late Cenozoic mountain building on ocean geochemical cycles, *Geology*, *16*, 649-653.

Raymo, M. E., L. E. Lisiecki, and K. Nisancioglu (2006), Plio-Pleistocene ice volume, Antarctic climate, and the global d18O record, *Science*, *313*.

Rohling, E. J., et al. (2013), Making sense of palaeoclimate sensitivity, *Nature*, *491*, 683 - 691.

Scheffer, M. (2009), *Critical transitions in Nature and Society*, Princeton University Press, Princeton and Oxford.

Scher, H. D., and E. E. Martin (2006), Timing and Climatic Consequences of the Opening of Drake Passage, *Science*, *312*, 428 - 430.

Schlitzer, R. (2010), Ocean Data View 4, version 4.3.6, http://odv.awi.de, edited.

Sexton, P. F., and S. Barker (2012), Onset of 'Pacific-style' deep-sea sedimentary carbonate cycles at the mid-Pleistocene transition, *Earth and Planetary Science Letters*, *321-322*, 81-94.

Shackleton, N. J. (1974), Attainment of isotope equilibrium between ocean water and the benthonic foraminifera genus *Uivergerina*: Isotopic changes in the ocean during the last glacial, *Colloques Internationaux du Centre National de la Recherche Scientifique*, *219*, 203-209.

Shackleton, N. J., and S. Crowhurst (1997), Sediment fluxes based on an orbitally tuned time scale 5 Ma to 14 Ma, Site 926, *Proceedings of the Integrated Ocean Drilling Program, Scientific Results*, *154*, 69-82.

Shackleton, N. J., S. J. Crowhurst, G. P. Weedon, and J. Laskar (1999), Astronomical Calibration of Oligocene-Miocene Time, *Philosophical Transactions: Mathematical, Physical and Engineering Sciences*, *357*(1757), 1907-1929.

Shackleton, N. J., M. A. Hall, I. Raffi, L. Tauxe, and J. C. Zachos (2000), Astronomical calibration age for the Oligocene-Miocene boundary, *Geology*, *28*(5), 447-450.

Smith, W. H. F., and D. T. Sandwell (1997), Global seafloor topography from satallite and ship depth soundings, *Science*, *277*, 1957 - 1962.

Sosdian, S., and Y. Rosenthal (2009), Deep-Sea Temperature and Ice Volume Changes Across the Pliocene-Pleistocene Climate Transition, *Science*, *325*, 306 - 310.

Sprovieri, M., N. Sabatino, N. Pelosi, S. J. Batenburg, R. Coccioni, M. Lavarone, and S. Mazzola (2013), Late Cretaceous orbitally-paced carbon isotope stratigraphy from the Bottaccione Gorge (Italy), *Palaeogeography, Palaeoclimatology, Palaeoecology*, *379-380*, 81-94.

Tauxe, L., and P. Hartl (1997), 11 million years of Oligocene geomagnetic field behaviour, *Geophysical Journal International*, *128*, 217 - 229.

Tauxe, L., P. Tucker, N. P. Petersen, and J. L. LaBrecque (1984), Magnetostratigraphy of Leg 73 sediments*Rep.*, US Governmental Printing Office, Washington, DC.

Tian, J., Q. Zhao, P. Wang, Q. Li, and X. Cheng (2008), Astronomically modulated Neogene sediment records from the South China Sea, *Paleoceanography*, *23*.

Torrence, C., and G. P. Compo (1998), A Practical Guide to Wavelet Analyses, *Bull. Am. Met. Soc.*, *79*(1).

Tripati, A., J. Backman, H. Elderfield, and P. Ferretti (2005), Eocene bipolar glaciation associated with global carbon cycle changes, *Nature*, *436*, 341 - 346.

Van Dam, J. A., H. Abdul Aziz, M. Angeles Alvarez Sierra, F. J. Hilgen, L. W. van den Hoek Ostende, L. J. Lourens, P. Mein, A. J. van der Meulen, and P. Pelaez-Campomanes (2006), Long-period astronomical forcing of mammal turnover, *Nature*, *443*(7112), 687-691.

Van de Wal, R. S. W., B. De Boer, L. J. Lourens, P. Köhler, and R. Bintanja (2011), Reconstruction of a continuous high-resolution CO2 record over the past 20 million years, *Climate of the Past*, *7*, 1459-1469.

Vandenberghe, N., F. J. Hilgen, and Speijer (Eds.) (2012), *The Paleogene Period*, Elsevier.

Von der Heydt, A., and H. A. Dijkstra (2005), Flow reorganizations in the Panama Seaway: A cause for the demise of Miocene corals?, *Geophysical research letters*, *32*.

Von der Heydt, A., and H. A. Dijkstra (2006), Effect of ocean gateways on the global ocean circulation in the late Oligocene and early Miocene, *Paleoceanography*, *21*.

Wade, B. S., and H. Pälike (2004), Oligocene climate dynamics, *Paleoceanography*, *19*(4).

Wang, P., W. L. Prell, P. Blum, and e. al. (2000), Initial Reports: Leg 184*Rep.*, College Station, TX.

Weedon, G. P. (1997), Data report: Measurements of Magnetic Susceptibility for the Oligocene and lower Miocene of Site 925*Rep.*

Weedon, G. P., N. J. Shackleton, and P. N. Pearson (1997), The Oligocene time scale and cyclostratigraphy on the Ceara Rise, Western Equatorial Atlantic*Rep.*

Weltje, G. J., and R. Tjallingii (2008), Calibration of XRF core scanners for queantitative geochemical logging of sediment cores: Theory and application, *Earth and Planetary Science Letters*, *274*, 423-438.

Westerhold, T., U. Röhl, and J. Laskar (2012), Time scale controversy: Accurate orbital calibration of the early Paleogene, *Gechemistry, Geophysics, Geosystems*, *13*(6).

Wilson, D. S., and B. P. Luyendyk (2009), West Antarctic paleotopography estimated at the Eocene-Oligocene climate transition, *Geophysical Research Letters*, *36*.

Woodruff, F., and S. M. Savin (1989), Miocene deepwater oceanography, *Paleoceanography*, *4*(1), 87-140.

Wright, J. D., and K. G. Miller (1992), Miocene stable isotope stratigraphy, Site 747, Kerguelen Plateau, *Proceedings of the Ocean Drilling Program, Scientific Results, Scientific Results, Vol. 120*.

Wright, J. D., K. G. Miller, and R. G. Fairbanks (1992), Early and middle Miocene stable isotopes: Implications for deepwater circulation and climate, *Paleoceanography*, *7*(3), 357-389.

Zachos, J. C., B. P. Flower, and H. A. Paul (1997), Orbitally paced climate oscillations across the Oligocene/Miocene boundary, *Nature*, *388*(6642), 567-570.

Zachos, J. C., G. R. Dickens, and R. E. Zeebe (2008), An early Cenozoic perspective on greenhouse warming and carbon-cycle dynamics, *Nature*, *451*(7176), 279-283.

Zachos, J. C., D. Kroon, P. Blum, and e. al. (2004), Initial Reports: Leg 208*Rep. Volume 208*, Ocean Drilling Program.

Zachos, J. C., B. N. Opdyke, T. M. Quinn, C. E. Jones, and A. N. Halliday (1999), Early Cenozoic glaciation, antarctic weathering, and seawater 87Sr/86Sr: is there a link?, *Chemical Geology*, *161*, 165-180.

Zachos, J. C., N. J. Shackleton, J. S. Revenaugh, H. Palike, and B. P. Flower (2001a), Climate Response to Orbital Forcing Across the Oligocene-Miocene Boundary, *Science*, *292*(5515), 274-278.

Zachos, J. C., M. Pagani, L. Sloan, E. Thomas, and K. Billups (2001b), Trends, Rhythms, and Aberrations in Global Climate 65 Ma to Present, *Science*, *292*, 686-693.

Zeeden, C., F. J. Hilgen, S. K. Hüsing, and L. J. Lourens (2014), The Miocene astronomical time scale 9 - 12 Ma: New constraints on tidal dissipation and their implications for paleoclimatic investigations, *Paleoceanography*, *29*, 296 - 307.

Zeeden, C., F. J. Hilgen, T. Westerhold, L. J. Lourens, U. Röhl, and T. Bickert (2013), Revised Miocene splice, astronomical tuning and calcareous plankton biochronology of ODP Site 926 between 5 and 14.4 Ma, *Palaeogeography, Palaeoclimatology, Palaeoecology*, *369*, 430-451.

Zhang, Y. G., M. Pagani, Z. Liu, S. Bohaty, and R. DeConto (2013), A 40-million-year history of atmospheric CO2, *Phil. Trans. R. Soc. A*, *371*.